ASSESSING THE USE OF NORMALIZED DIFFERENCE CHLOROPHYLL INDEX TO ESTIMATE CHLOROPHYLL-A CONCENTRATIONS USING LANDSAT 5 TM AND LANDSAT 8 OLI IMAGERY IN THE SALTON SEA, CALIFORNIA

by

Alejandra G. Lopez

A Thesis Presented to the
FACULTY OF THE USC DORNSIFE COLLEGE OF LETTERS, ARTS AND SCIENCES
University of Southern California
In Partial Fulfillment of the
Requirements for the Degree
MASTER OF SCIENCE
(GEOGRAPHIC INFORMATION SCIENCE AND TECHNOLOGY)

May 2023

To my parents, siblings, and loving partner

Acknowledgements

I would like to thank my advisor, Dr. Elisabeth Sedano, for her insight, encouragement, and patience throughout the completion of this project. I would also like to thank my committee members, Dr. Yi Qi and Dr. Diana Ter-Ghazaryan for their expertise, feedback, and guidance.

Table of Contents

List of Tables

List of Figures

List of Abbreviations

2BDA	Two-Band Algorithm
3BDA	Three-Band Algorithm
AOI	Area of Interest
AR	Alamo River
BoR	Bureau of Reclamation
FLH	Florence Line Height
IOPs	Inherent Optical Properties
IWRM	Integrate Water Resource Management
MIR	Middle Infrared
MNDWI	Modified Normalized Difference Water Index
NDCI	Normalized Difference Chlorophyll Index
NDVI	Normalized Difference Vegetation Index
NDWI	Normalized Difference Water Index
NIR	Near Infrared
NR	New River
NWI	New Water Index
QSA	Quantification Settlement Agreement
RS	Remote Sensing
ST	Salton Trough
US	United States
USGS	United States Geological Survey
WQ	Water Quality

WQMPs	Water Quality Management Plan
WWR	Whitewater River

Abstract

The Salton Sea is the largest body of water in the State of California and has experienced a decline in water quality within the last fifty years. This inland body of water serves as a reservoir for agricultural runoff and maintains high concentrations of pesticides and nutrients that place surrounding communities and ecological environments at risk. As a result of the degradation and eutrophic state of the Salton Sea, it is important to identify historical trends and methodologies that can be used for future water quality assessments. Traditional water quality assessments are conducted onsite and require extensive financial and human resources. In order to mitigate some of these costs while continuing to monitor water quality, more efficient assessment techniques must be explored. This study explores one such technique by examining the use of remote sensing techniques and the Normalized Difference Chlorophyll Index (NDCI) to assess chlorophyll-a concentrations in the Salton Sea from 2002 to 2020 using Landsat 5 TM and Landsat 8 OLI imagery. To assess the accuracy of this method, the NDCI is compared against two-band and three-band algorithms proposed by literature. Results indicate that the NDCI has largely underestimate chlorophyll-a concentrations within the Salton Sea and has incorrectly suggested small variations across the temporal range. Linear regression results further reveal a weak linear regression between NDCI, 2BDA and 3BDA values and in-situ measurements.

Chapter 1 Introduction

The Salton Sea is the largest body of waterbody in the State of California, spanning approximately 340 square miles between the Riverside and Imperial counties (Cantor and Knuth 2019; Carpelan 1958). Deviations in weather conditions, increasing water demand and unprecedented water drought episodes have contributed to the altering landscape of Southern California (Cohen 2019; Doede and De Guzman 2020; Johnston et al. 2019). In addition to local policies, environmental factors have contributed to the receding shoreline and poor water quality (WQ) of the Salton Sea. Scholars and government agencies have categorized the Salton Sea as an ecological disaster. This classification is attributed to its eutrophic state and uncommonly high concentration of nutrients that have contributed to the collapse of multiple fish populations (Bradley, Ajami, and Porter 2022; Forsman 2014; Riedel 2016). The Salton Sea faces an uncertain future, as the termination of water deposits from the Colorado River, its increased reliance for agricultural drainage and rising interest for lithium extraction within its lakebed. Thus, the continued monitoring of the Salton Sea's WQ is critical and calls for the adoption of efficient monitoring methods. The aim of this study is to (1) use the Normalized Difference Chlorophyll Index (NDCI) to assess historical chlorophyll-a concentrations within the Salton Sea from 2002 to 2020, and (2) assess the accuracy and performance of this method against two-band (2BDA) and three-band (3BDA) algorithms.

The remainder of this chapter is sectioned into four sections. Section 1.1 provides a historical overview of the Salton Sea, including how the modern-day Salton Sea was formed. Section 1.2 discusses the motivations behind this work, including the need for more extensive data collection within this waterbody. Section 1.3 provides a general overview of the

methodology that was implemented within the study. Lastly, section 1.4 outlines how the remainder of the remainder of the thesis is structured and formatted.

1.1. Salton Sea Overview

The Salton Sea is an inland body of water that is situated in Southern California, approximately 35 miles north of the US-Mexico border and 32 miles south of the Coachella Valley (Figure 1) (Cohen, Morrison, and Glen 1999; Doede and DeGuzman 2020). The waterbody has a maximum depth of 51 feet and a surface area of 340 square miles (Cohn 2000; King et al. 2011; Tompson 2016). The closed basin is bounded by multiple mountain ranges, including the Santa Rosa, Chocolate, Peninsular and Orcopia mountains (Tompson 2016).

Geologically, the Salton Sea lies 200 feet below sea level and atop the Salton Trough (ST). The ST is a rift valley formed along the San Andreas fault that is filled with high tectonic activity (Cohen, Morrison, and Glenn 1999). The movement of the Pacific and North American plates have formed local geothermal hotspots around the Salton Sea. These hotspots can exceed 680 degrees Fahrenheit in depths greater than 8,000 feet (Ajala et al. 2019; Tompson 2016). Multiple earthquakes have been documented within the region, the largest occurring within El Centro in 1940 and measuring 7.1 on the Richter scale (Cohen, Morrison, and Glenn 1999). The ST also lays above a deeper underground sink that extends more than 20,000 feet and is composed of alluvial deposits (Cohen, Morrison, and Glenn 1999). In 1997, the volume of groundwater was estimated to range between 1.1 to 1.3 billion acre-feet (Tompson 2016). The water remains inaccessible owing to its high depth and salinity levels (Tompson 2016).

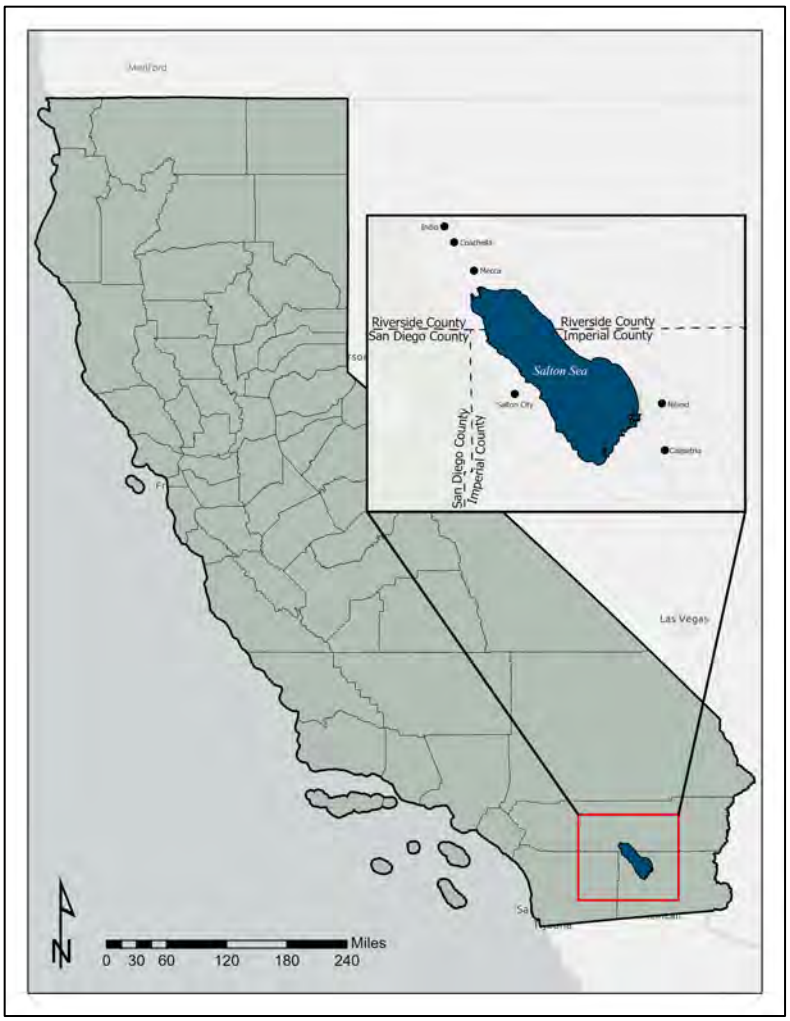

Figure 1. Salton Sea vicinity

Historically, the Colorado River periodically inundated parts of the Salton Sink, also called the Salton Basin, and creating a vast, intermittent lake. The ancient Lake Cahuilla had a surface area of approximately 2,200 square miles and an estimated evaporation rate of 1.52 to 2.05 meters per year (Waters 1983). When left undisturbed, the lake would take approximately 47 to 64 years to evaporate completely (Laylander 1997; Rockwell, Meltzner and Haaker 2018). Through the examination of historical records dating between 1774 and 1750, researchers confirmed this timeframe as the last time the Colorado River had naturally streamed into the ST. Expedition records dating between 1771 and 1776 confirmed the absence of the lake in later

years due to the high heat caused by the desert climate (Cohen 2019; Rockwell, Meltzner and Haaker 2018). Despite this arid climate and limited supply of irrigated water, the Salton Basin has a prolonged history of human settlement that dates back 12,000 years, including modern-day Torres Martinez Desert Cahuilla Indians and the Cabazon Band of Mission Indians (Cohen, Morrison, and Glenn 1999; Cohn 2000; Delfino 2006). Native American groups were able to reside and prosper within this dry climate due to the availability of fish and respite the recurrent bodies of water brought forth.

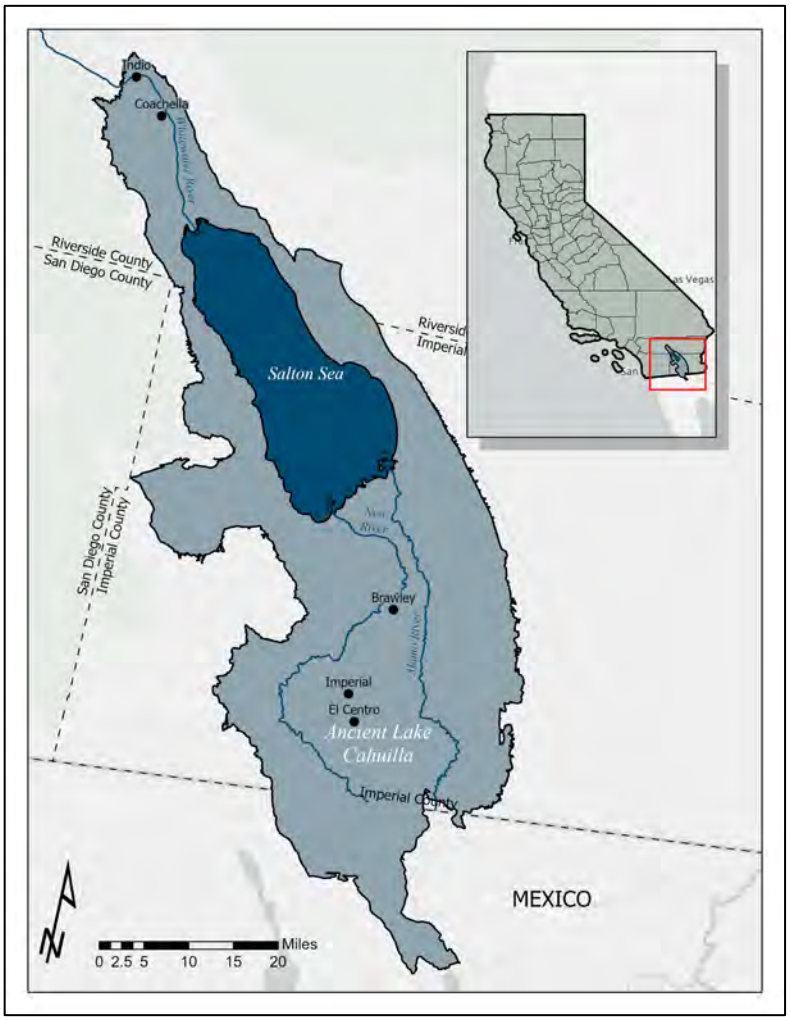

Figure 2. Ancient Lake Cahuilla

The expansion of irrigation within the region commenced in 1901 with the construction of a massive canal system. The $150,000 investment by George Chaffey to the California Development Company was used to build irrigation canals that would facilitate the transfer of water deposits from the Colorado River to the Imperial Valley (Cannon 2022; Kershner 1953). California Development Company had lain the framework of a canal system that required additional enhancements, as the irrigation canals were frequently obstructed by silt and sediments (Cohen, Morrison, and Glenn 1999). During the Winter of 1904 to 1905, the Colorado River experienced heavy rain and snowmelt that resulted in three floods overflowing into the Alamo Canal (Ross 2020). The modern-day Salton Sea was formed between 1905 and 1906 when floodwaters originating from the Colorado River ruptured an irrigation canal in the Imperial County and proceeded to flow into the Salton Sink for 18 months (Cohen 2019; Tompson 2016). At the height of the flooding, nearly 6 billion cubic feet of water was discharged into the Salton Basin (Cohen, Morrison, and Glenn 1999; Kennan 1917).

Despite its rapid formation, the Salton Sea quickly became a critical habitat for migrating birds and an area of interest (AOI) for real estate developers. The Colorado River floods naturally populated the waterbody with fish. In the 1950s, the California Department of Fish and Game introduced additional fish populations, including corina, sargo and croaker fish (Associated Press 2015; Riedel 2016; Sheikh and Stern 2020; Taylor 2018; Tompson 2016). The introduction of additional fish populations and continual water deposits from the Colorado River cemented the Salton Sea as a recreational lake. At its tourism peak, the Salton Sea boasted more visitors than the Yosemite National Park, including celebrity guests Frank Sinatra and the Beach Boys (Clouse 2016; Gutierrez 2009; Picone 2021; Vizzo 2017). All these activities pointed to a thriving tourist site that could serve as a sister location to the Palm Springs area. By the 1990s,

an evident decline in fish populations pointed toward a deteriorating environment caused by the declining WQ in the Salton Sea.

Throughout most of the 20th century, Salton Sea water levels were maintained through water deposits originating from the Colorado River and agricultural drainage from surrounding agricultural communities. The modern-day Salton Sea would have followed the same evaporation trajectory as Lake Cahuilla had it not been designated by President Coolidge as an agricultural sump in 1924 (Cohen 2019). Toward the end of the 1990s, the State of California was pressured by Wyoming, Utah, Colorado, Nevada, New Mexico Arizona, and the Federal government to decrease water consumption originating from the Colorado River (Cohen 2019). The Colorado River is the largest provider of water to California, as it supplies more than 60 percent of the water used by the Southern California region, see Figure 3 (Forsman 2014). The Law of the River annually allocates California around 4.4 million acre-feet of water and this base allotment was exceeded between 1983 and 1996 (Cohen, Morrison, and Glen 1999; Forsman 2014). The State of California had taken advantage of apportionments that went unused by other states and was consequently instructed by the Secretary of Interior to develop a plan to reduce Colorado River water consumption.

In 2003, Coachella Valley Water District, Imperial Irrigation District, San Diego County Water Authority, and the Metropolitan Water District of Southern California mutually signed the "Quantification Settlement Agreement" (QSA) that diverted Colorado River water resources from the Salton Sea to the San Diego County (Tompson 2016; Forsman 2014; Cohen, Morrison, and Glenn1999). Colorado River water deposits into the Salton Sea decreased by 10 percent and completely halted in 2018 (Levers, Skaggs, and Schwabe 2019). Prior to the QSA, the Salton Sea was already experiencing high levels of salinity due to the evaporation of water and

concentrations of salt. As a terminal lake, the Salton Sea does not have any physical outlets and loses water volume through evaporation. An estimated 1.35 million acre-feet of water were deposited annually into the Salton Sea to maintain water levels, 75 percent of which stems from agricultural drainage (Cohen, Morrison, and Glenn 1999).

Figure 3. Colorado River basin

According to the Imperial Irrigation District, the Salton Sea basin can experience temperatures exceeding 100 degrees Fahrenheit and generate conditions that allow for high annual evaporation rates. Roughly 1,300,000 acre-feet of water evaporates annually from the Salton Sea and scholars predict this amount will increase with ongoing climate changes,

primarily due to the effects of increasing drought episodes and decreasing precipitation rates (Cohen, Morrison, and Glenn 1999; Marshall 2017). Figure 4 illustrates precipitation rates within the Salton Sea between 1914 to 1994. The average annual precipitation rate of three inches per year are too low to offset the annual evaporation rate of five feet per year (Cohen, Morrison, and Glenn 1999; Hughes 2020). The reduction in contributing water resources and increased dependence on agricultural runoff has led the waterbody to shrink in size and experience poor WQ effects which impact wildlife and surrounding communities. In 2020, the State of California ceased WQ monitoring in the Salton Sea, and it has since become the responsibility of local agencies and non-profit organizations to continue assessing its WQ.

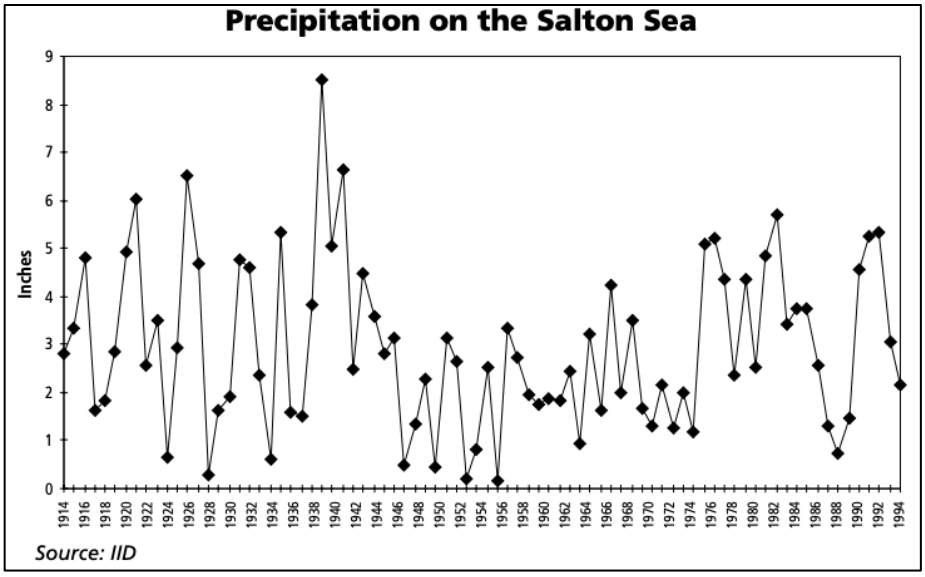

Figure 4. Precipitation on the Salton Sea between 1914 to 1994. Source: Cohen et al. 1999

1.2. Motivations

Interest and motivation for this research project stems from the unique circumstances that have led to the decline in the overall WQ of the Salton Sea and the complex dynamics that stem from the Coachella and Imperial valley regions.

1.2.1. Human Health

In combination with lower precipitation rates, the QSA has accelerated the shrinking of the Salton Sea and increased exposure to lakebed sediment (Parajuli and Zender 2018). The Salton Sea has served as a reservoir for agricultural runoff and the exposed lakebed sediment is enriched with pesticides that date back to the 1930s, such as dichlorodiphenyltrichloroethane and aldrin (Kim, Kabir, and Jahan 2017). The health and well-being of communities surrounding the Salton Sea is of great importance, especially when they have historically been inhabited by underserved population groups. In 1970, 57 percent of the total population in Imperial Valley self-identified as White and 36 percent identified as Hispanic (Mead 2016). By 2010, the Imperial Valley boasted a population of 180,000 and 74 percent of the population identified as Hispanic.

Farzan et al. (2019) also determined that communities situated within close proximity to the Salton Sea had a higher percentage of asthma prevalence among children (22.4%) than other communities in the United States (US) (8.4%). This occurrence was largely associated to the receding lakebed that resulted in approximately 40 to 80 tons of dust being released into neighboring areas. The small particulates originating from the lakebeds are miniscule and easily respirable by humans, consequently affecting the respiratory health of people in nearby communities.

1.2.2. Lack of State Action

In recent years, the State of California has encountered a lot of criticism surrounding their lack of organized efforts to address and improve the ongoing conditions of the Salton Sea. The state has held multiple meetings and considered various proposals to identify a sustainable management plan that will address rising concerns. In 2018, the State of California released a 10-

year management plan centered on aquatic habitat restoration and dust suppression around the edge of the Salton Sea. Although this initiative is a step forward, the plan is centered around smaller areas and does not address the overarching dilemma of poor WQ. In order to propose any larger scale mitigation efforts, there is a need for WQ data to be accessible. At the moment, WQ assessments are predominately performed at onsite locations and require a large workforce to collect water samples. Since January 2020, the State of California, and Bureau of Reclamation (BoR) have ceased WQ monitoring of the Salton Sea. Local entities and non-profit organizations have taken it upon themselves to perform WQ assessments and fill the gap left by these government agencies.

1.2.3. Economic Development

Since 2018, the State of California has held multiple discussions regarding the possibility of extracting lithium mineral from the Salton Sea Basin. In March 2020, the California Energy Commission released a report that outlined the proposed project and stated this venture would produce nearly 600,000 tons of lithium per year that could result in $7.2 billion project (Ventura 2020). The demand for lithium-ion batteries has increased since 2008 due to their use within electric vehicles and power grids (Agusdinata et al. 2018). The State of California recently passed a law that would require all sales of passenger vehicles within the state to be electric vehicles by 2035. Beyond California, it is estimated that the global demand of lithium will steadily increase and exceed the resources available by 2025 (Wanger 2011).

At the time of writing this thesis, the California Energy Commission is requesting bid proposals from companies to determine the best approach in extracting lithium using geothermal technology which may reduce some environmental impact; however, many environmentalists have already expressed major concerns (Gammon 2022). Most of the environmental impacts are

centered on polluting water sources, increasing carbon dioxide emissions, and creating a water table reduction that may lead to a drier lakebed in the Salton Sea.

1.2.4. Gap in Current Literature

The study will help build upon progress made within the spatial sciences, as it explores the application of NDCI in assessing chlorophyll-a concentration using Landsat 5 Thematic Mapper (TM) and Landsat 8 Operational Land Imager (OLI) imagery. The NDCI has been assessed using Landsat 8 OLI imagery, but studies have not incorporated Landsat 5 TM to conduct a temporal analysis. The study also creates a framework that can be reproduced across other bodies of water and across different temporal ranges. The research benefits local community members by highlighting shrinkage rates and poor WQ in the Salton Sea. Moreover, the study aims to address a scientific gap in the literature surrounding WQ within the Salton Sea. The majority of the current literature in the Salton Sea is centered on salinity levels and the rate in which the body of water is shrinking. Very few studies attempt to apply semi-empirical indices to assess WQ parameters. Lastly, the results of this study and studies alike can aid local agencies in assessing the Salton Sea and inform policy.

1.3. Methodological Overview

The methodology adopted in this study can be segmented into three different sections. The first section consisted of evaluating peer-reviewed articles to identify common trends and methodologies used to assess chlorophyll-a concentrations within inland bodies of water. Upon analyzing the literature, semi-empirical modeling methods were deemed suitable for conducting temporal analysis of chlorophyll-a concentrations in the Salton Sea. Semi-empirical indices, such as the NDCI, are useful since they can be reproduced and compared across different bodies of water and temporal ranges. In the second section, the study focused on the application of the

NDCI across the Salton Sea. This step entailed the use of Landsat 5 TM and Landsat 8 OLI imagery to capture the selected temporal range (2002 to 2020). The third section assessed the accuracy and performance of the NDCI by running multiple linear regressions against other notable two-band (2BDA) and three-band (3BDA) algorithms. The 2BDA and 3BDA were selected based on peer-reviewed articles that demonstrated comparable or better results than the NDCI in assessing chlorophyll-a presence using Landsat imagery.

1.4. Thesis Overview

The thesis is comprised of five organized chapters. Chapter 2 provides a comprehensive literature review of related work centered on WQ assessments, remote sensing (RS) modeling approaches and RS indices for WQ assessments. Chapter 3 describes the data sources and provides an overview of the methodology adopted within the study. Chapter 4 summarizes the findings from the adopted methodology and applied analysis. Lastly, Chapter 5 discusses the results, identifies limitations of the study and outlines future work.

Chapter 2 Literature Review

In this chapter, a survey of the literature related to traditional sampling methods, RS imagery in WQ assessments, WQ parameters and RS data is presented. The findings of the literature were used to inform the methodology and the direction of the overall study.

2.1. Traditional Water Quality Monitoring and Assessment Methods

Water shortages and low precipitation rates have historically been documented by early civilizations and have contributed to the adoption of water management practices aimed at preserving water resources (Behmel at al. 2016; Neary, Ice, and Jackson 2007). In the 20th century, the concept of water management gained renewed interest owing to population growth and limited access to natural resources. In 1972, the US enacted the Clean Water Act, which regulated the discharge of pollutants into US waterbodies and established WQ standards (Keiser and Shapiro 2019). In 1992, the United Nations Earth Summit introduced the Integrate Water Resource Management (IWRM) process to participating nations (Saravanan, McDonald, and Mollinga 2009; Savenije and Van der Zaag 2008). IWRM is a framework that promotes equitable and sustainable approaches to managing water and land resources. Savenije and Van der Zaag (2008) state that there is an emerging consensus on IWRM and water management necessitating an integrated approach, but there remain some issues that are unresolved. Biswas (2008) analyzes existing literature surrounding IWRM and identified 41 components that would need to be integrated to water resource management, including WQ, water demand, economic factors, ground water estimates, municipal water activities and land related issues. Although Biswas (2008) disputes the ability for this approach to be truly implemented there has been an increase in Water Quality Management Plans (WQMPs) within the past thirty years.

WQPMs are long-term programs designed to monitor aquatic environments, in order to better respond to emerging problems and assess developing water trends (Behmel et al. 2016; Bartram and Ballance 1996). WQPMs require standardized WQ assessments and continual evaluation of all monitoring activity. Behmel at al. (2016) and Strobl and Robillard (2008) outline eight different elements necessary for the implementation of WQMPs. These include (1) identifying program objectives, (2) determining location of sampling sites, (3) selecting relevant WQ parameters, (4) defining sampling frequencies, (5) calculating necessary human and fiscal resources, (6) establishing logistics and quality control checks, (7) launching data distribution platform and (8) assessment on use of public data distributed. Madrid and Zayas (2007) concur on the importance of these elements, but also include sampling as an additional element.

Madrid and Zayas (2007) also highlight the importance of maintaining sampling equipment, following post sampling procedure and maintaining clear record-keeping of samples collected. Figure 5 illustrates the various processes and considerations associated with collecting a water sample. WQ assessments are an integral part of WQPMs and consist of both data collection and data analysis processes. Traditional WQ assessments predominately use water sampling as part of their data collection process in combination with laboratories to conduct measurements of the collected samples. According to Madrid and Zayas (2007), water samples must abide by strict processing requirements to maintain the integrity of specimen and ought to be representative of the environment being evaluated. There are two kinds of water sampling approaches concerning the time a sample is collected, discrete and composite samples (Cassidy et al. 2018; Matamoros 2012). Discrete or grab samples are single samples collected within a single container. These types of samples represent the chemical composition of the waterbody at a given time and place and are primarily used when temporal considerations are not of

importance. In contrast, composite samples consist of multiple samples collected within 24 hours and combined within a single container.

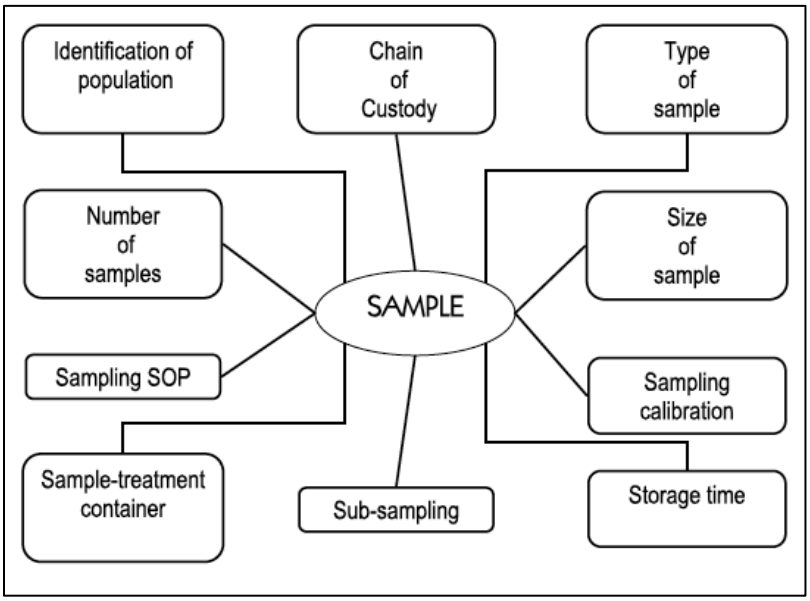

Figure 5. Sampling plan. Source: Madrid and Zayas 2007

Traditional water sampling methods for chemical pollutants include spot, instrumental and extraction sampling (Cassidy et al. 2018; Madrid and Zayas 2007). Spot or bottle sampling is a peer-reviewed method that has been widely adopted for governing and legislative efforts (Madrid and Zayas 2007). Spot sampling consists of individuals taking manual water samples at onsite locations using a bottle to extract the water. This approach is predominately used within surface waters, as individuals would be required to be onshore or on a boat. To ensure there is minimal cross contamination, the bottle is rinsed multiple times with the surface water prior to collecting the final sample (EPA 2017; Madrid and Zayas 2007). After the water sample has been extracted, the water undergoes instrumental analysis within a laboratory or onsite location. Water samples transported to laboratories are stored within a cooler at 4 to 6 degrees Celsius to ensure the temperature does not breakdown the contaminants during transit (EPA 2017). To

extract water samples from waters that exceed 0.5 meters, the bottle is open upon entry and lowered to the desired depth using a rope or cable (Madrid and Zayas 2007).

Although conventional sampling methods have become the norm within WQMPs, they have discernable limitations. Spot sampling can be categorized as being discrete, as it consists of taking a singular water sample at a given location and time (Cassidy et al. 2018; Matamoros 2012). This approach fails to reflect intermittent contamination and can be susceptible to quality control errors (Gagnon et al. 2007; Madrid and Zayas 2007). Because traditional sampling methods are conducted manually, they require high financial and human resources that limit the frequency of testing and the number of sampling sites. There are also concerns on the type of instruments that are used to measure water samples, given that they can vary across long-term programs and between laboratories. Schaeffer et al. (2013) and Madrid and Zayas (2007) agree that WQMPs should adopt novel approaches and emerging tools to conduct water monitoring. Some of these new approaches include using onsite sensors, RS imagery and online monitoring systems.

2.2. Water Quality Parameters

This section outlines different WQ parameters that are of importance to any WQ assessment. WQ is a measurement that allows us to determine the chemical, biological and physical characteristics of water in order to assess any degradation on WQ. These measurements allow the assessment of degradation on WQ. WQ indicators can be further categorized into subgroups, including chemical (e.g., dissolved oxygen, pH, organic compounds, and nutrients), biological (e.g., algae and bacteria), physical (e.g., temperature, turbidity, clarity, color, and salinity), and other (odor, color, and floating material). These subgroups are important to differentiate, as

screening tests will vary according to the selected WQ parameter and the overall objective of the study (Gholizadeh, Melesse, and Reddi 2016; Gorde and Jadhav 2013; Usali and Ismail 2010).

Stakeholders and local agencies have an avid interest in identifying WQ parameters that are best suited for a given body of water, as they are often adopted and standardized within local WQMPs. The selection of WQ parameters is dependent on the conditions surrounding the AOI and publications released. Multiple studies have been conducted around the Salton Sea to determine its physical and chemical compositions. Local and state agencies have equally conducted their own assessments, yet much of the data and findings remains unpublished (Holdren and Montano 2002). The earliest publication conducted on the Salton Sea regarding WQ dates back to the MacDougal publication of 1907. The journal examined major ion compositions including sodium chloride, magnesium chloride, magnesium sulphate, potassium sulphate, calcium sulphate, magnesium sulphate and calcium carbonate against other sources of sea water and determined high levels of salinity within the Salton Sea (Holdren and Montano 2002; MacDougal 1907). Publications thereafter centered on the concentrations of nutrients, metals and pesticides and have contributed to local WQMPs and WQ parameter selections.

2.2.1. Suspended Sediments

The US Environmental Protection Agency defines “suspended sediments” as fine inorganic specks of silt and clay that measure less than 0.063 millimeters. Also included are fine sands between 0.63 to 0.25 millimeters and other grainy matter found within the water column (Droppo 2001; Spehar, Taylor, and Cormier 2002). According to Ritchie, Zimba and Everitt (2003), suspended sediments are the most common water pollutant within the surface of freshwater systems. Traditional water assessments measure concentrations of suspended sediment by collecting water samples and transporting them to labs.

2.2.2. Chlorophyll and Algae

Chlorophyll is a green pigment and natural compound that allows plants to absorb sunlight and undergo photosynthesis (EPA 2022; Ritchie, Zimba, and Everitt 2003). There are two types of chlorophyll: chlorophyll-a and chlorophyll-b. Chlorophyll-a is the primary pigment of photosynthesis and it absorbs orange and violet light between 430 to 660 nanometers (Martin 2019). Chlorophyll-b is an accessory pigment that absorbs light between 450 to 650 nanometers. This pigment is not always present within the photosynthesis process and will pass absorbed light to the primary pigment (Martin 2019). Chlorophyll-a is often used as an indicator of algae growth and has been adopted in WQ assessments to manage eutrophic bodies of water. Eutrophication refers to high concentrations of nutrients in a lake, river or other bodies of water (Ansari et al. 2010; Dorgham 2014; Lin et al. 2021; Qin et al. 2013). Algae are native to freshwater systems, but excessive amounts result in high plant-life density and occasionally dead oxygen zones or loss of aquatic life (Ansari et al. 2010; Bhateria and Jain 2016; EPA 2022; Dorgham 2014).

2.2.3. Temperature

Temperature is a physical WQ indicator that measures the thermal energy of a constituent. Thermal energy is the movement of molecules and atoms and can be transmitted between constituents as heat (Ling et al. 2017; Raman et al. 2017; Verones et al. 2010). The transfer of heat to water bodies can occur by means of natural phenomena or human activity; excessive amounts are thermal pollution (Bhateria and Jain 2016; Raman et al. 2017; Ritchie et al. 2013). Outside of measuring thermal energy, high temperatures can decrease dissolved oxygen levels and regulate the type of aquatic species that reside in a river or lake (Bhateria and Jain 2016; Vasistha and Ganguly 2020).

2.2.4. Salinity

Salinity is a physical WQ indicator that measures dissolved salt concentrations in a waterbody (EPA 2022b; Wang and Xu 2012). Salt originates from three main sources: (1) evaporated ocean water, (2) landscape weathering and (3) other environmental settings, such as drainage water and road salts (Dailey, Welch, and Lyons 2014; Obianyo 2019; Nielsen et al. 2003). Small quantities of water are suitable for aquatic life and plants, but higher amounts negatively affect the viability of eggs and marine plant seeds (Nielsen et al. 2003). Compared to oceans, inland waters have lower salinity levels and higher variations in salinity due to seasonal water deposits, evaporation rates and precipitation frequency (Gholizadeh et al. 2016). Hua (2017) performed a WQ assessment on the Malacca River in Malaysian and determined that high salinity pollution resulted from pesticide usage in nearby rubber and oil plantations. This study echoes numerous studies conducted around the Salton Sea, which conclude that salinity pollution was largely attributed to pesticide usage and nearby agricultural practices (Bradley et al. 2022; Cohen 2019; Gao et al. 2022).

2.3. Water Quality and Remote Sensing

Multiple academic studies have reported on the effectiveness of using RS techniques and tools to better monitor WQ (Madrid and Zayas 2007; Schaeffer et al. 2013; Usali and Ismail 2010). RS as process for obtaining information on an object, AOI or through the use of satellites and sensors that are able to measure reflected and emitted radiation (Gholizadeh, Melesse, and Reddi 2016; Usali and Ismail 2010). In the past decades, there have been advancements in sensors, satellites and modeling approaches used in WQ assessment. The following subsections explore these topics further.

2.3.1. Sensors and Satellites Used for Water Quality Assessments

Technological advancements and public-facing NASA missions have made RS imagery readily available. However, it has not been commonly incorporated into WQ assessments and overarching WQMPs. The selection of RS imagery for water assessment is largely dependent upon the satellites and their associate multispectral sensors; other factors to consider include temporal range and spatial resolution. RS sensors measure the physical properties of an object or environment through the emission of heat, radiation, sound, light or motion (Gholizadeh, Melesse, and Reddi 2016; Sanderson 2010; Zhu et al. 2018).

Sensors can be categorized into two broad categories, airborne and spaceborne sensors. Airborne sensors are mounted on aircrafts (i.e., helicopters, balloons, or aircrafts) and were first introduced in 1859 when Gasper Felix Tourmachon captured the first aerial image of Paris on a hot air balloon (Waghmare and Suryawanshi 2017; Zhu et al. 2018). Aerial sensors are flexible instruments better suited for smaller waterbodies, as they require smaller pixel sizes (Gholizadeh, Melesse and Reddi 2016). Costs associated with airborne data can drastically increase as the surface area increases—standard cost of 350 dollars per square mile—and is one of the main impediments within its broader application in WQ assessments (Chipman, Olmanson, and Gitelson 2009; Gholizadeh, Melesse, and Reddi 2016).

Spaceborne or satellite sensors are aboard spacecrafts and satellites orbiting the earth's atmosphere (Gholizadeh, Melesse and Reddi 2016; Roy, Behera and Srivastav 2017). Satellite-derived data have lower associated costs and are more readily available, given fixed revisiting time frames. In terms of spatial resolution, satellite data tends to be coarse to moderate and ranges between 30 to 120 meters. Table 1 contains common spaceborne sensors and satellites used in WQ assessments, such as SPOT-5, MODIS, Landsat, Terra and Sentinel 2. Table 1 was compiled based on data from Gholizadeh, Melesse and Reddi (2016) and this literature review.

Table 1. Common Spaceborne Satellites Used in Water Quality Assessments

Satellite	*Sensor*	*Launch Year*	*Spectral Bands (mm)*		*Spatial Resolution (m)*	*Swath Width (km)*	*Revisit Interval (Days)*
Landsat 5	Thematic Mapper (TM)	1984	Band 1: 0.45 - 0.52 Band 2: 0.52 - 0.60 Band 3: 0.63 - 0.69 Band 4: 0.77 - 0.90	Band 5: 1.55 - 1.75 Band 6: 10.40 - 12.50 Band 7: 2.09 - 2.35	30 m 30 m	185 km	16
Landsat 5	Multispectral Scanner (MSS)	1984	Band 4: 0.5 - 0.6 Band 5: 0.6 - 0.7 Band 6: 0.7 - 0.8 Band 7: 0.8 - 1.1		60 m	185 km	18
Landsat 7	Enhanced Thematic Mapper Plus (ETM+)	1999	Band 1: 0.45 - 0.52 Band 2: 0.52 - 0.60 Band 3: 0.63 - 0.69 Band 4: 0.77 - 0.90	Band 5: 1.55 - 1.75 Band 6: 10.40 - 12.50 Band 7: 2.09 - 2.35 Band 8: 0.52 - 0.90	15 m 30 m 60 m	183 km	16
Landsat 8	Operational Land Imager (OLI) and Thermal Infrared Sensor (TIRS)	2013	Band 1: 0.43 - 0.45 Band 2: 0.45 - 0.51 Band 3: 0.53 - 0.59 Band 4: 0.64 - 0.67 Band 5: 0.85 – 0.88 Band 6: 1.57 – 1.65	Band 7: 2.11 - 2.29 Band 8 : 0.50 - 0.68 Band 9: 1.36 - 1.38 Band 10: 10.60 - 11.19 Band 11: 11.50 -12.51	15 m 30 m 100 m	170 km	16
Sentinel 2	Multi-Spectral Instrument (MSI)		Band 1: 0.43 - 0.45 Band 2: 0.45 - 0.52 Band 3: 0.54 - 0.57 Band 4: 0.65 - 0.68 Band 5: 0.69 - 0.71 Band 6: 0.73 - 0.74 Band 7: 0.77 - 2.29	Band 8: 0.78 - 1.38 Band 8A: 0.85 - 0.87 Band 9: 0.93 - 0.95 Band 10: 1.36 - 1.39 Band 11: 1.56 - 1.65 Band 12: 2.1 - 2.28	10 m 20 m 60 m	290 km	10
SPOT - 5	HRG	2005	Band 1: 0.50 - 0.59 Band 2: 0.61 - 0.68 Band 3: 0.78 - 0.89 Band 4: 1.58 – 1.75		2.5 m 5 m 10 m 20 m	60 km	2 - 3
Terra	Moderate Resolution Imaging Spectroradiometer (MODIS)	1999	Bands 1 to 19: 0.40 - 2.15 Bands 20 to 36: 3.66 - 14.28		250 m 500 m 1000 m	2330 km	1 - 2

2.3.2. Remote Sensing Modeling Approaches

The use of RS imagery in WQ dates to the 1970s with the work of Ritchie et al. (1974). The study focused on the use of RS techniques to identify and estimate the presence of suspended sediment within six Mississippi reservoirs (Ritchie et al. 1974; Usali and Ismail 2010). The study resulted in the following empirical equation:

$$Y = A + BX \quad \text{or} \quad Y = AB^X \tag{1}$$

where Y is the RS measurement (i.e., reflectance, energy, radiance), X represents the WQ parameter and A and B are empirically derived factors (Ritchie, Zimba, and Everitt 2003). This empirical equation was then adopted by other researchers to examine various WQ parameters such as suspended matter, algae, and temperature. Beyond the development of empirical equations, RS techniques have continued to evolve and now include semi-empirical, analytical and semi-analytical models. These models are bio-optical algorithms that determine the concentration of nutrients using both optical qualities and in-situ WQ parameter measurements (Topp et al. 2020).

Empirical models remain the most common RS approach, as it involves fitting a linear regression between in-situ WQ measurements and spectral bands (Topp et al. 2020; Wang and Yang 2019). These models are highly dependent on the availability of in-situ data to validate the accuracy of the model and are rarely used across large temporal and spatial resolutions (Wang and Yang 2019). Gholizadeh, Melesse and Reddi (2016) argue that empirical models are not suited for all WQ parameters, especially those that rely on multispectral sensors that can yield ambiguous results. For example, researchers have long debated on the use of empirical methods to assess chlorophyll-a concentrations. Existing spectral satellites have difficulty differentiating between suspended sediments and chlorophyll-a spectral signals when large amounts of

sediments are present within eutrophic bodies of water. Wang and Yang (2019) conducted a literature review of current research using RS techniques for WQ assessments in China and determined that chlorophyll-a was the highest WQ indicator examined using empirical models. Figure 6 illustrates the number of publications for different indicators among different model types.

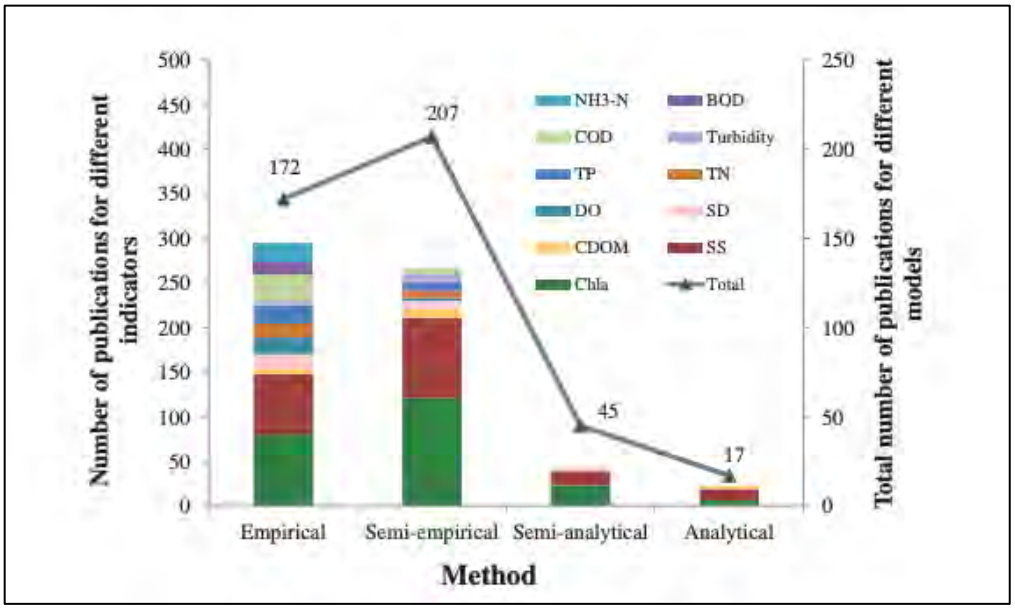

Figure 6. Modeling methods used in remote sensing. Source: Wang and Yang 2019

In contrast, semi-empirical methods use spectral band index values rooted in physical measurements to retrieve WQ parameters from RS imagery (Lednicka and Kubacka 2022; Mejia Avila, Torres-Bejarano, and Martinez Lara 2022; Topp et al. 2022). These models are designed to augment the spectral properties of the WQ indicators and reduce noise from other parameters. Since semi-empirical models are based on physical properties, model users are expected to have prior knowledge of sensors, spectral bands, and inherent optical properties (IOPs) to select appropriate RS imagery (Topp et al. 2022). IOPs are the scattering and absorption characteristics of water and suspended material (Lee 2006). Semi-empirical models are low cost and can be easily reproduced across different spatial and temporal scales (Mejia Avila, Torres-Bejarano and

Martinez Lara 2022). Wang and Yang (2019) and Topp et al. (2022) identified chlorophyll-a, suspended sediments, turbidity, and cyanobacteria as the most common WQ indicators used in semi-empirical modelling.

Both analytical and semi-analytical models are physics-based. They determine WQ concentrations by modeling surface water reflectance through IOPs of water and atmosphere (Gholizadeh, Melesse, and Reddi 2016; Topp et al. 2022). Analytical approaches are best suited for analyzing features that have distinct absorption values. Hence, they are not suited for measuring dissolved oxygen or suspended sediments whose absorption values can vary. Given that in-situ WQ measurement are used to parameterize semi-analytical models, they are often more accurate and thus more commonly used for assessing in inland bodies of water (Morel and Gordon 1980; Topp et al. 2020). However, due to their complex nature and high data requirements relative to empirical models, analytical models have lower application within WQ assessments (Wang and Yang 2019).

2.3.3. RS and Water Quality Parameters

In this section, an overview of RS techniques used to assess WQ parameters is provided. WQ parameters discussed within this section include suspended sediments, chlorophyll, temperature and salinity.

2.3.3.1. Suspended Sediments

There has been a growing consensus among researchers on the use of RS techniques to monitor suspended sediments. Current sensors and satellites (e.g., Landsat, IRS, and SPOT) are able to detect and quantify their optical signals, including Landsat, IRS, and SPOT (Sherman, Houser and Baas 2013; Usali and Ismail 2010). Because the quantity of signal returned from a sensor is correlated to the surface area of a particle, it can provide rough approximation of

suspended sediment concentrations (Sherman, Houser, and Baas 2013). To determine the optimal wavelength for use, researchers need to monitor in-situ measurements. Many studies have developed distinctive algorithms to establish a relationship between the concentration of suspended sediments and reflectance using in-situ data. However, since the algorithms are rooted in in-situ measurements, they cannot be repurposed for different bodies of water or even within large temporal scales for the same water body. Despite variance between studies, wavelengths between 700 and 800 nanometers have appeared to be the most effective in capturing suspended sediments (Ritchie, Zimba, and Everitt 2003; Usali and Ismail 2010). Figure 7 illustrates the relationship between reflectance and wavelength, as affected by the varying concentration levels of suspended sediments (Ritchie, Zimba, and Everitt 2003).

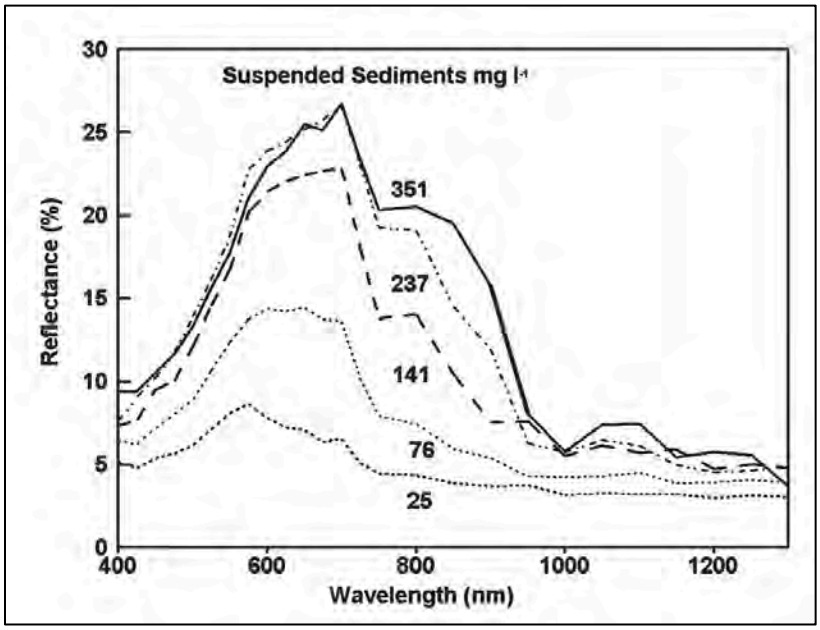

Figure 7. Relationship between wavelength and reflectance for suspended sediment concentrations. Source: Ritchie, Zimba, and Everitt 2003

2.3.3.2. Chlorophyll

Wang and Yang (2019) consider chlorophyll-a as the most studied WQ indicator in inland bodies of water and claim it is widely assessed across all RS models. In contrast,

Brezonik, Menken and Bauer (2005) and Ritchie, Zimba and Everitt (2003) claim most RS studies employ empirical models centered on the relationship between chlorophyll and reflectance values. Chlorophyll-a absorptions occur at shorter wavelengths, between 450 to 475 nanometers and between 650 to 680 nanometers (Ritchie, Zimba, and Everitt 2003). Figure 8 illustrates the relationship between wavelength and reflectance for differing chlorophyll concentrations. However, researchers are in agreement that existing satellites, such as SPOT and occasionally Landsat, sometimes have limitations to assessing chlorophyll concentrations. Strong signals emanating from suspended sediments can block chlorophyll-a reflectance. This occurrence is more prominent in bodies of water with low water volume and small surface areas.

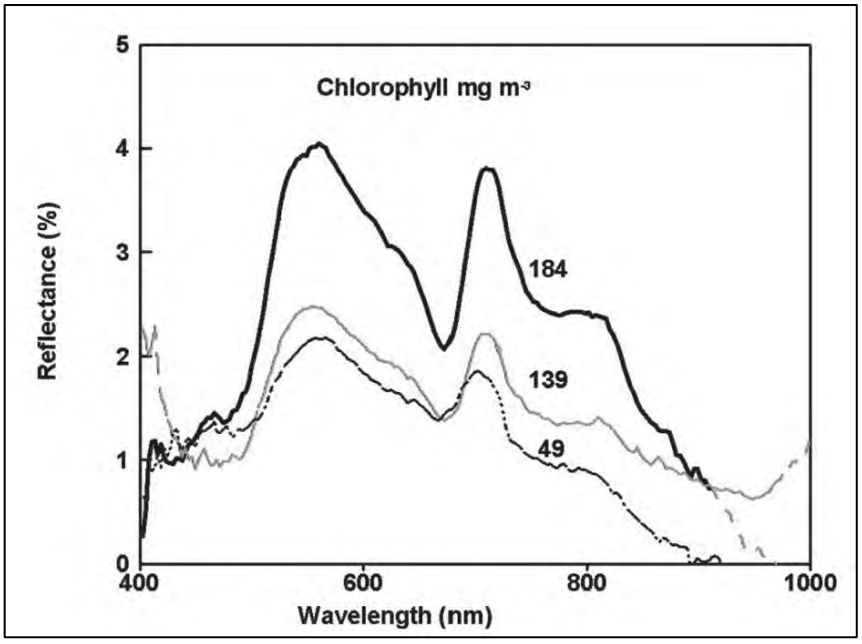

Figure 8. Relationship between wavelength and reflectance for chlorophyll concentrations. Source: Ritchie, Zimba, and Everitt 2003

2.3.3.3. Temperature

In RS studies, researchers employ thermal sensors aboard planes or rely on satellite imagery from MODIS and Landsat to measure temperature (Gholizadeh, Melesse, and Reddi 2016; Ritchie, Zimba, and Everitt 2013). Thermal infrared data incorporates middle wavelengths

ranging between 3 to 5 micrometers and long infrared wavelength ranging between 7 to 14 micrometers (Scafutto and de Souza Filho 2018; Wu et al. 2019).

2.3.3.4. Salinity

Similar to other WQ indicators, RS techniques can assist in monitoring water salinity using microwave wavelengths. Salinity is correlated with water conductivity. Changes in conductivity can be captured through microwave radiations (Lewis and Perkin 1978; Vinas 2012). Gholizadeh, Melesse and Reddi (2016), Ramadas and Samantaray (2018), Wang and Xu (2012), and Vinas (2012) identified numerous RS satellites suited for salinity, including Landsat, Aquarius, SEASAT and SMOS.

2.3.4. Remote Sensing Indices

In recent years, the use of semi-empirical methods and spatial indices to assess WQ parameters has increased. A spectral index is an equation that combines pixel values from more than one spectral band in multispectral images (Tran, Reef, and Zhu 2022). Spectral indices are derived from simple band ratios that use adding and subtracting bands to highlight targeted features and reduce environmental effects. Common spatial indices employ normalized difference, in which the band ratio is standardized by the sum of the two bands selected as shown in the following equation:

$$Normalized\ Difference\ = \frac{B_x - B_y}{B_x + B_y} \quad (2)$$

where B_x is the first selected band and B_y is the second selected band. This method ensures that the spatial index layer ranges between -1 and 1. Band ratios without standardization can vary in range and can be difficult to compare among one another.

There is an array of spatial indices that have been developed to highlight water bodies and WQ parameters, while filtering out surrounding landcover. One of the most common is the normalized difference water index (NDWI), which uses two separate equations to identify water in RS imagery. The first equation employs shortwave infrared (SWIR) and near infrared channels (NIR). It was first introduced by Gao (1996) and is expressed as follows:

$$NDWI\ (Gao\ 1996) = \frac{NIR-SWIR}{NIR+SWIR} \quad (3)$$

Gao's NDWI can assess water content within vegetation, as NIR and SWIR have a high correlation with vegetation water content (Gao 1996; Gao et al. 2015; Xu 2006). The second NDWI equation was introduced by McFeeters (1996). It employs NIR and green bands as shown in the following expression:

$$NDWI\ (McFeeters\ 1996) = \frac{Green-NIR}{Green+NIR} \quad (4)$$

McFeeter's NDWI highlights waterbodies by amplifying the reflectance of water using the green band and minimizing the reflectance of NIR seen in vegetation and other landcover types (McFeeters 1996; Xu 2006). This expression produces an index in which water features have high values and non-water feature have low or negative values, see Table 2. The NDWI has been used to extract bodies of water and is especially useful when the water surface area fluctuates through seasons or years.

Table 2. McFeeter's NDWI Pixel Range

Range	*Land use/Landcover Type*
-1.00 to -0.30	Drought, non-water surface
-0.30 to 0.00	Moderate Drought, non-water surface
0.00 to 0.20	Flooding
0.20 to 1.00	Water Surface

Xu (2006) argues McFeeter's NDWI generates positive values for urban-made structures and proposed the modified NDWI (MNDWI). The MNDWI equation uses middle infrared (MIR) and green bands as shown in the following equation:

$$MNDWI = \frac{Green-MIR}{Green+MIR} \quad (5)$$

According to Xu (2006), the MNDWI can generate higher values for waters of bodies, given the MIR's ability to absorb a higher percentage of light than NIR. The MNDWI should also produce lower pixel values for urban areas and structures (Nugroho 2013; Xu 2006). Nugroho (2013) assessed the NDWI, MNDWI and the new water index (NWI) to identify inundated areas within Java Island. The NWI was introduced by Yang et al. (2011) as a method for identifying and extracting bodies of water using the following equation:

$$NWI = \frac{Blue-(NIR+MIR1+MIR2)}{Blue+(NIR+MIR1+MIR2)} \quad (6)$$

Nugroho (2013) concluded that McFeeter's method provided more accurate results when compared against MNDWI and NWI. Similarly, Ali et al (2019) determined the usefulness and accuracy of using NDWI and MNDWI in extracting bodies of water, including those located in urban areas. In contrast, a study conducted by Jiang et al. (2021) determined that NDWI may not be suitable for identifying and extracting waterbodies that are frozen or are extremely large. Despite some reservations, the use of NDWI to extract bodies of water is a continued practice when assessing WQ parameters (Ali et al. 2019; Garg, Aggarwal, and Chauhan 2020; Haibo et al. 2011; Yue et al. 2020).

Aside from water indices used to identify and extract bodies of water, there has been a large development in RS algorithms used to assess WQ parameters, including chlorophyll-a. The majority of RS algorithms for chlorophyll-a have employed red and NIR channels, given that studies have shown blue and green band algorithms show inaccuracies when assessing

inland bodies of water with high turbidity (Mishra, Schaeffer, and Keith 2014). Mishra and Mishra (2012) developed the NDCI using red-edge and red bands as shown in the following equation:

$$NDCI = \frac{Red\ Edge - Red}{Red\ Edge + Red} \quad (7)$$

The spectral index was modeled after the normalized difference vegetation index (NDVI), which was initially introduced by Tucker (1979). The NDCI uses a spectral range that lies between 665 and 708 nm. This maximizes chlorophyll-a sensitivity and addresses several limitations found when using the 748 to 778 nm spectral range (Kamerosky, Cho and Morris 2015; Mishra, Schaeffer, and Keith 2014). The use of band ratio standardization ensures that the NDCI values not only range between -1 and 1, but also address seasonal variability. It was initially assessed using the Medium Resolution Imaging Spectrometer sensor aboard the ENVISAT and has since been tested across different sensors and satellites, including Landsat 8, Sentinel-2 and Worldview-3 (Buma and Lee 2020; Watanabe et al. 2015). Given that not all sensors have the capacity to capture RS imagery utilizing a red-edge band, the formula has been amended in multiple studies. The red edge band has been replaced with the NIR band and essentially models the NDVI as shown in the following equation:

$$Amended\ NDCI = \frac{NIR - Red}{NIR + Red} \quad (8)$$

In the RS community, there is a growing consensus that NDCI estimates chlorophyll-a concentrations more accurately when using Sentinel-2 versus Landsat-8 and WorldView-3 imagery (Beck et al. 2016; Caballero et al. 2020; Karimi, Hashemi and Aghighi 2022; Ogashawara and Moreno-Madrinan 2016). This consensus is largely attributed to the red-edge band that is present within Sentinel-2. However, there have been studies that demonstrate the usefulness of using Landsat imagery to apply NDCI. Buma and Lee (2020) assessed the use of

2BDA, 3BDA, florescence line height (FLH) and NDCI using Landsat 8, WorldView-3 and Sentinel-2 imagery on Lake Chad, Africa. Figure 9 contains the algorithms used to derive chlorophyll-a concentrations in Lake Chad. They determined that the four algorithms had an average R^2 of 0.74 when using Seninel-2 data. The 2BDA had the lowest R^2 value at ($R^2 = 0.60$) and the 3BDA had the highest ($R^2 = 0.95$). This value was in contrast with Landsat 8 that had an overall R^2 of 0.78, a slightly higher R^2 than Sentinel-2 data. The Landsat 8 performance diagnostics also revealed that 3BDA ($R^2 = 0.89$) and NDCI ($R^2 = 0.75$) performed better than 2BDA ($R^2 = 0.71$) and FLH ($R^2 = 0.73$).

Sensor Image	Index	Band Combination
Sentinel-2	2BDA	(band5)/(band4)
	3BDA	(1/band4) − (1/(band5)) x (band8b)
	NDCI	(band5) − (band4)/(band5) + (band4)
	FLH_violet	(band3) − [(band4) + (band2) − (band4)]
Landsat 8	2BDA	(band5)/(band4)
	3BDA	(band2) − (band4)/(band3)
	NDCI	(band5) − (band4)/(band5) + (band4)
	FLH_violet	(band3) − [(band4) + (band1) − (band4)]
WorldView-3	2BDA	(band6)/(band5)
	3BDA	(1/(band5)) − (1/(band6) x (band7))
	NDCI	(band6) − (band5)/(band6) + (band5)
	FLH_violet	(band3) − [(band5) + ((band1) − (band5))]

Figure 9. Algorithms to assess chlorophyll-a concentrations. Source: Buma and Lee 2020

Watanabe et al. (2015) conducted a similar assessment using only Landsat 8 imagery to determine chlorophyll-a concentration within a water reservoir in Brazil. The study examined various two-band and three-band models proposed by literature, including NDCI and the 2BDA performed within the Buma and Lee (2020) study (see Figure 10). Their findings revealed that the NIR-Red, NIR-Green and NIR-Blue ratios generated high R2 values and demonstrated their sensitivity towards detecting chlorophyll-a concentrations. The NDCI had one of the lowest R2 at 0.39, which contrasted greatly with the findings of Buma and Lee (2020). In terms of fitting the models, Watanabe et al. (2015) concluded that all algorithms illustrated satisfactory fits,

however, they underestimated the actual concentrations and were unable to accurately capture the correct trophic state. The NIR-Green ratio had the poorest results and NIR-Red (linear and polynomial) yielded the best fit. Watanabe et al. (2015) states the algorithms may be affected by the trophic state of the water feature and might display better results when used with other bodies of water. Overall, the benefit of continuing to use Landsat imagery to assess chlorophyll-a concentrations centers on its temporal range, given Sentinel-2 only launched in 2015.

Index	a	b	c	R^2	*p*-value
NIR/Red (Linear)	−77.16	925.001	–	0.7537	0.00000
NIR/Green (Linear)	−18.96	1289.84	–	0.6858	0.00000
NIR/Blue (Linear)	−58.90	742.33	–	0.7085	0.00000
NIR/Red (Polynomial)	−120.87	1179.72	−323.81	0.7555	0.00000
NIR/Green (Polynomial)	−149.72	2557.24	−2565.99	0.7085	0.00000
NIR/Blue (Polynomial)	−123.35	1058.23	−335.47	0.7156	0.00000
2B (Linear)	−124.72	213.73	–	0.3910	0.0006
3B (Linear)	71.212	603.15	–	0.5794	0.00001
NDCI (Linear)	53.361	767.2	–	0.3945	0.0006
2B (Polynomial)	−214.41	321.62	−30.63	0.3926	0.0006
3B (Polynomial)	33.95	918.36	−465.68	0.5963	0.00001
NDCI (Polynomial)	56.818	724.88	93.472	0.3946	0.0006

Linear fit $y = a + bx$; polynomial fit $y = a + bx + cx^2$

Figure 10. Algorithms used to assess chlorophyll-a concentrations using Landsat 8 OLI. Source: Watanabe et al. 2015

Chapter 3 Methods

The objective of this study is twofold: (1) use a semi-empirical RS index to perform a temporal analysis of chlorophyll-a presence between 2002 and 2020, and (2) assess the efficacy of the NDCI against 2BDA and 3BDA using linear regressions. Historically, WQMPs have been implemented using traditional WQ assessment methods that require high financial and labor resources. The use of NDCI to assess chlorophyll-a presence can help alleviate some of the resource requirements in WQMPs. The application of NDCI, 2BDA and 3BDA for WQ assessments have been examined in multiple studies and have proven to be comparable with empirical methods (Buma and Lee 2020; Das, Kaur, and Jutla 2021; Mishra and Mishra 2012; Xu et al. 2019a; Xu et al. 2019b).

This chapter summarizes the data and methodologies necessary for performing a temporal analysis of the Salton Sea using the NDCI. Section 3.1 provides a detailed description of the in-situ measurements and RS data sources. Section 3.2 expands on how the two datasets were prepared for use, including data cleaning, coordinate system projections and mosaicking RS imagery. Section 3.3 summarizes the application of NDWI to extract bodies of water and the application of NDCI to view chlorophyll-a presence in the Salton Sea. Lastly, Section 3.4 explains the linear regression assumptions and the application of linear regressions to assess the performance of NDCI against 2BDA and 3BDA. Figure 11 displays a general overview of the methodology.

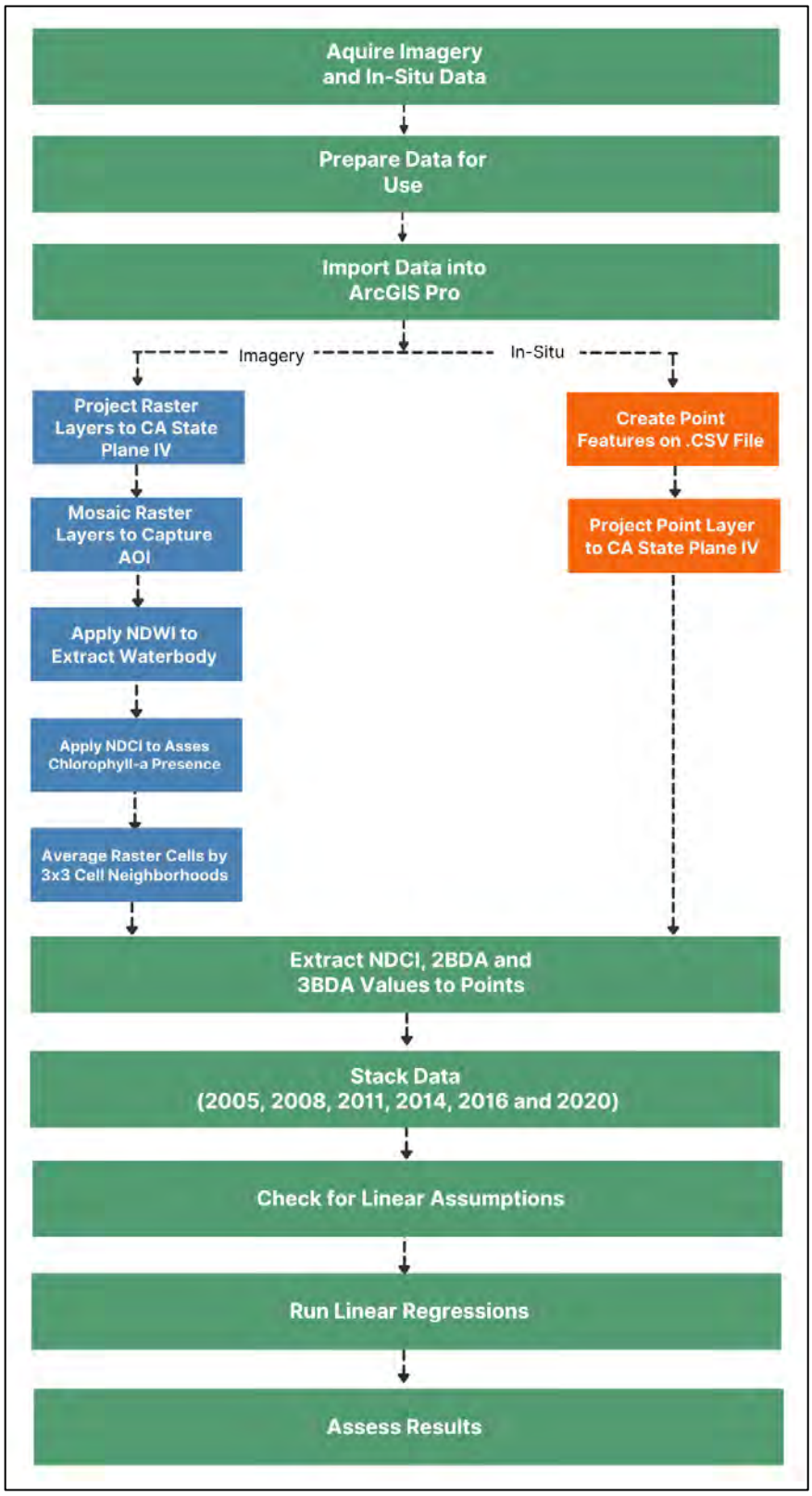

Figure 11. Overview of methodology

3.1. Data Description

The monitoring of WQ within inland waterbodies requires particular consideration to satellite imagery, as cloud coverage and atmospheric radiation can be impediments to assessing surface reflectance. Satellite imagery is the primary data type that is used within the study, while the in-situ chlorophyll-a measurements will serve to assess the use of the NDCI against 2BDA and 3BDA. Table 3 provides a brief overview of the imagery and in-situ data, including short descriptions and source specifics.

3.1.1. Landsat Imagery

The Landsat collection was established in 1972 with the launch of Landsat 1 and was predominantly inspired by the Apollo moon missions that resulted in early land surface images of the Earth (Irons and Dwyer 2010; Williams, Goward, and Arvidson 2006). According to the USGS, the main objective in establishing a RS satellite program was to allow civilians and scientists the opportunity to further explore the natural resources found within the planet (Goward et al. 2006; Loveland and Dwyer 2012). The satellite program was initially met with contention by the Department of Defense, which had concerns regarding near-real time RS data being readily available to the public. From a foreign relations perception, the Department of Defense was apprehensive of openly monitoring other countries without their explicit consent. Ultimately, the RS program was adopted, and it has since become the longest serving satellite program.

Table 3. Datasets Overview reach the velocity necessary to obtain orbit. Amongst all satellites,

Type of Data	***Source***	***Dataset***	***Description***	***Data Format***	***Spectral Resolution***	***Spatial Resolution***	***Temporal Resolution***
Satellite Imagery	United States Geological Survey (USGS)	Landsat 5 TM C2 U.S. Analysis Ready Data (ARD)	Dataset contains satellite imagery spanning from 2002 to 2020 and covers the extent of the Salton Sea. The dataset also has a level 1 processing and provides digital numbers (DN).	GeoTIFF	Band 1: 0.45 – 0.52 mm Band 2: 0.52 – 0.60 mm Band 3: 0.63 – 0.69 mm Band 4: 0.76 – 0.90 mm Band 5: 1.55 – 1.75 mm Band 6: 10.40 – 12.50 mm Band 7: 2.08 – 2.35 mm	30 meters 120 meters	16 - Days
Satellite Imagery	United States Geological Survey (USGS)	Landsat 8 OLI C2 U.S. Analysis Ready Data (ARD)	Dataset contains satellite imagery spanning from 2002 to 2020 and covers the extent of the Salton Sea. The dataset also has a level 1 processing and provides digital numbers (DN).	GeoTIFF	Band 1: 0.43 – 0.45 mm Band 2: 0.45 – 0.51 mm Band 3: 0.53 – 0.59 mm Band 4: 0.64 – 0.67 mm Band 5: 0.85 – 0.88 mm Band 6: 1.57 – 1.67 mm Band 7: 2.11 – 2.29 mm Band 8: 0.50 – 0.68 mm Band 9: 1.36 – 1.38 mm Band 10: 10.6 – 11.9 mm Band 11: 11.50 – 12.51 mm	15 meters 30 meters 100 meters 120 meters	16- Days
In-Situ	United States Bureau of Reclamation (USBR)	Salton Sea Data (2004 to 2020)	Dataset contains satellite imagery spanning from 2002 to 2020 and covers the extent of the Salton Sea. The dataset also has a level 1 processing and provides digital numbers (DN).	.CSV	N/A	N/A	Quarterly per Year

Since the successful launch of Landsat 1, the National Aeronautics and Space Administration has launched seven successful Landsat satellites (i.e., Landsat 2, Landsat 3, Landsat 4, Landsat 5, Landsat 7, Landsat 8, and Landsat 9) (Wulder et al. 2022). Landsat 6 launched on October 5, 1993, from the Vandenberg Air Force Base in California, but failed to Landsat 5 is the longest operating RS satellite. Landsat 5 orbited for 28 years and captured 2.5 million images before being discontinued in 2013 (Wulder et al. 2022). Similar to is predecessor, Landsat 5 carried aboard the Multispectral Scanner (MSS) and TM sensors. The MSS captured four spectral bands between 0.5 to 1.1 micrometers, whereas the TM sensors added mid-range infrared bands. In contrast, Landsat 7 carries the Enhanced Thematic Mapper Plus (ETM+) that offers higher quality products and the addition of a panchromatic band with a 15-meter resolution. In May 2003, the Scan Line Corrector, a mechanism responsible for the line of sight of the satellite, malfunctioned and was unable to be repaired (Scaramuzza and Barsi 2005). As a result, RS images in Landsat 7 are duplicated and follow a zig-zag pattern along the ground. Landsat 8 was launched in February 2013, and it carries two sensors, the OLI and the Thermal Infrared Sensor (TIRS) (Wulder et al. 2019; Wulder et al. 2022). The OLI contains nine spectral bands, including SWIR and panchromatic bands. Similar to other Landsat satellites, Landsat 8 OLI has a 16-day repeat cycle and a 30-meter spatial resolution. Landsat 9 is the latest satellite to be launched and it contains improved versions of the OLI and TIRS sensors.

The Landsat collection provides RS data to public users at different levels of processing and resolution. WQ studies commonly use level-1, level-2 or modified versions of level-1 and level-2 to assess surface reflectance and temperature values. Level-1 products consist of raw data products that are derived from the satellite sensors and have not undergone any processing or corrections. This minimal level of processing is common in the research community, given that it

allows users the flexibility to select the correction methodology best suited for their study. In contrast, level-2 data products have undergone radiometric and atmospheric corrections. These corrections often entail converting digital numbers to radiance and radiance to top of atmosphere (TOA) reflectance.

Due to the spatial, spectral, and temporal resolution requirements, this study employs Landsat Analysis Ready Data (ARD) that has been pre-processed, corrected and is ready to use. ARD data was developed by Global Land Analysis and Discovery and is processed using the following four steps for surface reflectance values: (1) conversion to TOA, (2) quality assessment of observations, (3) reflectance normalization and (4) temporal aggregation of images into 16-day composites (Potapov et al. 2012; Dwyer et al. 2018). Typical Landsat images have a spectral reflectance range from 0 to 1, but this process rescales the range from 1 to 40,000. This normalization of spectral values allows images originating from different Landsat satellites to be compared against one another.

Landsat 5 TM and Landsat 8 OLI U.S. ARD spanning from 2002 to 2020 (i.e., 2002, 2005, 2008, 2011, 2014, 2016 and 2020) was acquired using the USGS EarthExplorer. Landsat 7 ETM+ data was not employed within the study, given visible scanline errors within the AOI impeded the extraction and analysis of the waterbody. The selection of Landsat imagery was dependent on the following criteria: (1) RS image needed to be collected less than 16 days from when the in-situ measurements were collected, (2) RS image needed to fall between May and August to align with high temperatures, and (3) cloud coverage could not exceed 10 percent of image tile. Exceptions to the criteria were made in 2002, 2014 and 2020. In 2014, RS imagery surrounding the day of in-situ measurement collection had excessive cloud coverage and the selected RS imagery was collected 26 days prior to in-situ data. In 2020, in-situ measurements

were collected only in January of that year and were consequently incorporated in the study. Lastly, note that in-situ measurements were not collected by the BoR until 2004 and as such, no in-situ measurements were obtained for 2002. The selection for RS imagery for this year was guided by the preset May to August range, the month of July was selected.

3.1.2. In-Situ Data

As part of the Salton Sea Reclamation Act of 1998, the BoR was directed by the Department of Interior to investigate feasible options to manage salinity and water elevation at the Salton Sea (Cohn 2000; Sheikh and Stern 2020; Vessey 2000). The intention behind the act was to preserve fish and wildlife, increase recreational opportunities and aid in overall economic development of surrounding areas. The legislation was approved with the understanding that the Salton Sea would remain a reservoir for irrigation drainage. In collaboration with the Coachella Valley Water District and the Salton Sea Authority, the BoR collects quarterly water samples from preselected sampling stations located in and around the Salton Sea. As documented by the BoR, the samples are manually collected at mid-water depths using a YSI meter and the spot sampling method. The YSI meter can measure conductivity, water temperature, dissolved oxygen and salinity in real-time. Selenium, nitrogen, phosphorous, chlorophyll-a and other nutrients are measured at nearby laboratories.

In-situ measurements of the Salton Sea spanning between 2004 to 2020 were acquired from the BoR site. The study uses in-situ values collected between May and August for the following years: 2005, 2008, 2011, 2014, 2016 and 2020. The selected month range ensures that in-situ measurements are being captured during the hottest months within the region, in order to assess maximum values. Evaporation and temperature are correlated, and high temperatures cause higher evaporation rates that result in higher nutrient concentrations (Roland et al. 2012).

Table 4 provides a summary of in-situ measurements and Landsat imagery data collection dates and the date difference between them.

Year	*Landsat Satellite*	*Satellite Collection Date*	*In-Situ Collection Date*	*Date Difference*	*Known Limitations*
2002	Landsat 5 TM	07/04/2002	N/A	N/A	In-situ data not available prior to 2004
2005	Landsat 5 TM	06/26/2005	06/21/2005	05-Days	Missing latitude and longitude values
2008	Landsat 5 TM	08/21/2008	08/20/2008	01-Days	
2011	Landsat 5 TM	06/11/2011	06/02/2011	09-Days	
2014	Landsat 8 OLI	06/19/2014	05/28/2014	22-Days	Exceeds 16-Day criteria due to cloud coverage
2016	Landsat 8 OLI	05/23/2016	06/06/2016	13-Days	
2020	Landsat 8 OLI	01/11/2020	01/14/2020	03-Days	In-situ data only collected in January

Table 4. In-Situ and Remote Sensing Data Collection

3.2. Data Preparation

Given that the AOI spans across multiple RS imagery tiles, there were a few steps that needed to be implemented prior to applying NDWI and NDCI. Similarly, the in-situ data is formatted as a .csv file with multiple sheets that needed to be condensed and formatted prior to being imported into ArcGIS Pro 2.9.2. This section explains how the different datasets were prepared for use.

3.2.1. Landsat Imagery

Landsat 5 TM and Landsat 8 OLI surface reflectance data spanning from 2002 to 2020 were acquired through USGS EarthExplorer. The EarthExplorer interface allows public users to acquire RS imagery based on desired parameters, including satellites, sensors, temporal range, and cloud coverage percentage. The selected RS data for this study was downloaded in .TIFF file format via a compressed folder. The .TIFF files were unzipped upon download and imported into ArcGIS Pro 2.9.2. Attributing to the extended temporal range of this study, RS imagery

originating from Landsat 8 OLI and Landsat 5 TM imagery were used to capture all the preselected years. These two satellites have different sensors aboard and render RS bands with differing spectral ranges. Accordingly, the bands imported into the geographic information software are dependent on the year and associated satellite. For Landsat 5 TM imagery (i.e., 2002, 2005, 2008 and 2011), Band 1, Band 2, Band 3, and Band 4 were introduced. For Landsat 8 OLI imagery (i.e., 2014, 2016 and 2020), Band 2, Band 3, Band 4, and Band 5 were imported. Table 3 provides the spectral ranges of bands originating from Landsat 5 TM and Landsat 8 OLI.

At the time of import, the coordinate system for all raster band layers had not been predefined and were consequently projected to the NAD 1983 (2011) State Plane California VI (WKID: 0406) coordinate system. The Californian coordinate system is based on the North American Datum of 1983 and the Lambert conformal projection. The coordinate system divides the State of California and its counties into 6 different zones. Given that the Salton Sea extends across both the Riverside and Imperial counties, Zone IV of the California State Plane was selected for use.

After the RS bands had been projected, similar RS bands in a given year were combined into a single raster using the Mosaic tool. Figure 12 illustrates the mosaicked process of combining two raster layers into a singular raster layer.

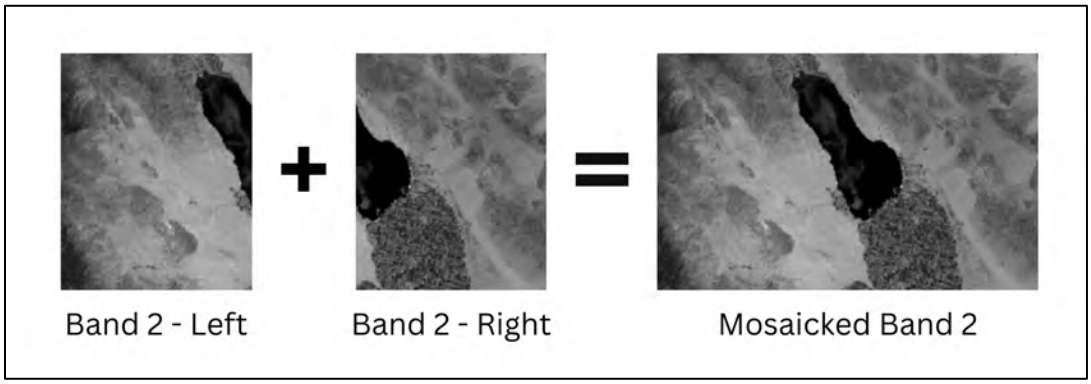

Figure 12. Mosaicked band 2 (2002)

3.2.2. In-Situ Data

The data was obtained from the BoR Lower Colorado Region website and downloaded in .csv file format. The original dataset contains multiple WQ parameter measurements taken at the various sampling stations, including depth, temperature, dissolved oxygen, pH, turbidity, chlorophyll-a, total dissolved oxygens, total suspended solids, calcium, magnesium, sodium, alkalinity, nitrate, salinity and phosphorous. Water samples were collected at multiple sampling stations, however, only six stations consistently provided data for the specified temporal range. Among those six stations, only three stations (SS1, SS2 and SS3) were in the Salton Sea. The other three stations were located at offsite locations, such as the Alamo River (AR), New River (NR) and Whitewater River (WWR). Note that these are streams of water that drain into the Salton Sea. Figure 13 illustrates the study area and the location of the different sampling stations.

The original in-situ dataset was modified to include only chlorophyll-a measurements that originated from SS1, SS2 and SS3 and spanned between May and August (January 2020 being an exception). For sampling events that captured two chlorophyll-a measurements, the average of the two measurements was recorded. This process allows us to capture a more accurate representation of the chlorophyll-a concentration. Moreover, the selected 2005 sampling event had missing latitude and longitude values that were replaced with values from the prior sampling event. The latitude and longitude for sampling stations vary slightly within each sampling event, less than one quarter of a mile.

After the in-situ dataset had been reformatted, it was uploaded as a single table into ArcGIS Pro 2.9.2. The table was then converted to a point feature layer using the XY to Point tool. This geoprocessing tool can generate a point layer based on latitude, longitude and z values obtained from a .txt or .csv file. Once the points had been created, they were projected to the

NAD 1983 (2011) State Plane California VI (WKID: 0406) coordinate system to ensure that all the new point features aligned with the raster data layers.

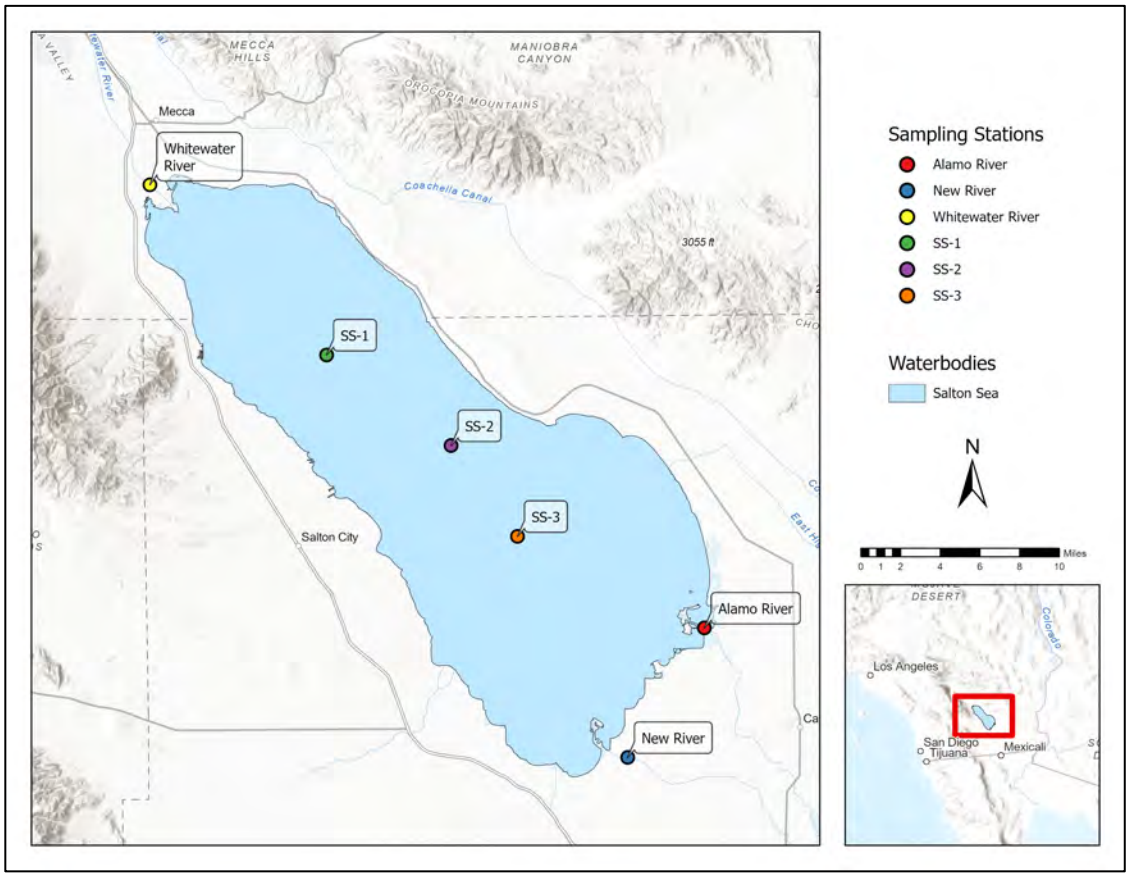

Figure 13. Sampling stations

3.3. NDWI, NDCI, 2BDA and 3BDA

This section introduces the application of NDWI, NDCI, 2BDA and 3BDA. After the RS imagery data had been projected and mosaicked, the NDWI expression was applied to extract the body of water. In recent years, the Salton Sea has experienced a decline surface area and the NDWI method allows for the water feature to be accurately delineated, see Figure 14. Surface area results will be discussed further in Chapter 4. The Raster Calculator tool was used to perform the NDWI expression, see the following equations:

$$NDWI_{Landsat\ 5\ TM} = \frac{Band\ 2 - Band\ 4}{Band\ 2 + Band\ 4} \quad (9)$$

$$NDWI_{Landsat\ 8\ OLI} = \frac{Band\ 3 - Band\ 5}{Band\ 3 + Band\ 5} \quad (10)$$

This process generated a new NDWI raster layer that enhanced water surfaces and ranged from -1 to 1, see Table 2. To extract the extent of the body of water, the raster layer needed to be converted to a binary layer prior to being converted to a polygon feature. Before proceeding with these steps, the symbology of the raster layer needed to be altered from stretch to classify. Classify symbology allocates a color to each group of values and allows users to determine the number of classes and method to which the values will be grouped. This additional step was necessary to facilitate the reclassification process that would need to occur thereafter. Through the use of two classifications and the manual method, water features were classified into a separate grouping from vegetation and other land surfaces.

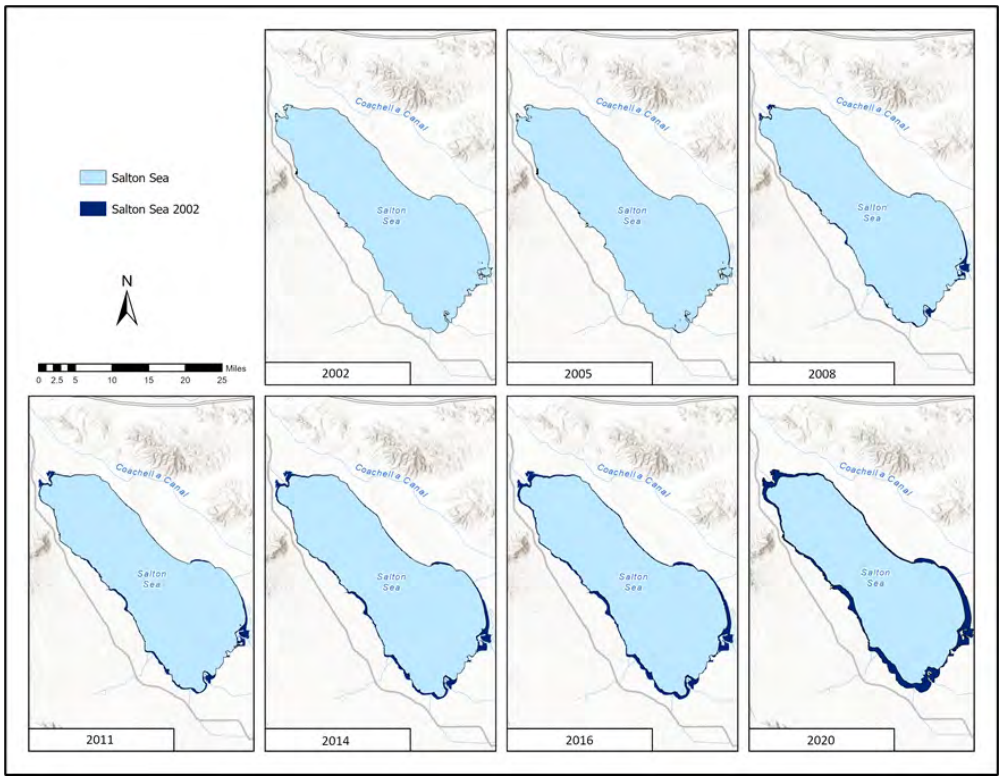

Figure 14. Salton Sea surface area

After modifying the symbology, the NDWI values were reclassified to 1 and 2 values. The reclassified layer was subsequently converted to a polygon layer, pixels with similar values were grouped into individual polygons. This step facilitated the selection of the body of water and its export as a new feature layer. The executed layer consisted of a water boundary for a specific year. The new water boundary layers were then used to clip the initial mosaicked raster layers to the extent of the body of water.

Once the mosaicked raster layers had been clipped, the next step consisted of assessing the presence of chlorophyll-a in the Salton Sea. This was implemented using the following NDCI formulas within the Raster Calculator tool:

$$NDCI_{Landsat\ 5\ TM} = \frac{Band\ 4 - Band\ 3}{Band\ 4 + Band\ 3} \tag{11}$$

$$NDCI_{Landsat\ 8\ OLI} = \frac{Band\ 5 - Band\ 4}{Band\ 5 + Band\ 4} \tag{12}$$

The tool rendered a layer consisting of NDCI values that ranged from 1 to -1. To ensure that all years were comparable, the symbology was altered from stretch to classify. The classifications were determined based on the distribution of the NDCI values across the different years (see Appendix A for distributions).

To assess NDCI differences between the years, NDCI differencing was applied using the following expression:

$$\Delta NDCI = NDCI_{Y1} - NDCI_{\ y2} \tag{13}$$

The subtraction of pixels generated a raster layer that ranged from -1 to 1, zero values indicated no change. Positive values indicated negative change and negative values indicated positive change in chlorophyll-a presence.

The NDCI was then compared against other 2BDA and 3BDA to assess its accuracy and performance. Watanabe et al. (2015) and Buma and Lee (2020) compared the NDCI to various 2BDA and 3BDA and their findings revealed NIR-Red, NIR-Green, NIR-Blue and 3BDA had generated higher adjusted R-squares than the NDCI. Higher adjusted R-square values are indicative of good model fit and 2BDA and 3BDA were therefore incorporated within the study. The NIR-Red ratios were calculated using the following equations:

$$NIR - Red_{Landsat\ 5\ TM} = \frac{Band\ 4}{Band\ 3} \tag{14}$$

$$NIR - Red_{Landsat\ 8\ OLI} = \frac{Band\ 5}{Band\ 4} \tag{15}$$

The Raster Calculator tool was then used to calculate the following NIR-Green expressions:

$$NIR - Green_{Landsat\ 5\ TM} = \frac{Band\ 4}{Band\ 2} \tag{16}$$

$$NIR - Green_{Landsat\ 8\ OLI} = \frac{Band\ 5}{Band\ 3} \tag{17}$$

After the NIR-Green expression had been applied across all years, the NIR-Blue equation was applied:

$$NIR - Blue_{Landsat\ 5\ TM} = \frac{Band\ 4}{Band\ 1} \tag{18}$$

$$NIR - Blue_{Landsat\ 8\ OLI} = \frac{Band\ 5}{Band\ 2} \tag{19}$$

Lastly, the Raster Calculator tool was used to calculate the following 3BDA suggested by Buma and Lee (2020):

$$3BDA_{Landsat\ 5\ TM} = \frac{Band\ 1 - Band\ 3}{Band\ 2} \tag{20}$$

$$3BDA_{Landsat\ 8\ OLI} = \frac{Band\ 2 - Band\ 4}{Band\ 3} \tag{21}$$

3.4. Global Regressions

Regression analysis is a statistical method used to assess the relationship between dependent and explanatory variables. Linear regressions were performed for NDCI, NIR-Red, NIR-Green, NIR-Blue and 3BDA. The regression models will assess the accuracy in which NDCI estimates chlorophyll-a concentrations in the Salton Sea and how it performs against the other 2BDA and 3BDA. The linear regressions were performed in ArcGIS Pro 2.9.2 and the program requires the dependent and independent variables to be within the same dataset. Because raster values will need to be extracted and conjoined to the point layer, a neighborhood operation was performed on the raster layers prior to the extraction of values. This additional step will ensure that the extracted values represent the average value of 3 x 3 neighborhood cells (rectangle shape), instead of a singular point. After this step had been completed, a spatial analyst tool was used to extract the raster values to the sampling points and the raster values were recorded in the attribute table of the output feature layer.

To perform a linear regression, it is recommended that the dataset contain at least ten data observations for each independent variable. The in-situ dataset only captured chlorophyll-a measurements from three sampling sites that were directly on the Salton Sea. This meant that each year (excluding 2002) had three data points observations that could contribute to the linear regression and would individually not meet the observation criteria. To address this limitation, the data points across all years were stacked within a single table. The new table was created in Microsoft Excel, reimported into ArcGIS 2.9.2, and projected accordingly to the NAD 1983 (2011) State Plane California VI (WKID: 0406) coordinate system.

3.4.1. Linear Regression Assumptions

There are four linear assumptions that can affect the output results of a model. The first assumption is linearity, and it assumes the relationship between dependent and independent values is linear. The second assumption is homoscedasticity, and it assumes equal variance in the residuals. The third assumption is no multicollinearity, and it assumes independent values are not correlated within one another. The last assumption is the Gaussian distribution of error terms, and it assumes residuals are normally distributed.

In an attempt to assess whether the dataset meets the linear assumptions, explanatory data analysis was conducted on all variables. The dataset was constructed around in-situ data measurements and the algorithm ratios were extracted and subsequently adjoined to the dataset. Table 5 provides a summary statistic of all the variables, and it includes their minimum, maximum, mean, median, standard deviation and sample size. Average chlorophyll-a is the independent variable for all the regression models, and it has the largest range of values from 4.15 to 256.56. The median and mean value are widely apart at 46.64 and 72.98 respectively and suggest high variance. In contrast, all the dependent variables tend to have smaller ranges between their minimum and maximum values. The sampling size of all variables is on the smaller side with 18 samples; however, it meets the 10 observations per variable threshold.

Table 5. Summary of Statistics

Variable	*Type*	*Minimum*	*Maximum*	*Mean*	*Median*	*Std. Deviation*	*Sample Size*
NDCI	Dependent	-0.05	-0.01	-0.02	-0.01	0.01	18
NIR-Red	Dependent	0.88	0.97	0.95	0.96	0.02	18
NIR-Green	Dependent	0.81	0.95	0.92	0.93	0.37	18
NIR-Blue	Dependent	0.92	1.00	0.96	0.96	0.02	18
3BDA	Dependent	-0.03	0.97	0.31	-0.00	0.46	18
Avg. Chlorophyll	Independent	4.15	265.56	72.98	45.64	72.98	18

Scatterplots are commonly used to evaluate the linearity assumption. They are able to provide insight into the relationship between variables and can be used to identify the degree of linearity and slope. Figure 15 displays the relationship between the NDCI and average chlorophyll-a variables. The R^2 for these two variables is low at 0.01 and it indicates that the relationship between the variables is not linear. Based on the distribution of points, the slopes appear to be negative with strong gaps between the values.

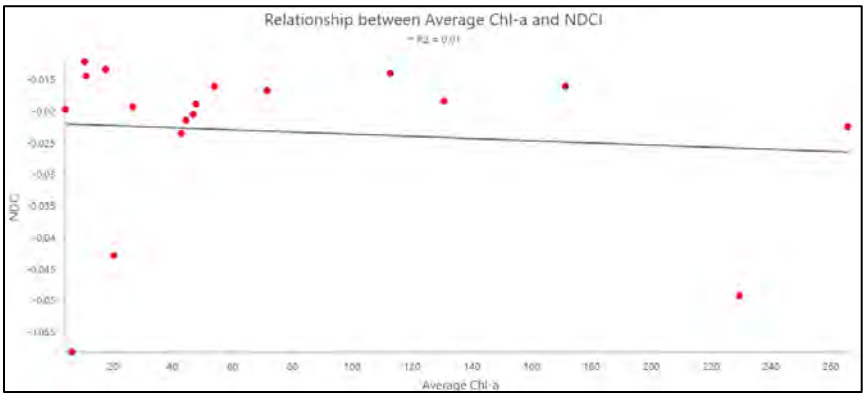

Figure 15. Relationship between average chlorophyll-a and NDCI

When we examine the relationship between NIR-R and average chlorophyll-a, the relationship appears to be non-linear, see Figure 16. The R^2 is 0.01 and the points distribution suggests a negative slope with large gaps between values. There are also outliers that indicate large and small average chlorophyll-a values.

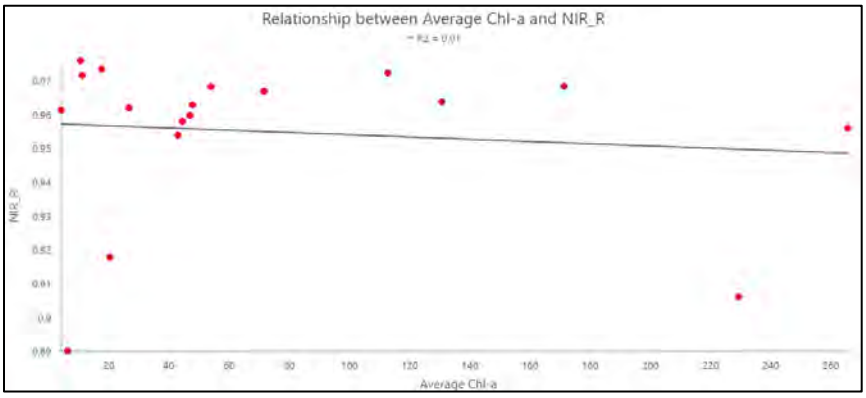

Figure 16. Relationship between average chlorophyll-a and NIR-Red

Figure 17 displays the relationship between NIR-G and average chlorophyll-a. The R^2 in this relationship is 0, indicating no linearity between the independent and dependent variables. The distribution of points also suggests the slope is near 0. When compared to NIR-Red, both 2BDA demonstrate the same outliers within the independent variable.

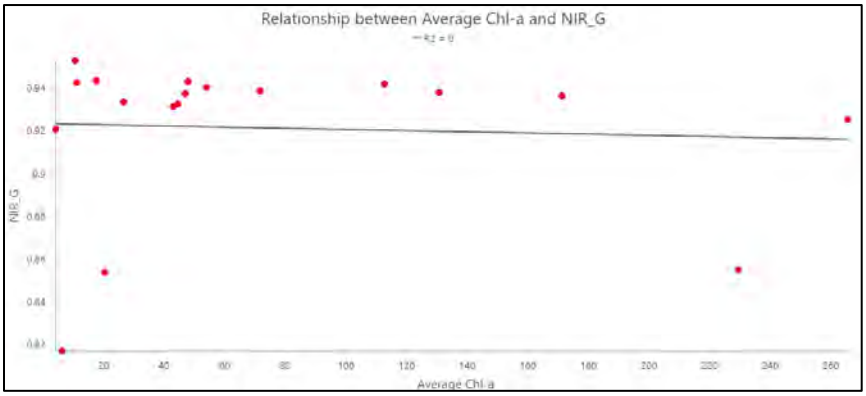

Figure 17. Relationship between average chlorophyll-a and NIR-Green

Figure 18 illustrates the relationship between NIR-B and average chlorophyll-a. The R^2 in this relationship is 0 and it indicates there is no linearity between the variables. Compared to the other 2BDA, NIR-Green has a more scattered distribution making it difficult to assess whether it has a negative or positive association.

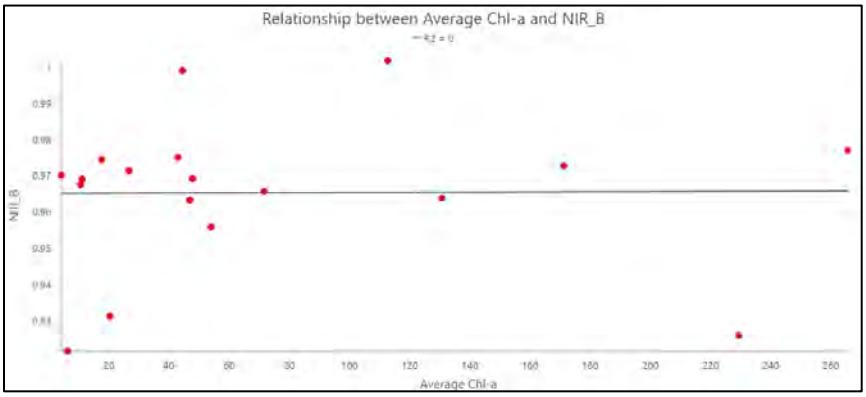

Figure 18. Relationship between average chlorophyll-a and NIR-Blue

Lastly, Figure 19 illustrates the relationship between 3BDA and average chlorophyll-a. The R^2 in this relationship is 0.33 and the clustering of points at opposite ends suggests a

bimodal distribution. Compared to NDCI and 2BDA, 3BDA has a larger gap between values and no clear association.

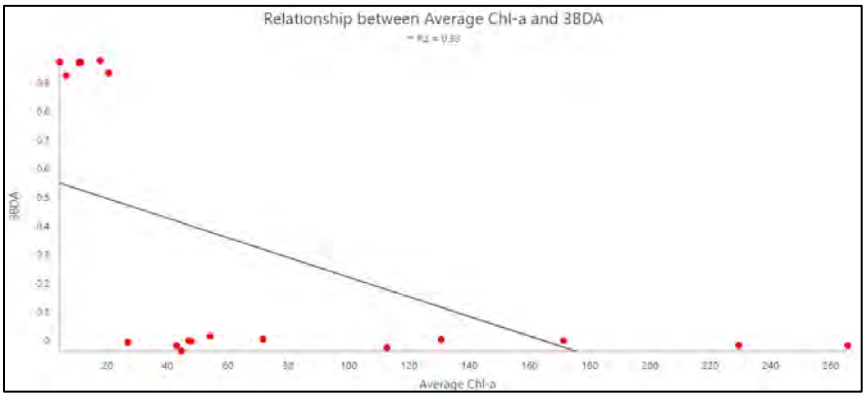

Figure 19. Relationship between average chlorophyll-a and 3BDA

The scatterplot findings align with the individual histograms of the variables shown in Figure 20. In the figure, the NDCI, NIR-R and NIR-G values skew largely to the right. In contrast, average chlorophyll-a and NIR-B tend to skew to the left. The 3BDA values are bimodal, as data is clustered away from the mean and median. Non-linear relations are normally addressed by transforming the independent or dependent variables using a linear transformation.

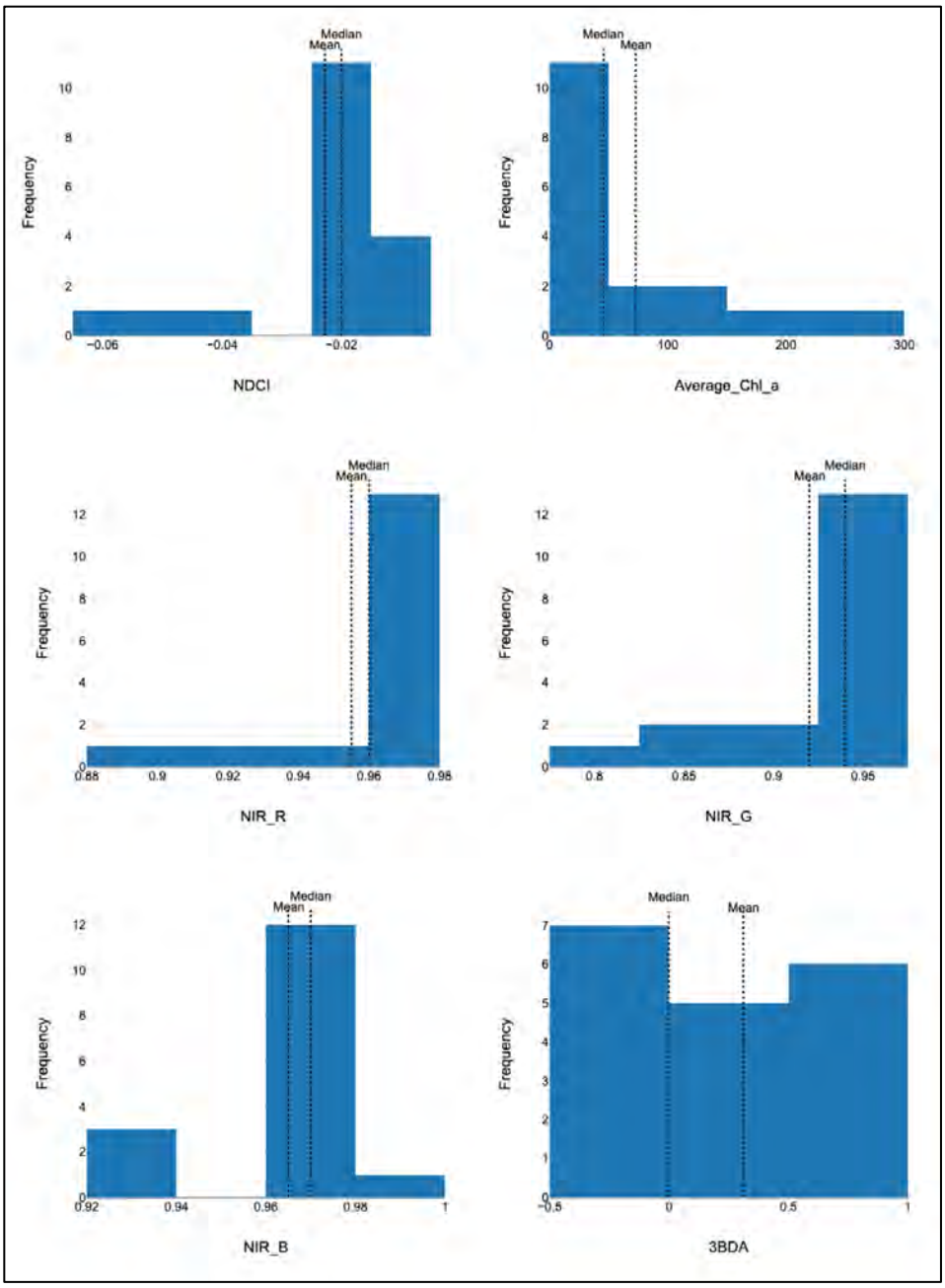

Figure 20: Histograms of variables

The distribution of error terms were evaluated using quantile-quantile plots. Figure 21 illustrates that the error terms are not normally distributed across the majority of the variables. NDCI, NIR-R, NIR-B and NIR-G have larger gaps between values and are lightly tailed. They also have a comparable number of outliers within third quadrant. In regard to 3BDA and average chlorophyll-a, the error terms are heavily tailed and more rightly skewed, respectively.

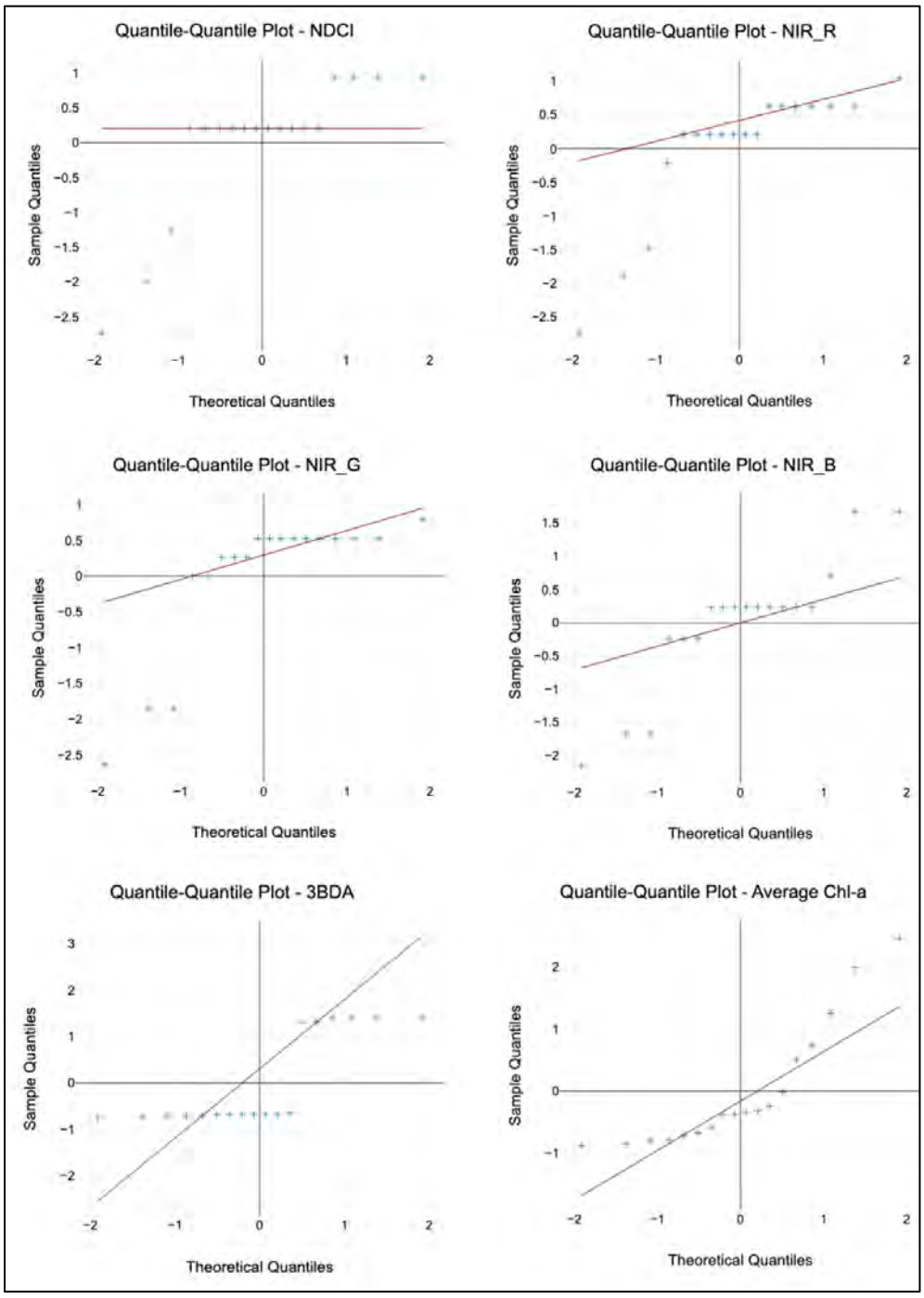

Figure 21. Quantile-Quantile plots of variables

As previously described, an assumption of linear regression is no multicollinearity among the independent variables. In this study, each linear regression was ran with one independent variable and one dependent variable. This means that there was no correlation among the

independent variables, as there was only one. This assumption is normally assessed using the variance inflation factor.

To address the issue of linearity and distribution, the independent and dependent variables were transformed using linear transformations. Negative values and outliers were taken into account when selecting the box-cox transformation for the dependent variables. For the independent variable, a logarithm transformation was used to correct the skewness of the variable values. Despite the transformations, the R^2 for majority of the variables remained low. For example, NDCI and NIR-Red increased to an R^2 of 0.08. While NIR-Green rose to a value of 0.21 and 3BDA maintained an R^2 of 0.33. NIR-Blue maintained a low R^2 after transformation with 0.02. Collectively, the R^2 are low and still demonstrate the low linearity between the variables. To further offset low linearity, outliers were removed from the dataset. The alternative solution would be to include additional data points to fill in the large value gaps, but this was not readily available.

3.4.2. Linear Regression

The Generalized Linear Regression is a tool that can be used to fit continuous, binary and count models. The linear performs an array of diagnostic tests that help us understand whether the model is useful or if there is additional work to be done (Esri n.d.). The first diagnostic examines the significance and robustness of explanatory variables. The second diagnostic observes the coefficient of each explanatory variable to ensure they capture the relationship you are expecting, whether it be positive or negative. The third diagnostic assesses whether the model includes redundant variables through the computation of the variance inflation factor (VIF). The fourth diagnostic considers the distribution of the model's residuals through the Jarque-Bera test.

The fifth diagnostic evaluates the overall performance of the model through adjusted R^2 and Akaike's information criterion (AIC).

For the linear regression, the NDCI values were imputed as the dependent variable and the in-situ chlorophyll-a measurements as the independent variable. Each data observation was examined using a continuous model (ordinary least squares). Ordinary least squares is a continuous model used estimate coefficients and model the relationship between dependent and explanatory variables (Esri n.d.). The process was repeated for NIR-Red, NIR-Green, NIR-Blue and the 3BDA. Linear regression results are summarized in Chapter 4.

Chapter 4 Results

This chapter presents chlorophyll-a patterns identified in the temporal analysis and the results of the linear regression analysis. NDCI values, NDCI changes and linear regression results are quantified, tabulated, and spatially presented in maps across the temporal range of the study. Section 4.1 describes chlorophyll-a presence in the Salton Sea from 2002 to 2020 and evaluates the NDCI differences across those years. Section 4.2 describes the linear regression results of NDCI, 2BDA and 3BDA.

4.1. Temporal Analysis of Chlorophyll-a Presence using NDCI

This section explores how chlorophyll-a concentrations temporally fluctuated and steadily increased throughout the years. The NDCI was used to assess chlorophyll-a concentrations in the Salton Sea and the raster layers range between -1 and 1. Higher values represent higher concentrations of chlorophyll-a in the waterbody. Table 6 illustrates the correlation between NDCI values and in-situ chlorophyll-a (µg/L) concentrations. These pixel ranges and associated concentrations were first introduced by Mishra and Mishra (2012) and were used in this study to quantify chlorophyll-a concentrations within the Salton Sea.

While NDCI values range from -1 to 1, the symbology of each NDCI map was chosen to highlight changes in pixel values. The symbology classifications were based on the distribution of pixel values across all years. The symbology was then applied to all NDCI layers to ensure they are comparable against one another. Moreover, Table 7 was adopted from Tas, Can and Koloren (2011) to explain the correlation between chlorophyll-a concentrations (µg/L) and trophic states.

Table 6. NDCI Pixel Range (Adopted from Mishra and Mishra 2012)

NDCI Range	*Chlorophyll-a Range (µg/L)*
-1.00 to -0.10	<7.5
-0.10 to 0.00	7.5 to 16
0.00 to 0.10	16 to 25
0.10 to 0.20	25 to 33
0.20 to 0.40	33 to 50
0.40 to 0.50	> 50
0.50 to 1.00	Severe Algae Bloom

In addition to calculating NDCI values for all years, NDCI differences were calculated between two selected years (e.g., 2002 and 2005). The NDCI difference layers also had their symbology modified based on pixel value distribution. Pixel values depicted in shades of blue experienced a decrease in chlorophyll-a concentrations from the first year to the second year. Whereas pixel values depicted in shades of red experienced an increase in chlorophyll-a concentration from the first year to the second year. Darker hues for either color translated to higher pixel differences and lighter hues to minimal or no pixel difference.

Table 7. Chlorophyll-a and Trophic States (Adopted from Tas, Can and Koloren et al. 2011)

Trophic State Levels	*Average*	*Max*
Ultraoligotrophic	<1	< 2.5
Oligotrophic	<2.5	<8
Mesotrophic	2.5 – 8	8 - 25
Eutrophic	8 - 25	25 -75
Hypereutrophic	> 25	>75

4.1.1. Chlorophyll-a Presence in 2002

In 2002, the Salton Sea extended 365.71 square miles. A total of 1,052,428 pixel values were assessed for NDCI. The pixel values had a range of 0.24, a minimum of -0.18 and a

maximum of 0.05. The pixel values also had a mean of -0.31 and a median of -0.02. As shown in Figure 22, most of the visible pixel values are less than -0.02. According to the pixel range introduced by Mishra and Mishra (2012), the chlorophyll-a concentration should range between 7.5 to 16 µg/L. Chlorophyll-a concentrations that range between these values tend to indicate eutrophic bodies of water, high nutrient concentrations and condensed plant populations. Although, the NDCI values are minimal there is discernable differences at the mouths of the WWR, AR and NR. NDCI values are noticeably higher in AR and NR and may be indicative of higher agricultural runoff water and higher pesticide concentrations. In contrast, the WWR has smaller NDCI values along its cove and the higher NDCI values are constrained to the shoreline.

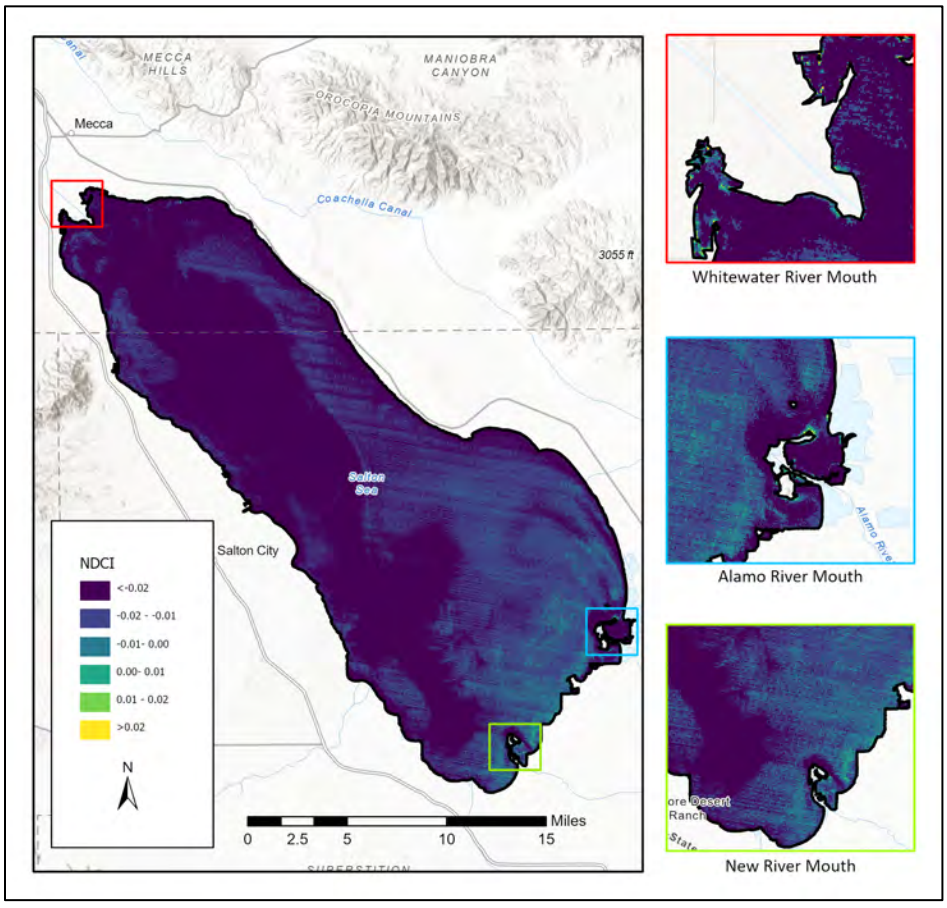

Figure 22. NDCI 2002

4.1.2. Chlorophyll-a Presence in 2005

In 2005, there is a slight reduction in the Salton Sea with a surface area of 364.62 square miles. A total of 1,049,292 pixel values were assessed in the NDCI. The range is 0.24, the minimum is -0.17 and the maximum is 0.06. Compared to the 2002 pixel values, the range remained the same and the overall NDCI range moved by 0.01 or less. The mean is -0.03 and the median is -0.02, indicating a chlorophyll-a concentration that ranges between 7.5 to 16 µg/L. In Figure 23, one can also detect a small plume of higher NDCI values located northwest of the AR and these values range between 0.01 and 0. At the WWR mouth, values range between 0.02 to 0.06, indicating a chlorophyll-a concentration of 16 to 25 µg/L. The AR and NR also appear to demonstrate higher concentrations, especially when compared the rest of pixel values in the Salton Sea.

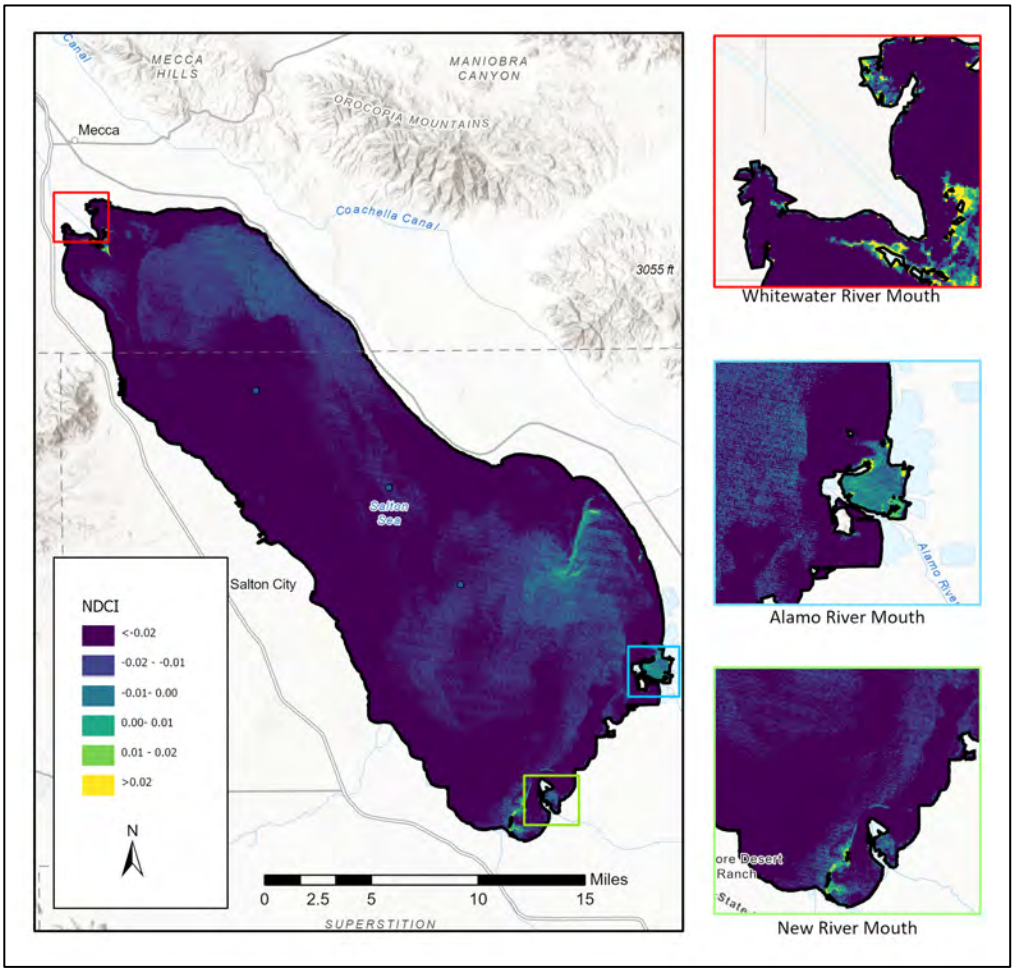

Figure 23. NDCI 2005

Figure 24 illustrates the NDCI difference amid 2002 and 2005 and 48 percent of all the pixel values fall within the 0.00 to 0.05 array. This range indicates that there was an overall decrease or no change in NDCI values between 2002 and 2005. The larger reduction of pixel values occurred alongside the northern and western shorelines of the Salton Sea. Less than 4 percent of NDCI values had pixel changes that differed more than -0.05.

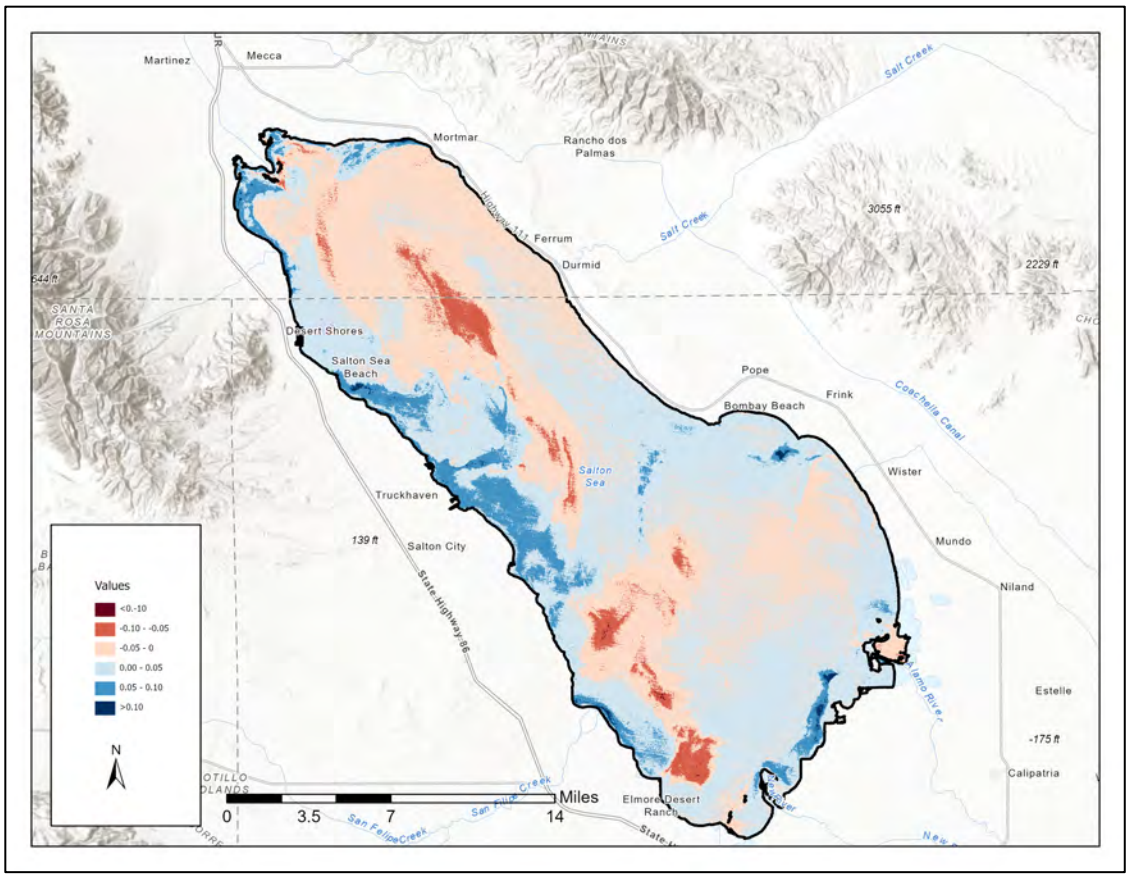

Figure 24. NDCI difference from 2002 to 2005

4.1.3. Chlorophyll-a Presence in 2008

By 2008, the Salton Sea had been further reduced in size with a surface area that extended 356.61 square miles. For the 2008 NDCI assessment, a total of 1,026,255 values were evaluated. The range of these values is 0.34, the maximum is 0.06 and the minimum is -0.28 (Figure 25). From a visual perspective, 2008 appears to have NDCI values that are mainly less than -0.02 with smaller areas fluctuating between -0.02 and 0. Based on the NDCI pixel range, chlorophyll-a concentrations still range between 7.5 to 16 µg/L. When we observe the rivers mouths, a noticeable difference is their overall reduction in surface area and lower NDCI values. There is however a visible area surrounding the perimeter of the Salton Sea that appear to have elevated NDCI values compared to the rest of the extent.

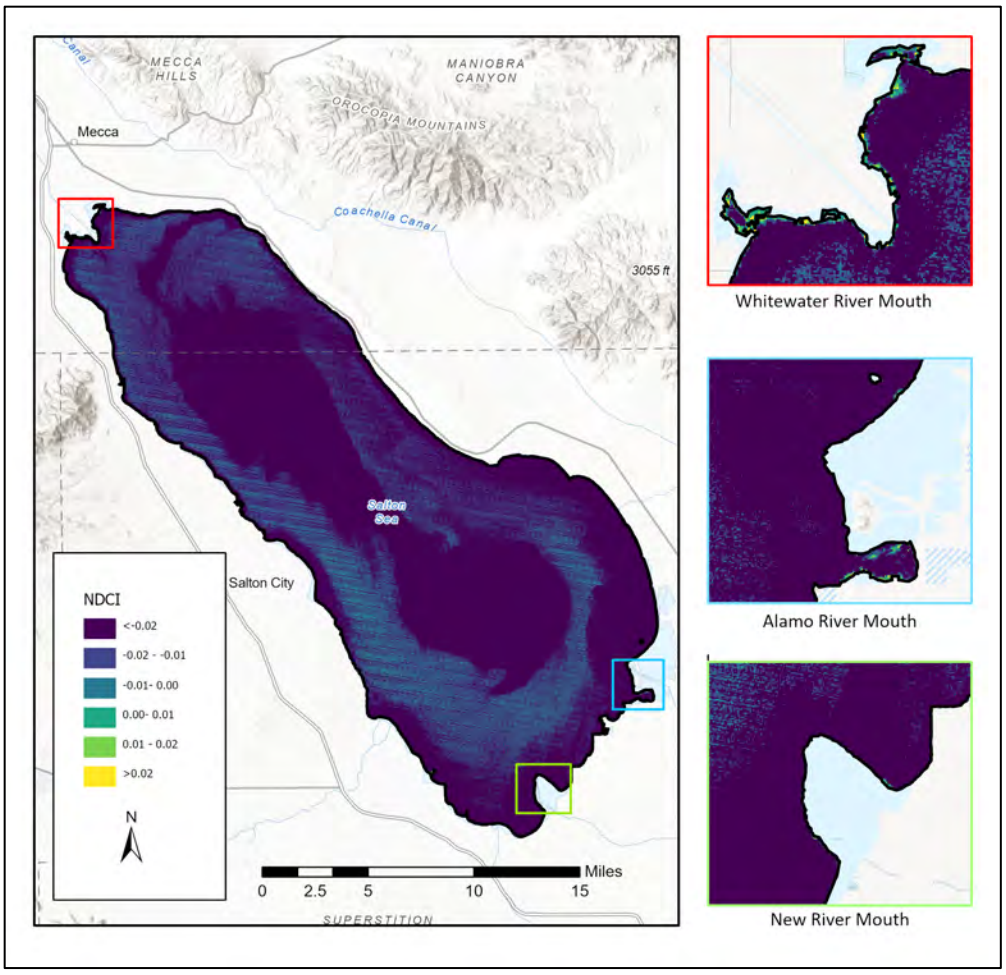

Figure 25. NDCI 2008

Compared against 2005 values, the range has grown by 0.10 values and the maximum has grown by 0.03 values (Figure 26). Whereas the differentiation between 2002 and 2005 had lower NDCI values along the west shoreline of the Salton Sea, the 2005 and 2008 differentiation reveal that there has been an increase in NDCI values within this year range.

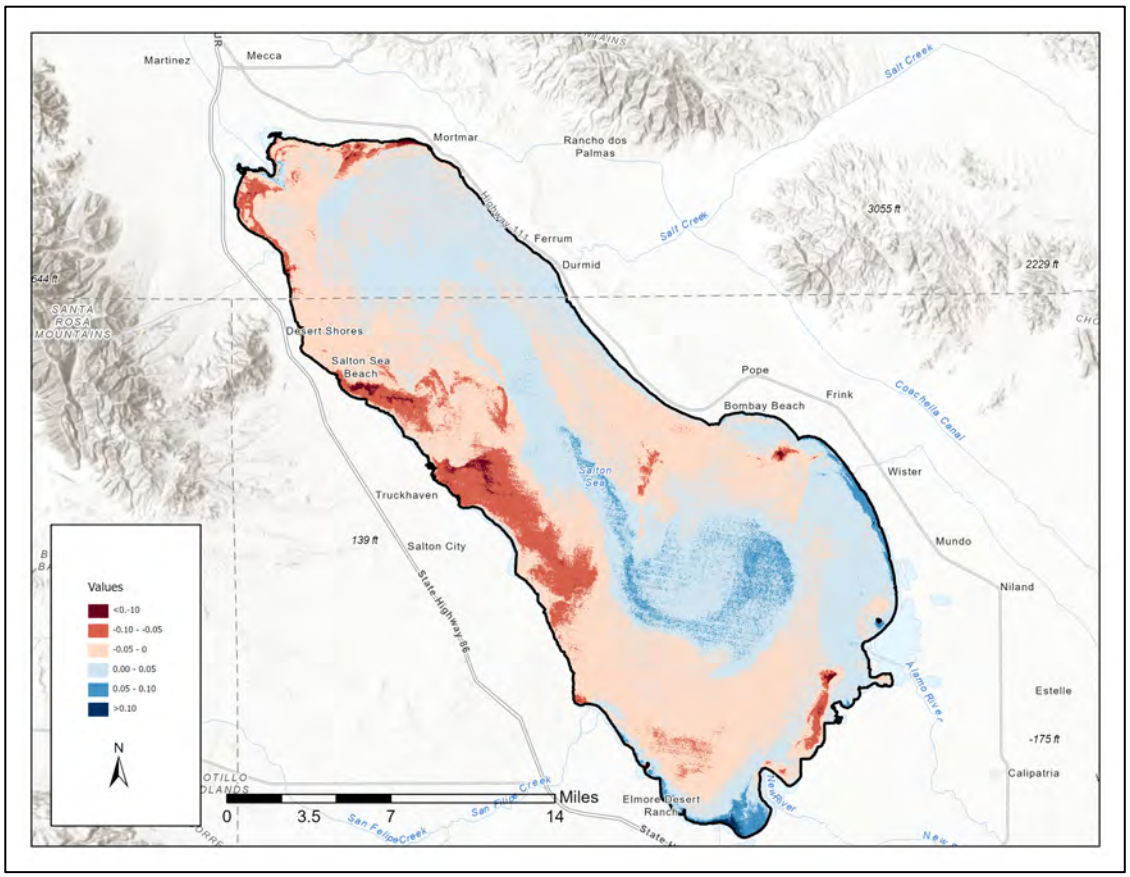

Figure 26. NDCI difference from 2005 to 2008

4.1.4. Chlorophyll-a Presence in 2011

In 2011, the Salton Sea further reduced in size to 352.32 square miles. A total of 1,013,895 pixel values were processed for the NDCI, the range was 0.19, the minimum was -0.12 and the maximum was 0.06. The mean and median pixel value for this year was -0.01. Compared to previous year, 2011 has the shortest range at 0.19 and the smallest maximum at 0.19. The maximum value of 0.06 has remained consistent between 2008 and 2011. NDCI values across the extent of the waterbody appear to have risen and broaden from <0.02 to a range between -1 and 0 (Figure 27). When we examine the pixel count per classification, 44 percent of all NDCI values fall within the -0.02 to -0.01 range and 17 percent fall between -0.01 to 0. In

terms of the WWR, AR and NR mouths, there is a notable decrease in NDCI values. This is especially true when compared to the original 2002 values.

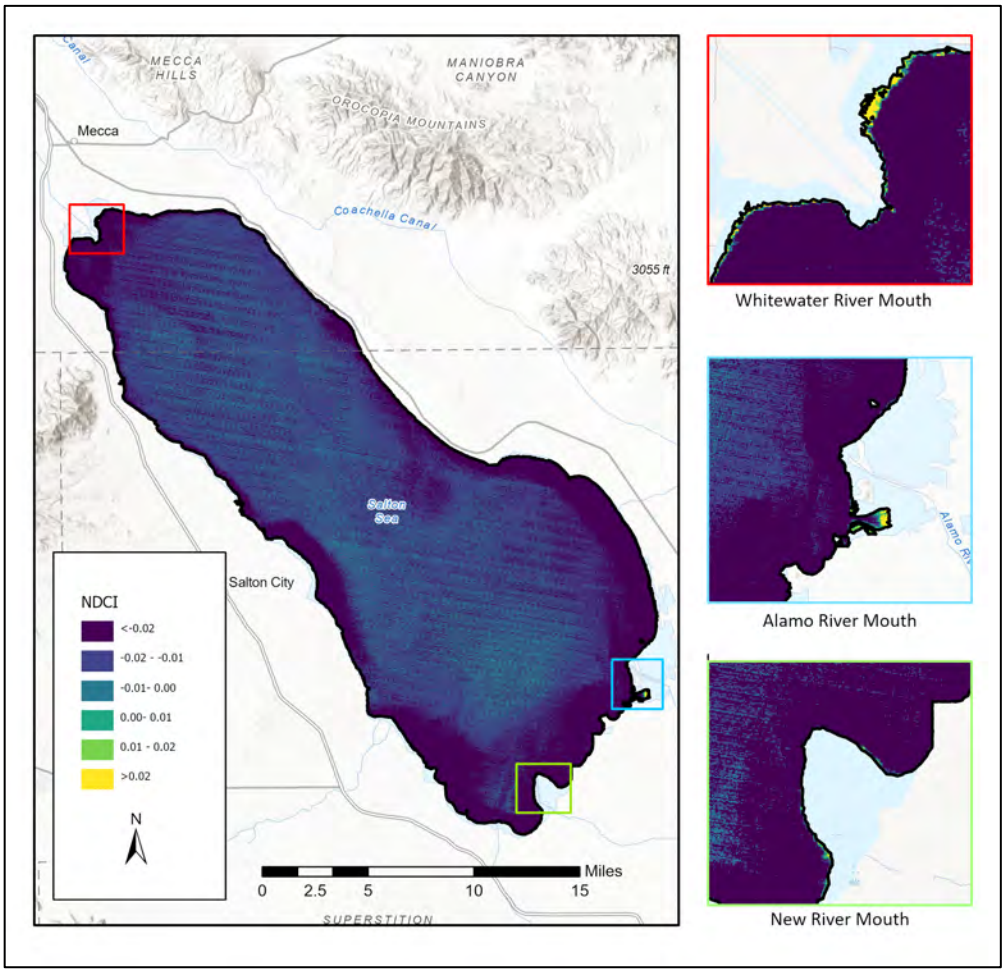

Figure 27. NDCI 2011

In Figure 28, the NDCI values from 2008 and 2011 were differenced and the majority of the Salton Sea extent is shaded in light red and blue shades. This suggests that NDCI values between 2008 and 2011 largely remained the same and if they deviated from the previous year, it was by less than 0.05 pixel values. The dark red plume at the southern part of the Salton Sea implies that there was a higher increase in NDCI values from 2008 to 2011.

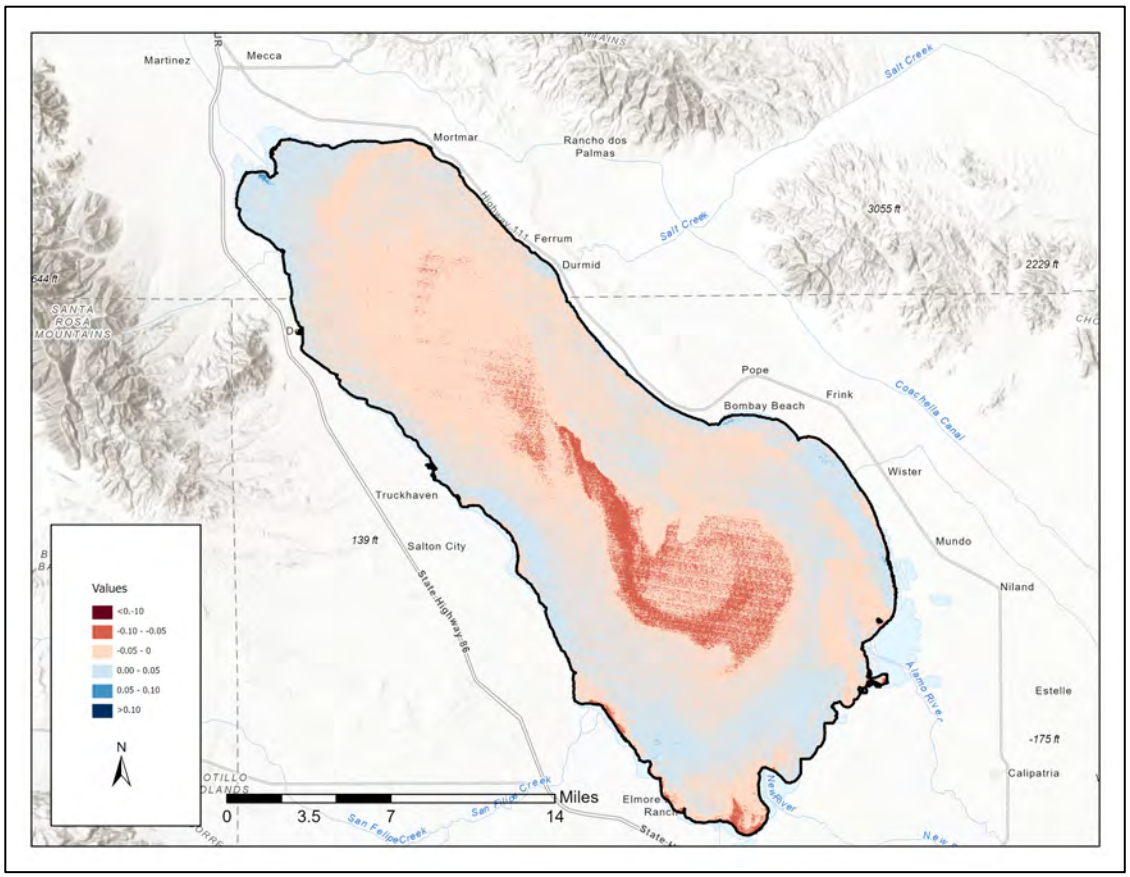

Figure 28. NDCI difference from 2008 to 2011

4.1.5. Chlorophyll-a Presence in 2014

For 2014, a total of 997,611 pixel values were assessed for the NDCI, given that the surface area of the Salton Sea extended only 346.66 square miles. The range for these pixels was 0.24, the minimum was -0.17 and the maximum was 0.06. These values deviate only by 0.01 from the original NDCI values in 2002. However, in 2014 there are three notable NDCI ranges: -1 to -0.02, -0.02 to -0.01 and -0.01 to 0. The -0.02 to -0.01 had the largest surface area at 44 percent and this differentiates from previous years that had overall lower NDCI values (Figure 29). When we examine the river mouths, AR and NR continue to have lower NDCI values and WWR continues to display more elevated ranges. Seen as most of the values remain below 0, chlorophyll-a concentration should continue to range between 7.5 to 16 µg/L.

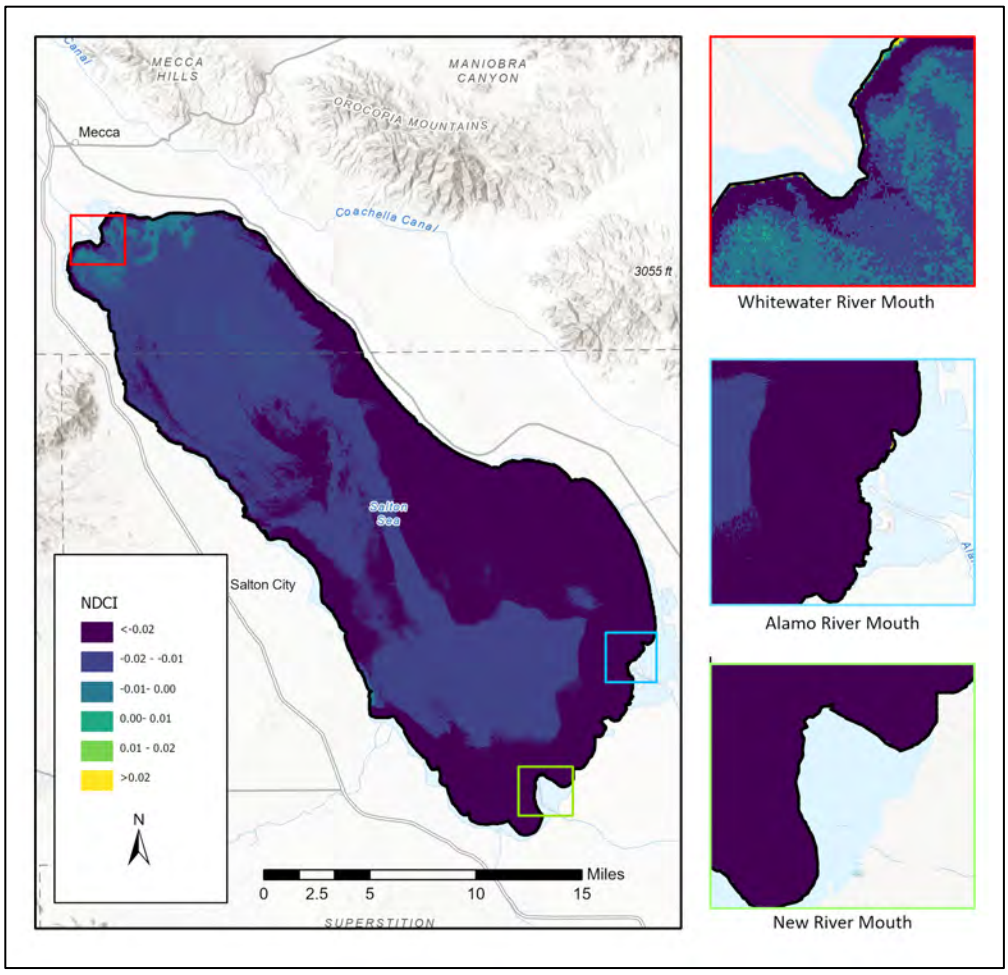

Figure 29. NDCI 2014

In comparing 2011 to 2014, it is evident that there has been a general decline in NDCI values along the southern shoreline (see Figure 30). This may be linked to lower water deposits or lower nutrient concentrations within the southern water streams, given that high nutrient concentrations prompt the production of algae bloom and chlorophyll-a. The remainder of the Salton Sea extent experienced smaller deviations from 2011 NDCI values.

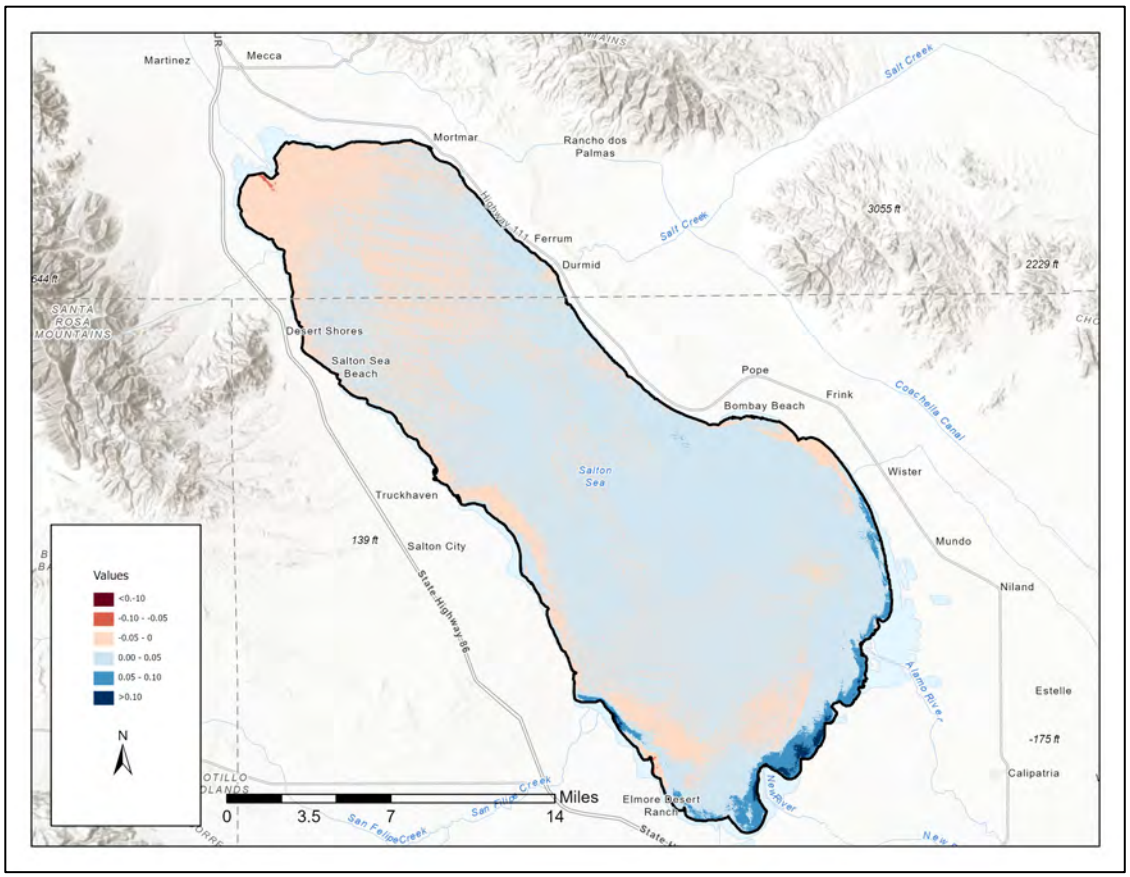

Figure 30. NDCI difference from 2011 to 2014

4.1.6. Chlorophyll-a Presence in 2016

In comparison to the previous year, the Salton Sea in 2016 had a decreased surface area of 341.10 square miles. A total of 981,626 pixels were assessed for NDCI and the mean and median was -0.03 and -0.02 respectively. The range for this year increased to 0.31from 0.24 in 2014. The minimum value was -0.17 and the maximum value was 0.10, indicating that there were areas within the Salton Sea that had chlorophyll-a concentration between 15 to 25 µg/L. NDCI values largely ranged between -1 to 0, most of the -0.02 to -0.01 pixels were located at the northern portion of the Salton Sea (Figure 31). NDCI values for AR and NR appear to remain the same to 2014, whereas WWR illustrates an overall decrease in NDCI values. Along the lower

west shoreline, there also appears to be an increase in NDCI values from the -0.02 to -0.01 range to the -0.01 to 0 range.

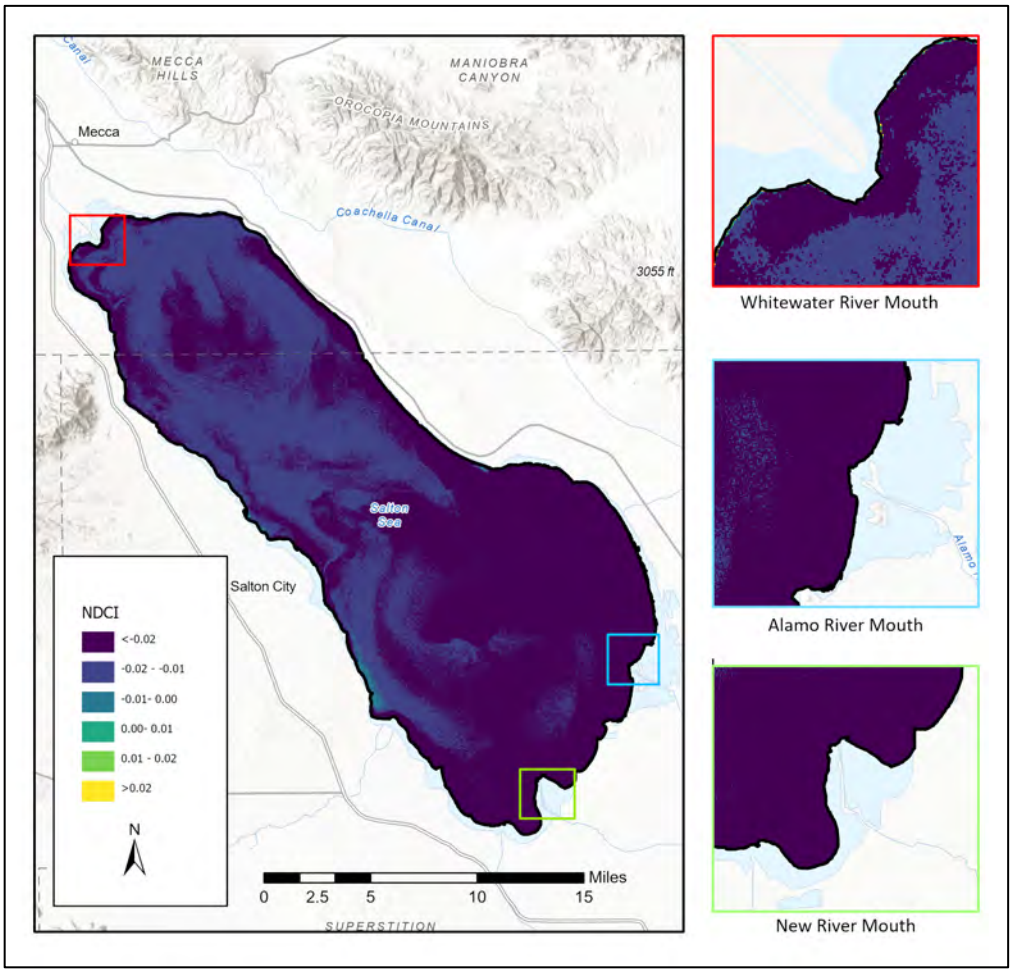

Figure 31. NDCI 2016

In Figure 32, we can examine NDCI difference between 2014 to 2016, the difference in NDCI values does not appear to be too great. Although not visible to eye, the largest difference occurred at the southern eastern area of the Salton Sea. In this area, there was a difference of 0.10 pixel values from the previous year.

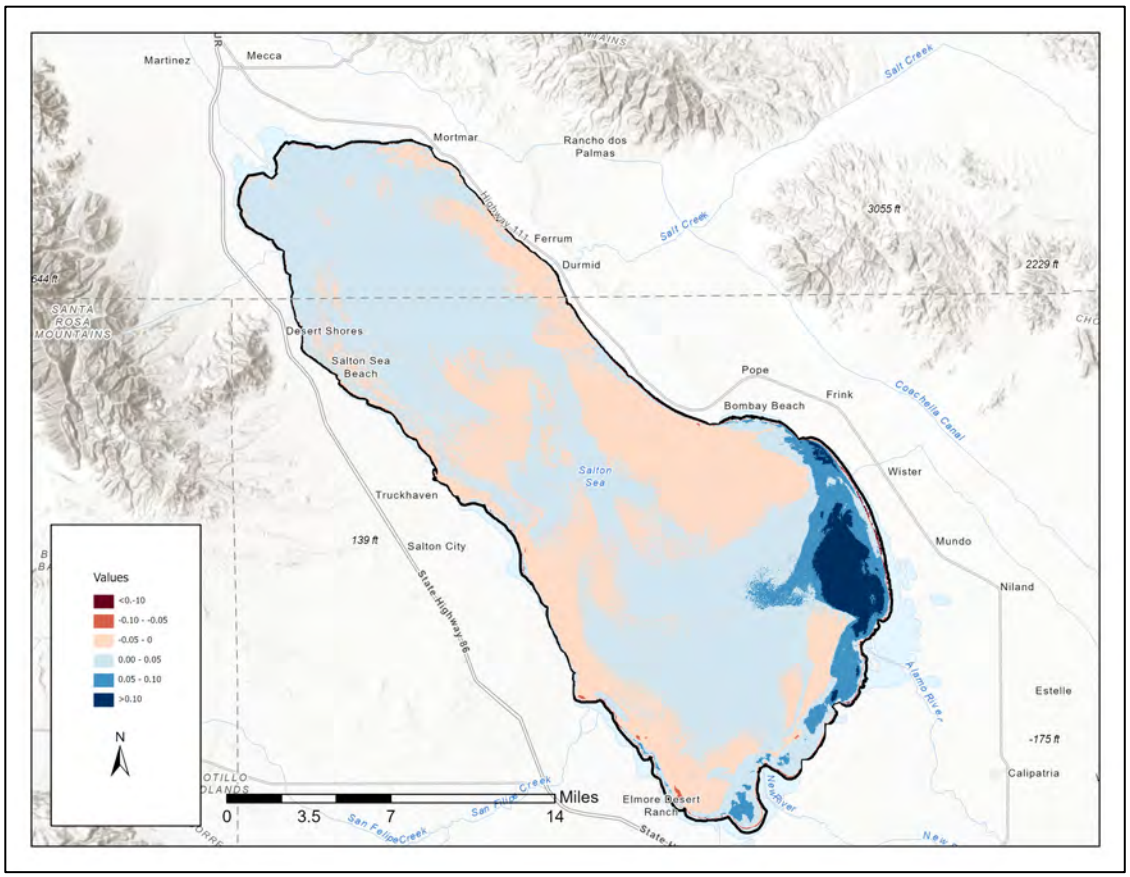

Figure 32. NDCI differenced from 2014 to 2016

4.1.7. Chlorophyll-a Presence in 2020

By 2020 the Salton Sea had a surface area of 326.75 square miles, the majority of its NDCI values range from -0.02 to -0.0. These values indicate a continual chlorophyll-a concentration of 7.5 to 16 µg/L. A total of 940,317 pixel values were assessed in the NDCI, the range is 0.27, the minimum is -0.19 and the maximum is 0.08. In contrast to early years, the AR has NDCI values less than -0.02. Both the NR and WWR had higher NDCI values along their shoreline (Figure 33). In the middle of the Salton Sea, we can also discern small areas with higher chlorophyll-a concentrations.

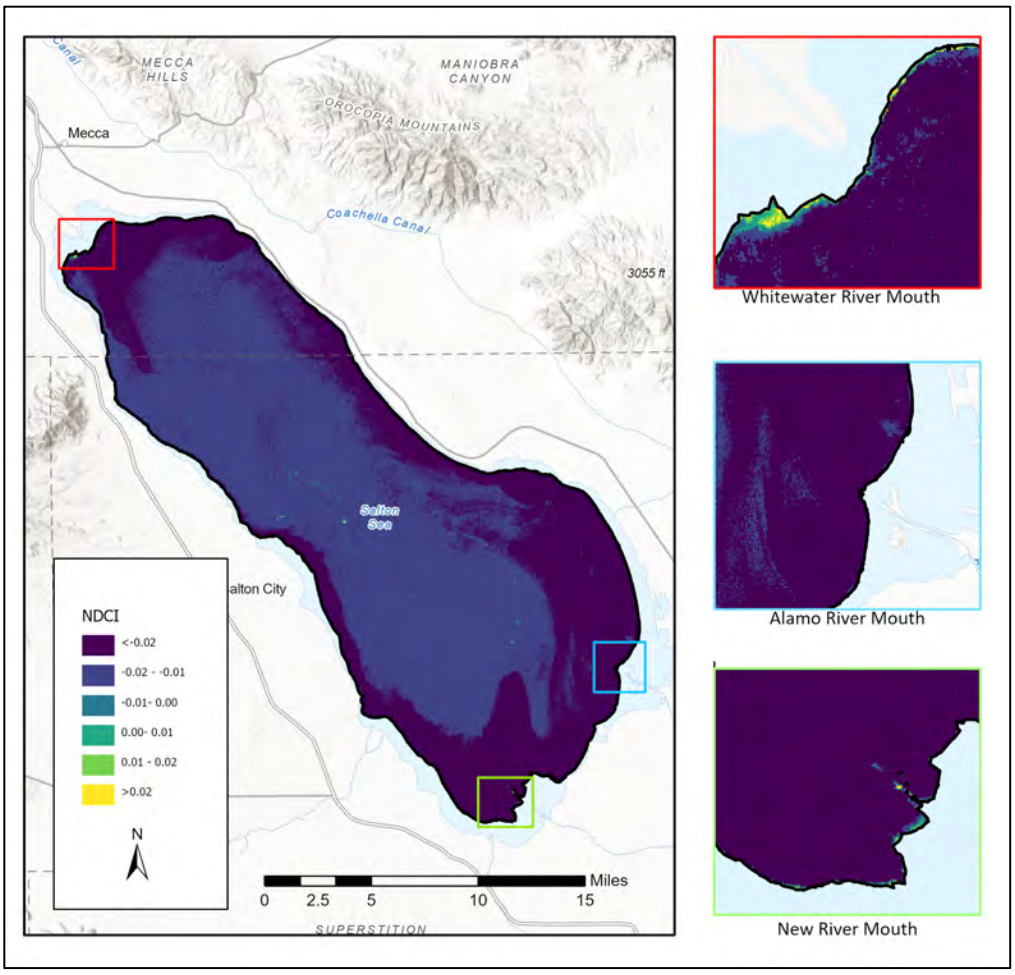

Figure 33. NDCI 2020

The quantifiable difference between 2016 and 2020 reveals a large increase in chlorophyll-a concentrations within the southern portion of the Salton Sea (Figure 34). Note that this is the same area that experienced a decline in NDCI from 2014 to 2016.

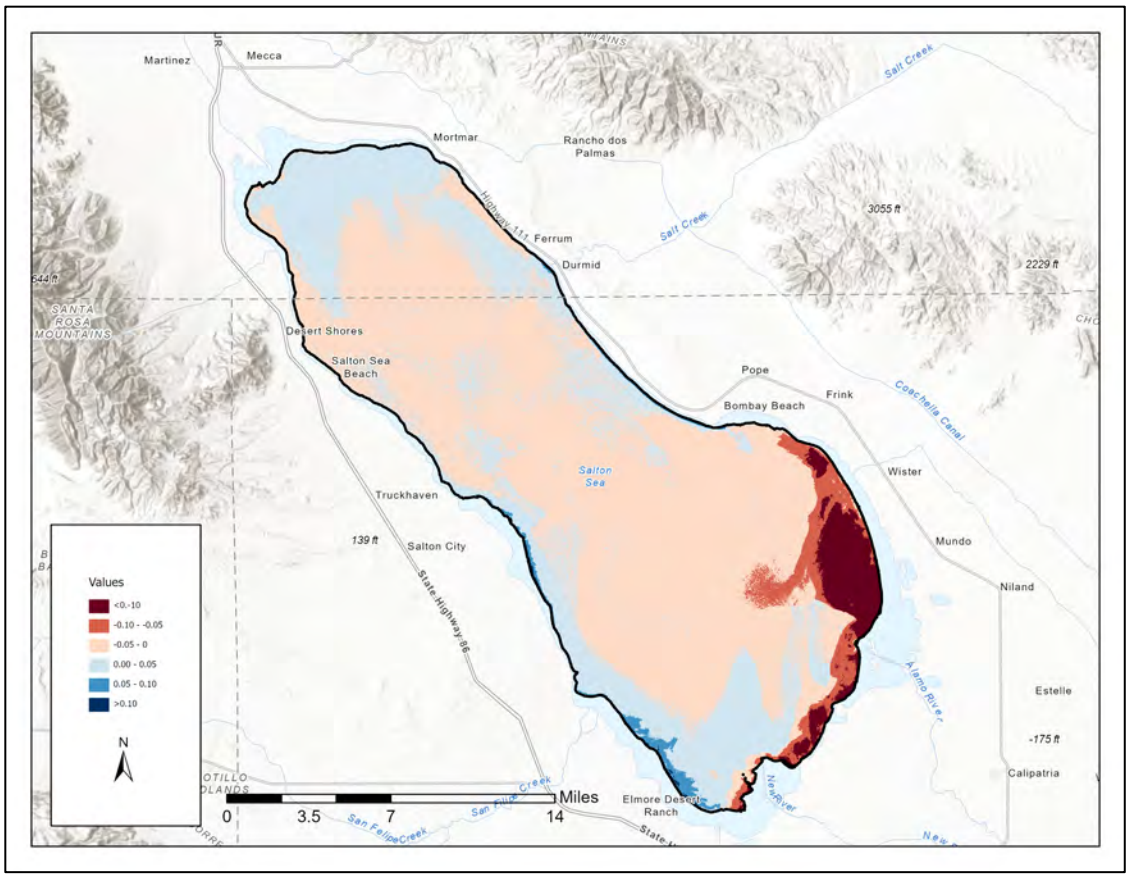

Figure 34. NDCI differences from 2016 to 2020

NDCI difference values from 2002 to 2020 reveal that there has been a general increase in chlorophyll-a concentrations within the Salton Sea (Figure 35). The majority of the variation between these years is minimal, as it fluctuates between 0 to 0.05 values. However, these findings indicate that the Salton Sea is largely eutrophic and that the overall chlorophyll-a concentrations are slowly rising. The northern and western areas of the Salton Sea experienced the greater change in water quality, value differentiations were as high as -0.10. We can also see that the southern portion of the Salton Sea experienced a slighter decrease in NDCI values, specifically around the AR mouth.

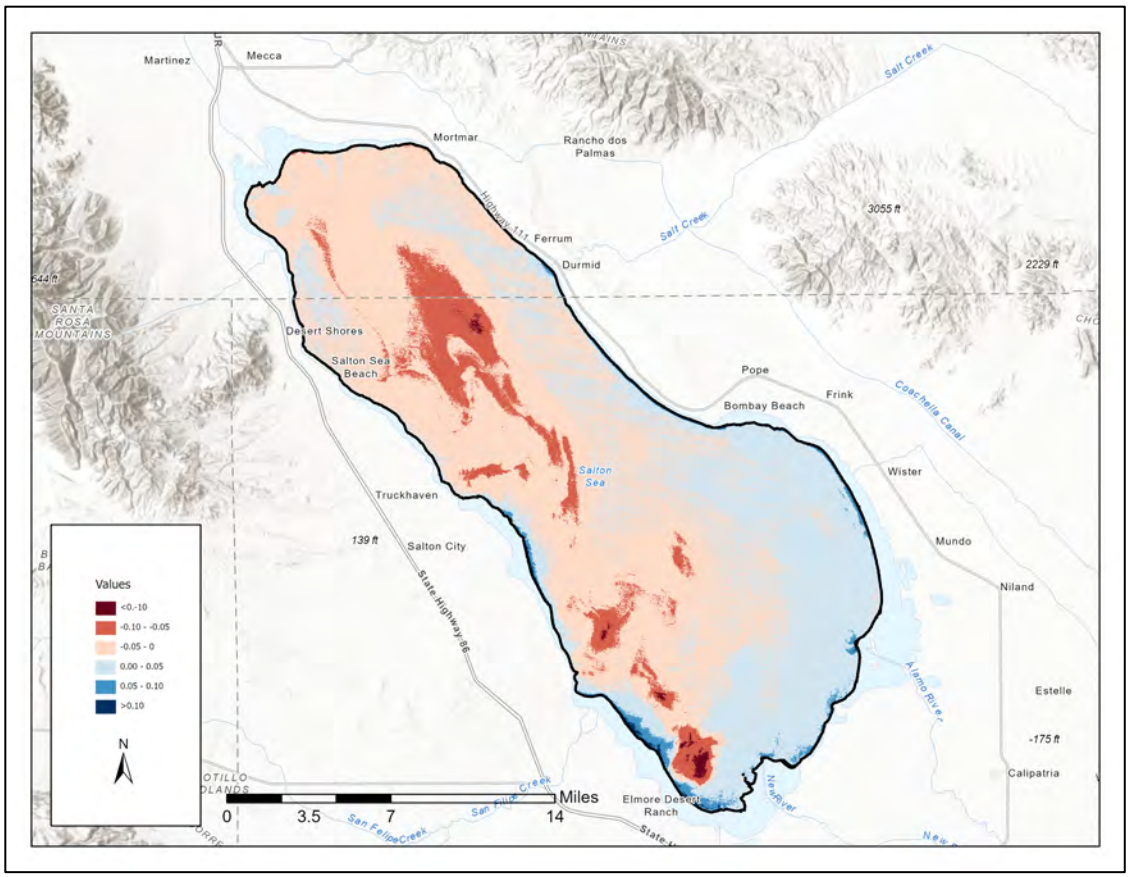

Figure 35. NDCI differences from 2002 to 2020

4.2. Assessment of NDCI against 2BDA and 3BDA

Table 8 provides a summary overview of the linear regression. The NDCI regression model demonstrated a weak linear fit between the dependent and independent variable, meaning that the independent variable was unable to add value to the model. This regression model had an AIC^2 value of -104.40 and higher AIC^2 values are indicative of poor model performance; regardless if the value is negative or positive. The NDCI regression also had a small R^2 of -0.0005 that indicates a low level of correlation between variables. Because the p-value for average chlorophyll-a was greater than the significance level of 0.05, we fail to reject the null hypothesis that the coefficients are not zero.

Table 8. Summary of Linear Regression Results

Band Ratios	*Intercept*	*Coefficient*	*Std. Error*	*t-Statistic*	*P-Value*	*R^2*	*AIC^2*
NDCI	0.9866	-0.0007	0.0011	-0.9661	0.3547	-0.0055	-104.4077
NIR-Red (2BDA)	0.9737	-0.0021	0.0021	-0.9836	0.3511	-0.0043	-87.2594
NIR-Green (2BDA)	1.9503	-0.0029	0.0017	-1.7151	0.1143	0.1392	-92.9739
NIR-Blue (2BDA)	0.9640	0.9640	0.0044	0.5193	0.6138	-0.0648	-68.2995
3BDA	0.0049	-0.0341	0.0003	-1.0250	0.3240	0.0036	-79.1229

For NIR-Red, the intercept is 0.9737 and the coefficient is -0.0021. This means that an increase in average chlorophyll-a results in a 0.0021 decrease in NIR-Red values. The standard error is 0.0021 and it suggests that the sample population does not deviate too largely from a true mean population. The t-value is -0.9836 and the p-value for the coefficient of average chlorophyll -a is 0.35. Since the p-value is greater than the significance level of 0.05, the variable is not statistically significant, and we are unable to reject the null hypothesis that the coefficient is not zero. The AIC^2 for NIR-Red is -87.25 and it indicates a relatively poorer model compared to NIR-Blue model. The R^2 is low at -0.0043 and it suggests that the model is doing a poor job at explaining the variance of the dependent variable.

Unexpectedly, out of all the regression models NIR-Green had the highest R^2 at 0.13. The AIC^2 value remains larger than the NIR-Blue model, which had the lowest AIC^2 out of all the models. In a study conducted by Watanabe et al. (2015), NIR-Green had the lowest R^2 compared to the rest of the NIR-based 2BDA. The 3BDA model had an R^2 of 0.0036 and while it remains low, it was the model with the second highest value. It was difficult to assess the performance of the NDCI model against the rest of the regression models, when the R^2 were negative, and the independent variable proved to statistically insignificant.

Table 9 provides a list of the in-situ measurements and their associated NDCI values. The table also includes the expected NDCI range given the in-situ measurement and the correlated

trophic state based on the in-situ measurements. When we compare the NDCI and in-situ measurements, it is evident that the NDCI underestimated the chlorophyll-a concentrations and assigned incorrect NDCI values. Chlorophyll-a concentrations that varied more than 95µg/L were assigned the same NDCI values. Between 2005 and 2008, we can see that Salton Sea had the highest fluctuation in chlorophyll-a concentrations. Based on these limited in-situ measurements, we can conclude that the Salton Sea is moving toward a hypereutrophic state versus a eutrophic state.

Table 9. Comparison of NDCI and In-Situ Measurements

Year	*In- Situ Chlorophyll-a Concentrations (µg/L)*	*Measured NDCI Value*	*Expected NDCI Range*	*In-Situ Trophic State*
2005	229.44	-0.05	0.50 to 1.00	Hypereutrophic
2005	265.56	-0.02	0.50 to 1.00	Hypereutrophic
2005	171.26	-0.02	0.50 to 1.00	Hypereutrophic
2008	20.34	-0.04	0.00 to 0.10	Eutrophic
2008	4.16	-0.02	-1.00 to -0.10	Mesotrophic
2008	6.26	-0.06	-1.00 to -0.10	Mesotrophic
2011	10.56	-0.01	-1.00 to -0.10	Eutrophic
2011	17.57	-0.01	0.00 to 0.10	Eutrophic
2011	11.07	-0.01	0.00 to 0.10	Eutrophic
2014	112.70	-0.01	0.50 to 1.00	Hypereutrophic
2014	47.79	-0.02	0.20 to 0.40	Hypereutrophic
2014	42.91	-0.02	0.20 to 0.40	Hypereutrophic
2016	26.66	-0.02	0.10 to 0.20	Hypereutrophic
2016	46.87	-0.02	0.20 to 0.40	Hypereutrophic
2016	44.42	-0.02	0.20 to 0.40	Hypereutrophic
2020	71.56	-0.02	0.50 to 1.00	Hypereutrophic
2020	130.69	-0.02	0.50 to 1.00	Hypereutrophic
2020	53.96	-0.02	0.50 to 1.00	Hypereutrophic

Chapter 5 Discussion

This study conducted a temporal analysis of chlorophyll-a concentrations within the Salton Sea from 2002 to 2020. The study also assessed the use of NDCI against 2BDA and 3BDA using linear regression models. The contributions of this work lie within developing a more holistic and efficient approach towards monitoring, predicting and safeguarding bodies of water. The use of RS imagery to conduct WQ assessments, as opposed to traditional WQ methods, ensures greater temporal and spatial coverage. The use of RS imagery can also aid policymakers and community members in avoiding the high costs associated with conventional water sampling methods while still making progress in monitoring and improving WQ. The results demonstrate the potential of incorporating RS imagery in WQMPs, but they still show the value in the continued collection of in-situ measurements. The linear regression findings revealed that the NDCI underestimated chlorophyll-a concentrations by a wide margin. The significance of these findings is that they highlighted the challenges and limitations of using RS imagery in WQ assessment. The remainder of this chapter summarizes the main findings from the temporal analysis and the linear regression models. A discussion of known limitations and challenges within the study are also presented. Lastly, areas of potential future work and analysis application are identified and discussed.

5.1. Discussion of Results

The temporal analysis evaluated chlorophyll-a concentrations in the Salton Sea. This process generated NDCI values for all the years considered within the selected temporal range (i.e., 2002, 2005, 2008, 2011, 2014, 2016 and 2020). The NDCI values primarily ranged between -0.02 and 0.02. This NDCI range indicates that the Salton Sea has maintained concentrations between 7.5 to 17 µg/L and 16 to 25 µg/L from 2002 to 2020. These chlorophyll-a

concentrations are in agreement with values measured in other eutrophic bodies of water and are indicative of poor WQ within the Salton Sea, specifically in relation to eutrophication (Mishra and Mishra 2012; Setmire et al. 2000). A eutrophic condition refers to an environment that is enriched with nutrients and experiences high plant life density and dead oxygen zones (Cohen 2019; Setmire et al. 2000). The eutrophic state of the Salton Sea was an expected outcome, given that it has served as an agricultural drainage since 1924 (Cohen 2019). Nevertheless, the extent of eutrophication of the Salton Sea is alarming and has led to a large decrease in diversity of aquatic life, increase in overall turbidity and has reduced the lifespan of the waterbody.

In terms of related work conducted on the Salton Sea, a study by Setmire et al. (2000) examined inflow, nutrient, and chlorophyll-a concentrations in the Salton Sea from 1968-69 and 1999. The study findings revealed chlorophyll-a concentrations averaged 25 µg/L, indicating that the Salton Sea had reached a eutrophic state as early as then. In 1999, the NR accounted for 46 percent of the inflow into the Salton Sea, the AR accounted for 32 percent and the WWR accounted for 6 percent. Setmire et al. (2000) and Cohen (1999) recognized areas surrounding the AR, NR and WWR experienced higher chlorophyll-a concentrations (an average of 70 µg/L) compared to the rest of waterbody. The temporal trends found in this study illustrate minimal variation of NDCI pixel values and indicate chlorophyll-a concentrations did not exceed 25 µg/L. Interestingly, when examining the difference in concentrations between 2002 and 2020, it is evident that there has been a decrease in inflow from the AR and NR and increase in WWR. Areas that were near the rivers experienced the highest change in in NDCI pixel values over the years, but changes were less than 0.10 values. This means that the temporal analysis was unable to identify areas that measured concentrations equal to or exceeding 70 µg/L.

Another goal of this study was to evaluate the performance of the NDCI in estimating chlorophyll-a concentrations and assessing its performance against other band ratio algorithms. This process generated statistical summaries for the NDCI, 2BDA and 3BDA models. None of the linear regression results had p-values less than 0.05 to signify statistical significance of the independent variable. The adjusted R2 for all the models was near 0 and it failed to indicate a strong linear relationship between the independent and dependent variables. This finding suggests Landsat imagery may not be suitable for estimating chlorophyll-a concentrations in the Salton Sea using NDCI, 2BDA and 3BDA.

The conclusions of this study can build upon previous works in this space and more insights can be gained when comparing these results against those found in similar studies. In the RS community, Sentinel-2 imagery has long been favored to assess chlorophyll-a presence due to the inclusion of the red-edge band. Buma and Lee (2020) evaluated the performance of NDCI, 2BDA, 3BDA and FLH using Sentinel-2 and Landsat 8 OLI imagery. Their findings revealed that NDCI (R2 = 0.75) and 3BDA (R2 = 0.89) performed relatively better than FLH (R2 = 0.73) and 2BDA (R2 = 0.71) when using Landsat 8 OLI imagery. When compared against Sentinel-2 imagery, NDCI and 3BDA had higher correlations with Worldview-3 measurements. Buma and Lee (2020) findings deviate from those of this study, given that the adjusted R2 for NDCI was -0.0055 and 0.0036 for 3BDA. The difference in results can be attributed to the use of Worldview-3 values in Buma and Lee (2020), while this study relied on the use of in-situ measurements.

Watanabe et al. (2015) conducted a study using Landsat OLI imagery and in-situ measurements to examine multiple two-band and three-band models, including NIR-R, NIR-G and NIR-B. Their findings revealed that the 2BDA (i.e., NIR-Red, NIR-Green and NIR-Blue)

performed better than the NDCI (R2 = 0.39). Most of the band ratios demonstrated acceptable model fits, but the linear regression models underestimated chlorophyll-a concentrations and incorrectly designated the associated tropic state. In this study, the NDCI values of the point features were compared against the in-situ measurements. This evaluation revealed that the NDCI also underestimated chlorophyll-a concentration in the Salton Sea by a wide margin. Points that had high chlorophyll-a concentrations (>70 µg/L) were given the same NDCI values as those that had low chlorophyll-a concentrations (> 5 µg/L). This finding shows limitations in the use of RS imagery and emphasizes the importance of having a large enough dataset of in-situ measurements to assess spatial indices. Moreover, the findings reveal that chlorophyll-a concentrations have fluctuated greatly between 2002 and 2020. Since 2011, the sampling stations have consistently recorded concentrations that exceed 25 µg/L and point toward a hypereutrophic Salton Sea.

5.2. Limitations and Challenges

Several limitations and challenges exist within this study, which lead to uncertainty in the results. A well-known constraint to performing traditional WQ assessment is the data collection process and the high associated costs. The original in-situ dataset was constructed by the BoR, which performed quarterly water sampling events at the Salton Sea from 2004 to 2020. In WQMPs, the WQ data collection process is usually pre-planned as it requires assembling a workforce and gathering water sensing equipment. The pre-planning process does not always extend to the final product and a known limitation in this study was the data quality of the in-situ dataset. The original dataset contained multiple data entry errors, including missing values, duplicated items and unstructured data formats. The study had initially planned to evaluate the Salton Sea every three years, beginning in 2002 to 2020. Missing values from the year 2017

made it difficult to maintain the intended temporal range. The original dataset also contained entries for all the sampling events conducted since 2004. The location of the sampling events varied across years and this inconsistency made it difficult to evaluate a single area temporally.

The second limitation of this study also results from issues in data-availability and is centered on the limited in-situ sampling size. The study evaluated six years (i.e., 2005, 2008, 2011, 2014, 2016 and 2020) of in-situ measurements, which only had three consistent sampling stations across all these years. This meant that between all six years, a total of only 18 data point were acquired for the study. The large fluctuation in chlorophyll-a concentrations means that the limited sampling size had a large range of values. When the data was being examined to meet linear assumptions, the scatterplots would identify maximum and minimum values as outliers. The values were removed in multiple iterations to increase the linearity between independent and dependent variables, but new outliers would then emerge. This limitation could have been mitigated had there been additional points to fill in the large gaps between in-situ values.

The third limitation of the study is the discrepancy between the days the RS imagery and in-situ data were collected. The study used linear regressions to better understand the relationship between band ratio values and in-situ measurements. It was important for the RS imagery to be collected within a similar time window to when the in-situ data collection occurred to ensure higher accuracy of assessment. However, when the in-situ measurements were collected, they were not intended to be used in conjunction with satellite imagery and the data collection process did not take into account cloud coverage, scanline errors or revisit intervals for Landsat satellites, which are important considerations for RS imagery This meant that RS imagery selected for the study were not always aligned with the days in which the in-situ measurements were collected, which introduced large uncertainty in the final results.

The final limitation of this study was the temporal range of the analysis. The temporal range spanned between 2002 to 2020 and required an RS program that was established prior to 2002. This limited the options in choice of RS programs that were publicly available and could be used within the analysis. The only program that met all criteria was Landsat imagery, however, this study showed the limitations of its use for WQ assessment. Sentinel-2 imagery could have been an option because it incorporates a red-edge band, but it was not established until 2014.

5.3. Future Work

Assessing chlorophyll-a concentrations is only one step in performing a complete WQ assessments on a body of water. There is a large array of WQ parameters that are spectrally active and can be assessed using RS imagery and RS techniques. Some of these spectrally active WQ parameters include temperature, turbidity, salinity, and suspended sediments (Topp et al. 2022). This project can serve as a framework for future studies that can conduct WQ studies using other parameters, as the analytical methods and workflows can be easily replicated. The semi-empirical component of the NDCI means that the algorithm is not dependent on in-situ measurements and can be reproduced in other bodies of water and across multiple temporal ranges. The framework can also be implemented when using other spatial indices, as they will require similar map algebra expressions. From a policy perspective, these analytical methods and workflows can be beneficial to local government and non-profit organization that seek to create more sustainable WQMPs.

Finally, future research can build upon this study by incorporating new satellite imagery from other RS programs. For instance, the original NDCI expression contains a red-edge band that captures the 748 to 778 nm spectral range. The red-edge band was replaced with a NIR band

when the NDCI was used with Landsat imagery. Thus, there is value in evaluating whether the original NDCI expression can accurately assess chlorophyll-a presence within the Salton Sea.

References

"60 Years Ago First Satellite Image of Earth." 60 Years Ago: First Satellite Image of Earth. Kennedy Space Center, August 7, 2019.

Agusdinata, D.B., W. Liu, H. Eakin, and H. Romero. 2018. "Socio-Environmental Impacts of Lithium Mineral Extraction: Towards a Research Agenda." *Environmental Research Letters* 13, no. 12: 16-20.

Ahn, J.M. and S. Lyu. 2020. "Selection of Priority Tributaries for Point and Non-Point Source Pollution Management." *KSCE Journal of Civil Engineering* 24, no. 4: 1060-1069..

Ajala, R., P. Persaud, J.M. Stock, G. S. Fuis, J.A. Hole, M. Goldman, and D. Scheirer. 2019. "Three-Dimensional Basin and Fault Structure From a Detailed Seismic Velocity Model of Coachella Valley, Southern California." *Journal of Geophysical Research: Solid Earth* 124*,* no. 5: 4728-4750.

Ali, M.I., G.D Dirawan, A.H. Hasim and M.R. Abidin, 2019. "Detection of Changes in Surface Water Bodies Urban Area With NDWI and MNDWI Methods. *International Journal on Advanced Science Engineering Information Technology* 9, no. 3: 946-951.

Ansari, A.A., G.S. Singh, G.R. Lanza, and W. Rast, eds. 2010. *Eutrophication: Causes, Consequences and Control* Vol. 1. Springer Science & Business Media

Armstrong, L.E. and E.C. Johnson. 2018. "Water Intake, Water Balance, and the Elusive Daily Water Requirement." *Nutrients* 10, no.12: 1-25.

Aulenbach, D.B. 1967. "Water--Our Second Most Important Natural Resource." *Boston College Industrial and Commercial Law Review* 9: 535-552.

Bartram, J. and R. Ballance, eds. 1996. *1996. Water Quality Monitoring: A Practical Guide to the Design and Implementation of Freshwater Quality Studies and Monitoring Programmes. CRC Press.*

Beck, R., S. Zhan, H. Liu, S. Tong, B. Yang, M. Xu, Z. Ye, Y. Huang, S. Shu, Q. Wu, and S. Wang. 2016. "Comparison of Satellite Reflectance Algorithms for Estimating Chlorophyll-a in a Temperate Reservoir Using Coincident Hyperspectral Aircraft Imagery and Dense Coincident Surface Observations." *Remote Sensing of Environment* 178: 15–30.

Behmel, S., M. Damour, R. Ludwig, and M.J. Rodriguez. 2016. "Water Quality Monitoring Strategies — A Review and Future Perspectives." *Science of The Total Environment* 571: 1312–29.

Bhateria, R. and D. Jain. 2016. "Water Quality Assessment of Lake Water: A Review." Sustainable *Water Resources Management* 2, no. 2: 161–73.

Biswas, A.K. 2008. “Integrated Water Resources Management: Is It Working?” *International Journal of Water Resources Development* 24, no. 1: 5–22.

Bradley, T., H. Ajami and W. Porter. 2022. “Ecological Transitions at the Salton Sea: Past, Present and Future.” *California Agriculture* 76, no. 1: 8–15.

Brezonik, P., K.D. Menken, and M. Bauer. 2005. “Landsat-Based Remote Sensing of Lake Water Quality Characteristics, Including Chlorophyll and Colored Dissolved Organic Matter (CDOM).” *Lake and Reservoir Management* 21, no. 4: 373–82.

Brothers, D.S., N.W. Driscoll, G.M. Kent, R.L. Baskin, A.J. Harding, and A.M. Kell. 2022. “Seismostratigraphic Analysis of Lake Cahuilla Sedimentation Cycles and Fault Displacement History beneath the Salton Sea, California, USA.” *Geosphere* 18, no. 4: 1354–76.

Buma, W.G. and S.I. Lee. 2020. “Evaluation of Sentinel-2 and Landsat 8 Images for Estimating Chlorophyll-a Concentrations in Lake Chad, Africa.” *Remote Sensing* 12, no. 15: 1-18.

Caballero, I., R. Fernández, O.M. Escalante, L. Mamán and G. Navarro. 2020. “New Capabilities of Sentinel-2A/B Satellites Combined with in Situ Data for Monitoring Small Harmful Algal Blooms in Complex Coastal Waters.” *Scientific Reports* 10, no. 1: 1-14.

Cannon, B.Q. 2022. “Irrigation, Reclamation, and Water Rights.” In *A Companion to American Agricultural History*, 314–26. John Wiley & Sons, Ltd.

Cantor, A., and S. Knuth. 2019. “Speculations on the Postnatural: Restoration, Accumulation, and Sacrifice at the Salton Sea.” *Environment and Planning A: Economy and Space* 51, no. 2: 527–44.

Carpelan, L.H. 1958. “The Salton Sea. Physical and Chemical Characteristics.” *Limnology and Oceanography* 3, no. 4: 373–386.

Cassidy, R., P. Jordan, M. Bechmann, B. Kronvang, K. Kyllmar, and M. Shore. 2018. “Assessments of Composite and Discrete Sampling Approaches for Water Quality Monitoring.” *Water Resources Management* 32, no. 9: 3103–3118.

Cheney, A.M., C. Newkirk, K. Rodriguez, and A. Montez. 2018. “Inequality and Health among Foreign-Born Latinos in Rural Borderland Communities.” *Social Science & Medicine* 215: 115–22.

Chipman, J.W., L.G. Olmanson, and A.A. Gitelson, 2009. “Remote Sensing Methods for Lake Management: A Guide for Resource Managers and Decision-Makers Developed By The North American Lake Management Society In Collaboration With Dartmouth College.” *Madison, WI: University of Minnesota, University of Nebraska and University of Wisconsin for the United States Environmental Protection Agency*.

Clouse, L.E., 2016. "The History, Current State, and Future of Tourism at the Salton Sea, California, USA." *Sustainability Of The Salton Sea: A Review of the Environmental, Economic, And Social Climate Around California's Largest Saline Lake*, p.48.

Cohen, M.J., 2019. Past and future of the Salton Sea.

Cohen, M.J., J.I. Morrison and E.P. Glenn, 1999. *Haven or hazard: The ecology and future of the Salton Sea*. Oakland, CA: Pacific Institute for Studies in Development, Environment and Security.

Cohn, J.P., 2000. Saving the Salton Sea. *Bioscience*, *50*(4), pp.295-301.

Crane, W.B. 1914. "The History of the Salton Sea." *Annual Publication of the Historical Society of Southern California* 9, no. 3: 215–24.

Dailey, K.R., K.A. Welch, and W.B. Lyons. 2014 "Evaluating the Influence of Road Salt on Water Quality of Ohio Rivers over Time." *Applied Geochemistry* 47: 25–35.

Damalas, C.A. 2009. Understanding Benefits and Risks of Pesticide Use. *Scientific Research and Essays* 4, no. 10: 945-949.

Damalas, C.A. and I.G. Eleftherohorinos. 2011. "Pesticide Exposure, Safety Issues, and Risk Assessment Indicators. *International Journal of Environmental Research and Public Health* 8, no. 5: 1402-1419.

Das, S., S. Kaur, and A. Jutla. 2021. "Earth Observations Based Assessment of Impact of COVID-19 Lockdown on Surface Water Quality of Buddha Nala, Punjab, India." *Water* 13, no. 10: 1-15.

Delfino, K. 2006. "Salton Sea Restoration: Can There Be Salvation for the Sea." *Pacific McGeorge Global Business & Development Law Journal* 19, no. 1: 157-172.

Doede, A.L. and P.B. DeGuzman. 2020. "The Disappearing Lake: A Historical Analysis of Drought and the Salton Sea in the Context of the GeoHealth Framework." *GeoHealth* 4, no. 9: 1-12.

Dorgham, M.M. 2014. "Effects of Eutrophication". In *Eutrophication: Causes, Consequences and Control: Volume 2*, 29-44. Springer Netherlands.

Droppo, I.G. 2001. "Rethinking What Constitutes Suspended Sediment." *Hydrological Processes* 15, no. 9: 1551–1564.

Dwyer, J.L., D.P. Roy, B. Sauer, C.B. Jenkerson, H.K. Zhang, and L. Lymburner. 2018. "Analysis Ready Data: Enabling Analysis of the Landsat Archive." *Remote Sensing* 10, no. 9: 1-19.

Elahi, E., C. Weijun, H. Zhang, and M. Nazeer. 2019. “Agricultural Intensification and Damages to Human Health in Relation to Agrochemicals: Application of Artificial Intelligence.” *Land Use Policy* 83: 461–74.

EPA. 2017. Quick guide to drinking water sample collection - *US EPA*. Environmental Protection Agency

EPA. 2022a. Indicators: Chlorophyll a. Environmental Protection Agency.

EPA. 2022b. Indicators: Chlorophyll a. Environmental Protection Agency.

Esri. n.d. What they don't tell you about regression analysis (no date) What they don't tell you about regression analysis-ArcGIS Pro | Documentation.

Farzan, S.F., M. Razafy, S.P. Eckel, L. Olmedo, E. Bejarano, and J.E. Johnston. 2019. “Assessment of Respiratory Health Symptoms and Asthma in Children near a Drying Saline Lake.” *International Journal of Environmental Research and Public Health* 16, no. 20: 1-15.

Forsman, T.N. 2014. “What the QSA Means for the Salton Sea: California’s Big Blank Check.” *Arizona State Law Journal* 46: 365-387.

Gagnon, B., G. Marcoux, R. Leduc, M.F. Pouet, and O. Thomas. 2007. “Emerging Tools and Sustainability of Water-Quality Monitoring.” *TrAC Trends in Analytical Chemistry, Emerging Tools as a New Approach for Water Monitoring* 26, no.4: 308–314.

Gammon, K. 2022. As Lithium Drilling Advances at the Salton Sea, Researchers Work out the Details. KCET.

Gao, B.C. 1996. “NDWI—A Normalized Difference Water Index for Remote Sensing of Vegetation Liquid Water from Space.” *Remote Sensing of Environment* 58, no. 3: 257–266.

Gao, J., J. Liu, R. Xu, S. Pandey, V.S.K.S Vankayala Siva, and D. Yu. 2022. “Environmental Pollution Analysis and Impact Study—A Case Study for the Salton Sea in California.” *Atmosphere* 13, no. 6: 1-23.

Gao, Y., J.P. Walker, M. Allahmoradi, A. Monerris, D. Ryu, and T.J. Jackson. 2015. “Optical Sensing of Vegetation Water Content: A Synthesis Study.” *IEEE Journal of Selected Topics in Applied Earth Observations and Remote Sensing* 8, no. 4: 1456–1464.

Garg, V., S.P. Aggarwal, and P. Chauhan. 2020. “Changes in Turbidity along Ganga River Using Sentinel-2 Satellite Data during Lockdown Associated with COVID-19.” *Geomatics, Natural Hazards and Risk* 11, no. 1: 1175–1195.

Garry, V. F. “Pesticides and Children*.” Toxicology and Applied Pharmacology*, Special Pediatric Volume 198, no. 2: 152–63. https://doi.org/10.1016/j.taap.2003.11.027.

Gholizadeh, M.H., A.M. Melesse, and L. Reddi. 2016. “A Comprehensive Review on Water Quality Parameters Estimation Using Remote Sensing Techniques.” *Sensor*s 1, no. 8: 1298.

Glenn, E.P., M.J. Cohen, J.I. Morrison, C. Valdés-Casillas, and K. Fitzsimmons. 1999. “Science and Policy Dilemmas in the Management of Agricultural Waste Waters: The Case of the Salton Sea, CA, USA.” *Environmental Science & Policy* 2, no. 4: 413–423.

Gobalet, K.W. and T.A. Wake. 2000. “Archaeological and Paleontological Fish Remains from the Salton Basin, Southern California.” *The Southwestern Naturalist* 45, no. 4: 514–520.

Goodchild, M.F. and L. Li. 2012. “Assuring the Quality of Volunteered Geographic Information.” *Spatial Statistics* 1: 110–120.

Gorde, S.P. and M.V. Jadhav. 2013. “Assessment of Water Quality Parameters: A Review.” *J Eng Res Appl* 3, no. 6: 2029-2035.

Goward, S., T. Arvidson, D. Williams, J. Faundeen, J. Irons, and S. Franks. 2006. “Historical Record of Landsat Global Coverage.” *Photogrammetric Engineering & Remote Sensing* 72*,* no. 10: 1155-1169.

Gutierrez, A., 2009. Dead Fish in the Desert: A Brief Photo-History of The Salton Sea. *History in the Making*, *2*(1), p.8.

Haftendorn, H.. 2000. “Water and International Conflict.” *Third World Quarterly* 21, no.1: 51–68.

Haibo, Y., W. Zongmin, Z. Hongling, and G. Yu, 2011. “Water Body Extraction Methods Study Based on RS and GIS.” Procedia Environmental Sciences, 2011 3rd International Conference on Environmental Science and Information Application Technology ESIAT 2011, 10 (January): 2619–24.

Hasmadi, M., H.Z. Pakhriazad, and M.F. Shahrin, 2009. “Evaluating Supervised and Unsupervised Techniques for Land Cover Mapping Using Remote Sensing Data.” *Geografia : Malaysian Journal of Society and Space* 5, no.1: 1–10.

Harrold, Z., M.M. Arienzo, M. Collins, J.M. Davidson, X. Bai, S. Sukumaran and J. Umek, 2022. “A Peristaltic Pump and Filter-Based Method for Aqueous Microplastic Sampling and Analysis.” *ACS ES&T Water* 2, no.2: 268–77.

Holdren, G.C. and A. Montaño. 2002. “Chemical and Physical Characteristics of the Salton Sea, California.” *Hydrobiologia* 473, no. 1: 1–21.

Hua, A.K., 2017. “Land Use Land Cover Changes in Detection of Water Quality: A Study Based on Remote Sensing and Multivariate Statistics.” *Journal of Environmental and Public Health 2017* (March): e7515130.

Hughes, B., 2020. “Turning Off the Tap: Will California Let the Salton Sea Go Down the Drain?” *California Western Law Review* 56, no. 1: 245-281.

Irons, J.R. and J.L. Dwyer. 2010. “An Overview of the Landsat Data Continuity Mission.” *Remote Sensing of Environment* 122: 11-21

Jiang, W., Y. Ni, Z. Pang, X. Li, H. Ju, G. He, J. Lv, K. Yang, J. Fu, and X. Qin, 2021. “An Effective Water Body Extraction Method with New Water Index for Sentinel-2 Imagery.” *Water* 13, no. 12: 1-17.

Johnston, J.E., M. Razafy, H. Lugo, L. Olmedo, and S.F. Farzan. 2019. “The Disappearing Salton Sea: A Critical Reflection on the Emerging Environmental Threat of Disappearing Saline Lakes and Potential Impacts on Children’s Health.” *Science of The Total Environment* 663: 804–17.

Jones, B.A. and J. Fleck. 2020. “Shrinking Lakes, Air Pollution, and Human Health: Evidence from California’s Salton Sea.” *Science of The Total Environment* 712 : 136490.

Kamerosky, A., H.J. Cho,. and L. Morris, 2015. “Monitoring of the 2011 Super Algal Bloom in Indian River Lagoon, FL, USA, Using MERIS.” Remote Sensing 7 (2): 1441–60.

Karimi, B., S.H. Hashemi and H. Aghighi, 2022. “Performance of Sentinel-2 and Landsat-8 Satellites in Estimating Chlorophyll-a Concentration in a Shallow Freshwater Lake.” Preprint. In Review.

Keiser, D.A. and J.S. Shapiro, 2019. “Consequences of the Clean Water Act and the Demand for Water Quality.” The Quarterly Journal of Economics 134 (1): 349–96..

Kennan, G., 1917. *The Salton Sea: An Account of Harriman’s Fight with the Colorado River*. Macmillan.

Kershner, F.D. 1953. “George Chaffey and the Irrigation Frontier.” *Agricultural History* 27, no. 4: 115–122.

Kim, K.H., E. Kabir, and S.A. Jahan. 2017. “Exposure to Pesticides and the Associated Human Health Effects.” *Science of The Total Environment* 575: 525–535.

King, J., V. Etyemezian, M. Sweeney, B.J. Buck, and G. Nikolich. 2011. “Dust Emission Variability at the Salton Sea, California, USA.” *Aeolian Research*, AGU Fall Meeting session on Aeolian Dust: Transport Processes, Anthropogenic Forces and Biogeochemical Cycling, 3 (1): 67–79.

“Landsat Science.” n.d. NASA. NASA. Accessed May 7, 2021.

Laylander, D. 1997. “The Last Days of Lake Cahuilla: The Elmore Site.” *Pacific Coast Archaeological Society Quarterly* 33, no. 2: 1-138.

Lednicka, B. and M. Kubacka. 2022. “Semi-Empirical Model of Remote-Sensing Reflectance for Chosen Areas of the Southern Baltic.” *Sensors* 22, no. 3: 1-23.

Lee, G.F., Jones, R.A. and Newbry, B.W. 1982. “Water Quality Standards and Water Quality.” *Journal (Water Pollution Control Federation)*: 1131-1138.

Lee, Z.P., 2006. Remote Sensing of Inherent Optical Properties: Fundamentals, Tests of Algorithms, and Applications. International Ocean Colour Coordinating Group (IOCCG).

Lewis, E.L. and R.G. Perkin, 1978. “Salinity: Its Definition and Calculation.” Journal of Geophysical Research: Oceans 83 (C1): 466–78. https://doi.org/10.1029/JC083iC01p00466.

Levers, L.R., T.H. Skaggs and K.A. Schwabe, 2019. “Buying Water for the Environment: A Hydro-Economic Analysis of Salton Sea Inflows.” Agricultural Water Management 213 (March): 554–67. https://doi.org/10.1016/j.agwat.2018.10.041.

Loveland, T.R. and J.L. Dwyer, 2012. “Landsat: Building a Strong Future.” Remote Sensing of Environment, Landsat Legacy Special Issue, 122 (July): 22–29. https://doi.org/10.1016/j.rse.2011.09.022.

Lichtenberg, E., 2002. “Chapter 23 Agriculture and the Environment.” In Handbook of Agricultural Economics, 2:1249–1313. Agriculture and Its External Linkages. Elsevier. https://doi.org/10.1016/S1574-0072(02)10005-3.

Lin, S.S., S.L. Shen, A. Zhou and H.M. Lyu, 2021. “Assessment and Management of Lake Eutrophication: A Case Study in Lake Erhai, China.” Science of The Total Environment 751 (January): 141618. https://doi.org/10.1016/j.scitotenv.2020.141618.

Ling, F., G.M. Foody, H. Du, X. Ban, X. Li, Y. Zhang and Y. Du, 2017. “Monitoring Thermal Pollution in Rivers Downstream of Dams with Landsat ETM+ Thermal Infrared Images.” Remote Sensing 9 (11): 1175. https://doi.org/10.3390/rs9111175.MacDougal, D.T., 1907. *The Desert Basins of the Colorado Delta. American Geographical Society.*

Madrid, Y. and Z.P. Zayas, 2007. “Water Sampling: Traditional Methods and New Approaches in Water Sampling Strategy.” TrAC Trends in Analytical Chemistry, Emerging tools as a new approach for water monitoring, 26 (4): 293–99. https://doi.org/10.1016/j.trac.2007.01.002.

Malmqvist, B. and S. Rundle, 2002. “Threats to the Running Water Ecosystems of the World.” Environmental Conservation 29 (2): 134–53. https://doi.org/10.1017/S0376892902000097.

Marshall, J.R., 2017. “Why Emergency Physicians Should Care About the Salton Sea.” Western Journal of Emergency Medicine 18 (6): 1008. https://doi.org/10.5811/westjem.2017.8.36034

Marti-Cardona, B., T.E. Steissberg, S.G. Schladow and S.J. Hook, 2008. Relating fish kills to upwellings and wind patterns in the Salton Sea. In The Salton Sea Centennial Symposium (pp. 85-95). Springer, Dordrecht.

Martin, L., 2019. What Are the Roles of Chlorophyll A & B?. Sciencing.

Matamoros, V., 2012. Equipment for water sampling including sensors.

McFeeters, S.K., 1996. "The Use of the Normalized Difference Water Index (NDWI) in the Delineation of Open Water Features." International Journal of Remote Sensing 17 (7): 1425–32. https://doi.org/10.1080/01431169608948714.

Mead, S.J.F., 2016. A Green Oasis in the Desert: The History of Immigration in the Imperial Valley. *Sustainability Of The Salton Sea: A Review Of The Environmental, Economic, And Social Climate Around California's Largest Saline Lake*, p.43.

Mejía Ávila, D., F. Torres-Bejarano and Z. Martínez Lara, 2022. "Spectral Indices for Estimating Total Dissolved Solids in Freshwater Wetlands Using Semi-Empirical Models. A Case Study of Guartinaja and Momil Wetlands." International Journal of Remote Sensing 43 (6): 2156–84. https://doi.org/10.1080/01431161.2022.2057205.'

Miller, W. and A. Rango, 1984. "Using Heat Capacity Mapping Mission (Hcmm) Data to Assess Lake Water Quality1." JAWRA Journal of the American Water Resources Association 20 (4): 493–501. https://doi.org/10.1111/j.1752-1688.1984.tb02831.x.

Mishra, S. and D.R. Mishra, 2012. "Normalized Difference Chlorophyll Index: A Novel Model for Remote Estimation of Chlorophyll-a Concentration in Turbid Productive Waters." Remote Sensing of Environment, Remote Sensing of Urban Environments, 117 (February): 394–406. https://doi.org/10.1016/j.rse.2011.10.016.

Mishra, D.R., B.A. Schaeffer and D. Keith, 2014. "Performance Evaluation of Normalized Difference Chlorophyll Index in Northern Gulf of Mexico Estuaries Using the Hyperspectral Imager for the Coastal Ocean." GIScience & Remote Sensing 51 (2): 175–98. https://doi.org/10.1080/15481603.2014.895581.

Morel, A.Y. and H.R. Gordon, 1980. "Report of the Working Group on Water Color." Boundary-Layer Meteorology 18 (3): 343–55. https://doi.org/10.1007/BF00122030.

Moses, M., E.S. Johnson, W.K. Anger, V.W. Burse, S.W. Horstman, R.J. Jackson, R.G. Lewis, K.T Maddy, R. McConnell, W.J. Meggs and S.H. Zahm, 1993. "Environmental Equity and Pesticide Exposure." Toxicology and Industrial Health 9 (5): 913–59. https://doi.org/10.1177/074823379300900512.

National Geographic Society, 2019. Freshwater Resources. *National Geographic Society*. Accessed March 17, 2022.

Neary, D.G., G.G. Ice and C.R. Jackson, 2009. "Linkages between Forest Soils and Water Quality and Quantity." Forest Ecology and Management, 258 (10): 2269–81. https://doi.org/10.1016/j.foreco.2009.05.027.

Nielsen, D.L., M.A. Brock, G.N. Rees and D.S. Baldwin, 2003. "Effects of Increasing Salinity on Freshwater Ecosystems in Australia." Australian Journal of Botany 51 (6): 655–65. https://doi.org/10.1071/bt02115.

Niepytalska, M. and P. Warschau, 2019. *The Salton Sea: An Eco-biography of California's Largest Lake* (Doctoral dissertation, Universitätsbibliothek der Ludwig-Maximilians-Universität).

Nugroho, J.T., 2013. Identification of Inundated Area Using Normalized Difference Water Index (NDWI) on Lowland Region of Java Island. *International Journal of Remote Sensing and Earth Sciences (IJReSES)*, *10*(2).

Obianyo, J.I., 2019. "Effect of Salinity on Evaporation and the Water Cycle." Emerging Science Journal 3 (4): 255–62. https://doi.org/10.28991/esj-2019-01188.

Ogashawara, I., L. Li and M.J. Moreno-Madriñán, 2016. "Slope Algorithm to Map Algal Blooms in Inland Waters for Landsat 8/Operational Land Imager Images." Journal of Applied Remote Sensing 11 (1): 012005. https://doi.org/10.1117/1.JRS.11.012005.

Omer, N.H., 2019. "Water Quality Parameters." In Water Quality - Science, Assessments and Policy, edited by Kevin Summers. IntechOpen. https://doi.org/10.5772/intechopen.89657.

Parajuli, S.P. and C.S. Zender, 2018. "Projected Changes in Dust Emissions and Regional Air Quality Due to the Shrinking Salton Sea." Aeolian Research 33 (August): 82–92. https://doi.org/10.1016/j.aeolia.2018.05.004.

Payán-Rentería, R., G. Garibay-Chavez, R. Rangel-Ascencio, V. Preciado-Martinez, L. Munoz-Islas, C. Beltrán-Miranda, S. Mena-Munguía, L. Jave-Suárez, A. Feria-Velasco and R. De Celis, 2012. "Effect of Chronic Pesticide Exposure in Farm Workers of a Mexico Community." Archives of Environmental & Occupational Health 67 (1): 22–30. https://doi.org/10.1080/19338244.2011.564230.

Picone, K., 2021. "Salton Sea: The Rise and Fall of a Toxic California Lake." All That's Interesting. All That's Interesting.

Pillsbury-Coyne, A., 2018. Policy Trials and Tribulations of the Salton Sea. UC San Diego: Climate Science and Policy.

Poole, G.C., J.B. Dunham, D.M. Keenan, S.T. Sauter, S.T., D.A. McCULLOUGH, C. Mebane, J.C. Lockwood, D.A. Essig, M.P Hicks, D.J. Sturdevant and E.J. Materna, 2004. "The Case for Regime-Based Water Quality Standards." BioScience 54 (2): 155–61. https://doi.org/10.1641/0006-3568(2004)054[0155:TCFRWQ]2.0.CO;2

Potapov, P.V., S.A. Turubanova, M.C. Hansen, B. Adusei, M. Broich, A. Altstatt, L. Mane and C.O. Justice, 2012. "Quantifying Forest Cover Loss in Democratic Republic of the Congo, 2000–2010, with Landsat ETM+ Data." Remote Sensing of Environment, Landsat Legacy Special Issue, 122 (July): 106–16. https://doi.org/10.1016/j.rse.2011.08.027..

Qin, B., G. Gao, G. Zhu, Y. Zhang, Y. Song, X. Tang, H. Xu and J. Deng. 2013. "Lake Eutrophication and Its Ecosystem Response." Chinese Science Bulletin 58 (9): 961–70. https://doi.org/10.1007/s11434-012-5560-x.

Ramadas, M. and A.K. Samantaray, 2018. "Applications of Remote Sensing and GIS in Water Quality Monitoring and Remediation: A State-of-the-Art Review." In Water Remediation, edited by Shantanu Bhattacharya, Akhilendra Bhushan Gupta, Ankur Gupta, and Ashok Pandey, 225–46. Energy, Environment, and Sustainability. Singapore: Springer. https://doi.org/10.1007/978-981-10-7551-3_13.

Råman Vinnå, L., A. Wüest and D. Bouffard, 2017. "Physical Effects of Thermal Pollution in Lakes: Physical Effects of Thermal Pollution." Water Resources Research 53 (5): 3968–87. https://doi.org/10.1002/2016WR019686.

Reis, S. 2008. "Analyzing Land Use/Land Cover Changes Using Remote Sensing and GIS in Rize, North-East Turkey." *Sensors* 8, no. 10: 6188–6202. https://doi.org/10.3390/s8106188.

Riedel, R., 2016. "Trends of Abundance of Salton Sea Fish: A Reversible Collapse or a Permanent Condition?" *Natural Resources* 07, no.10: 535. https://doi.org/10.4236/nr.2016.710045.

Richards, J.A., 2022. "Supervised Classification Techniques." In Remote Sensing Digital Image Analysis, edited by John A. Richards, 263–367. Cham: Springer International Publishing. https://doi.org/10.1007/978-3-030-82327-6_8.

Ritchie J.C., F.R. Schiebe, and J.R. McHenry, 1976. "Remote Sensing of Suspended Sediments in Surface Waters." *Photogramm. Eng. Remote Sens* 42: 1539-1545.

Ritchie, J.C., P.V. Zimba and J.H. Everitt, 2003. "Remote Sensing Techniques to Assess Water Quality." *Photogrammetric Engineering & Remote Sensing* 69, no. 6: 695–704. https://doi.org/10.14358/PERS.69.6.695.

Rockwell, T.K., A.J. Meltzner, and E.C. Haaker, 2018. Dates of the two most recent surface ruptures on the southernmost San Andreas fault recalculated by precise dating of Lake Cahuilla dry periods. *Bulletin of the Seismological Society of America*, *108*(5A), pp.2634-2649.

Ross, J.E., 2020. Formation of California's Salton Sea in 1905–07 was not "accidental". In *Changing Facies: The 2020 desert symposium field guide and proceedings* (pp. 103-116). Zzyzx, CA: Desert Symposium.

Rwanga, S.S. and J.M. Ndambuki. 2017."Accuracy Assessment of Land Use/Land Cover Classification Using Remote Sensing and GIS." *International Journal of Geosciences* 8, no.04: 611. https://doi.org/10.4236/ijg.2017.84033.

Rockwell, T.K., A.J. Meltzner and E.C. Haaker. 2018. "Dates of the Two Most Recent Surface Ruptures on the Southernmost San Andreas Fault Recalculated by Precise Dating of Lake Cahuilla Dry Periods." *Bulletin of the Seismological Society of America* 108, no.5A: 2634–2649. https://doi.org/10.1785/0120170392.

Rode, E. and J. Wilson, 2022. "Lithium Valley: A Look at the Major Players near the Salton Sea Seeking Billions in Funding." The Desert Sun. Palm Springs Desert Sun, May 15, 2022.

Roland, F., V.L.M. Huszar, V.F. Farjalla, A. Enrich-Prast, A.M. Amado, and J.P.H.B. Ometto, 2012. "Climate Change in Brazil: Perspective on the Biogeochemistry of Inland Waters." *Brazilian Journal of Biology* 72: 709–22. https://doi.org/10.1590/S1519-69842012000400009.

Roy, P.S., M.D. Behera, and S.K. Srivastav. 2017. "Satellite Remote Sensing: Sensors, Applications and Techniques." *Proceedings of the National Academy of Sciences, India Section A: Physical Sciences* 87, no.4: 465–72. https://doi.org/10.1007/s40010-017-0428-8.

Sanderson, R. 2010. "Introduction to Remote Sensing." *New Mexico State University*: 25-26.

Saravanan, V.S., G.T. McDonald, and P.P. Mollinga. 2009. "Critical Review of Integrated Water Resources Management: Moving beyond Polarised Discourse." *Natural Resources Forum* 33, no. 1: 76–86. https://doi.org/10.1111/j.1477-8947.2009.01210.x.

Savenije, H.H. and P. Van der Zaag. 2008. "Integrated Water Resources Management: Concepts and Issues." *Physics and Chemistry of the Earth, Parts A/B/C, Integrated Water Resources Management in a Changing World* 33, no. 5: 290–97. https://doi.org/10.1016/j.pce.2008.02.003.

Scafutto, R.D.P.M. and C.R. de Souza Filho, 2018. "Detection of Methane Plumes Using Airborne Midwave Infrared (3–5 Mm) Hyperspectral Data." Remote Sensing 10 (8): 1237. https://doi.org/10.3390/rs10081237.

Scaramuzza, P. and J. Barsi, 2005, October. Landsat 7 scan line corrector-off gap-filled product development. In *Proceeding of Pecora* (Vol. 16, pp. 23-27).

Schaeffer, B.A., K.G. Schaeffer, D. Keith, R.S. Lunetta, R. Conmy and R.W. Gould. 2013. "Barriers to Adopting Satellite Remote Sensing for Water Quality Management." *International Journal of Remote Sensing* 34, no. 21: 7534–44. https://doi.org/10.1080/01431161.2013.823524.

Setmire, J., C. Holdren, D. Robertson, C. Amrhein, J. Elder, R. Schroeder, G. Schladow, H. McKellar, and R. Gersberg, 2000, September. Eutrophic conditions at the Salton Sea.

In *A topical paper from the Eutrophication Workshop convened at the University of California at Riverside*.

Sheikh, P.A. and C.V. Stern, 2020. Salton Sea Restoration. LIBRARY OF CONGRESS WASHINGTON DC.

Sherman, D.J., C. Houser and A.C. Baas. 2013. "Electronic Measurement Techniques for Field Experiments in Process Geomorphology." *Treatise on Geomorphology*: 195–221. https://doi.org/10.1016/B978-0-12-374739-6.00401-2.

Smith, V.H. and D.W. Schindler. 2009. "Eutrophication Science: Where Do We Go From Here?" *Trends in ecology & evolution 24,* no. 4: 201-207.

Spehar, R., D. Taylor, and S. Cormier. 2022. *EPA*. Environmental Protection Agency.

Stanley, M. 2022. *Point source and nonpoint sources of Pollution*, *National Geographic Society*.

Strobl, R.O. and P.D. Robillard. 2008. "Network Design for Water Quality Monitoring of Surface Freshwaters: A Review." Journal of Environmental Management, Microbial and Nutrient Contaminants of Fresh and Coastal Waters, 87 (4): 639–48. https://doi.org/10.1016/j.jenvman.2007.03.001.

Tas, B., O. Can, and Z. Koloren. 2011. "Investigation on Photosynthetic Pigments Content of Lotic Systems (Blacksea River Basin, Ordu-Turkey). *Structure 1*: 417-426.

Taylor, M., 2018. "The Salton Sea: A Status Update". *Sacramento, CA: Legislative Analysts*.

The Associated Press. 2015. "History of the Salton Sea." Tribune. San Diego Union-Tribune.

Tompson, A.F. 2016. "Born from a Flood: The Salton Sea and Its Story of Survival." *Journal of Earth Science* 27, no. 1: 89–97. https://doi.org/10.1007/s12583-016-0630-7.

Topp, S.N., T.M. Pavelsky, D. Jensen, M. Simard, and M.R. Ross. 2020. "Research Trends in the Use of Remote Sensing for Inland Water Quality Science: Moving Towards Multidisciplinary Applications." *Water* 12, no. 1: 1-34. https://doi.org/10.3390/w12010169.

Tran, T.V., R. Reef, and X. Zhu. 2022. "A Review of Spectral Indices for Mangrove Remote Sensing". *Remote Sensing* 14, no. 19: 1-29. https://doi.org/10.3390/rs14194868.

Tucker, C.J. 1979. "Red and Photographic Infrared Linear Combinations for Monitoring Vegetation." *Remote Sensing of Environment* 8, no. 2: 127–150. https://doi.org/10.1016/0034-4257(79)90013-0.

Usali, N. and M.H. Ismail. 2010. "Use of Remote Sensing and GIS in Monitoring Water Quality." *Journal of Sustainable Development* 3, no. 3: 228-238. https://doi.org/10.5539/jsd.v3n3p228.

U.S. Environmental Protection Agency. 2022. *What are Water Quality Standards?*, *EPA*. Environmental Protection Agency.

U.S. Geological Survey, Water quality information by topic completed. *Water Quality Information by Topic | U.S. Geological Survey*. Accessed March 21, 2022.

U.S. Geological Survey, What is remote sensing and what is it used for? *What is remote sensing and what is it used for? | U.S. Geological Survey*. Accessed March 21, 2022.

Vasistha, P. and R. Ganguly. 2020. "Water Quality Assessment of Natural Lakes and Its Importance: An Overview." *Materials Today: Proceedings*, 3rd International Conference on Innovative Technologies for Clean and Sustainable Development, 32: 544–52. https://doi.org/10.1016/j.matpr.2020.02.092.

Ventura, S., 2020. "Selective Recovery of Lithium from Geothermal Brines." Accessed June 20, 2022.

Verones, F., M.M. Hanafiah, S. Pfister, M.A. Huijbregts, G.J. Pelletier and A. Koehler, 2010. Characterization factors for thermal pollution in freshwater aquatic environments. *Environmental Science & Technology*, *44*(24), pp.9364-9369.

Vessey, K.B. 2000. "Salton: A Sea of Controversy." *Journal of College Science Teaching* 30, no. 1: 67-69.

Viñas, M.J., 2012. *Notes from the field - measuring salinity from space*, *NASA*. NASA.

Vizzo, E.C. 2017. "The Salton Sea: An Unfished and Quickly Loved Foray." *The Trumpeter* 33, no.1: 81-91.

Waghmare, B. and M. Suryawanshi. 2017. A Review-Remote Sensing. *Int. J. Eng. Res. Appl* 7, no. 6: 52-54.

Wang, G., S. Mang, H. Cai, S. Liu, Z. Zhang, L. Wang, and J.L. Innes. 2016. "Integrated Watershed Management: Evolution, Development and Emerging Trends." *Journal of Forestry Research* 27, no. 5: 967–94. https://doi.org/10.1007/s11676-016-0293-3.

Wang, F. and Y.J. Xu. 2012. "Remote Sensing to Predict Estuarine Water Salinity." *Environmental Remote Sensing and Systems Analysis*; 85-108.

Wang, X. and W. Yang. 2019. "Water Quality Monitoring and Evaluation Using Remote Sensing Techniques in China: A Systematic Review. *Ecosystem Health and Sustainability* 5, no. 1: 47-56. https://doi.org/10.1080/20964129.2019.1571443.

Wanger, T.C. 2011. "The Lithium Future—Resources, Recycling, and the Environment." *Conservation Letters* 4, no. 3: 202-206. https://doi.org/10.1111/j.1755-263X.2011.00166.x.

Watanabe, F.S.Y., E. Alcântara, T.W.P. Rodrigues, N.N. Imai, C.C.F. Barbosa and L.H.D.S. Rotta. 2015. "Estimation of Chlorophyll-a Concentration and the Trophic State of the Barra Bonita Hydroelectric Reservoir Using OLI/Landsat-8 Images." *International Journal of Environmental Research and Public Health* 12, no. 9: 10391-10417.

Waters, M.R. 1983. "Late Holocene Lacustrine Chronology and Archaeology of Ancient Lake Cahuilla, California." *Quaternary Research* 19, no. 3: 373–387. https://doi.org/10.1016/0033-5894(83)90042-X.

Williams, D.L., S. Goward, and T. Arvidson, 2006. "Landsat: Yesterday, Today, and Tomorrow." *Photogrammetric Engineering & Remote Sensing* 72, no.10: 1171-1178.

Wu, Z., G. Snyder, C. Vadnais, R. Arora, M. Babcock, G. Stensaas, P. Doucette, and T. Newman, 2019. "User Needs for Future Landsat Missions." *Remote Sensing of Environment* 231 : 1-13. https://doi.org/10.1016/j.rse.2019.111214.

Wulder, M.A., T.R. Loveland, D.P. Roy, C.J. Crawford, J.G. Masek, C.E. Woodcock, R.G. Allen, M.C. Anderson, A.S. Belward, W.B. Cohen, and J. Dwyer. 2019. "Current Status of Landsat Program, Science, and Applications." *Remote Sensing of Environment* 225: 127–47. https://doi.org/10.1016/j.rse.2019.02.015.

Wulder, M.A., D.P. Roy, V.C. Radeloff, T.R. Loveland, M.C. Anderson, D.M. Johnson, S. Healey, Z. Zhu, T.A. Scambos, N. Pahlevan, and M. Hansen. 2022. "Fifty Years of Landsat Science and Impacts." *Remote Sensing of Environment* 280: 1-21. https://doi.org/10.1016/j.rse.2022.113195.

Xu, H. 2006. "Modification of Normalised Difference Water Index (NDWI) to Enhance Open Water Features in Remotely Sensed Imagery." *International Journal of Remote Sensing* 27, no. 14: 3025–3033. https://doi.org/10.1080/01431160600589179.

Xu, M., H. Liu, R. Beck, J. Lekki, B. Yang, S. Shu, E.L. Kang, R. Anderson, E. Johansen, E. Emery and M. Reif. 2019a. "A Spectral Space Partition Guided Ensemble Method for Retrieving Chlorophyll-a Concentration in Inland Waters from Sentinel-2A Satellite Imagery. *Journal of Great Lakes Research* 45, no. 3: 454-465.

Xu, M., H. Liu, R. Beck, J. Lekki, B. Yang, S. Shu, Y. Liu, T. Benko, R. Anderson, R. Tokars, and R. Johansen. 2019b. "Regionally and Locally Adaptive Models for Retrieving Chlorophyll-a Concentration in Inland Waters From Remotely Sensed Multispectral and Hyperspectral Imagery*." IEEE Transactions on Geoscience and Remote Sensing* 57, no. 7: 4758–4774. https://doi.org/10.1109/TGRS.2019.2892899

Yang, J. and X. Du. 2017. "An Enhanced Water Index in Extracting Water Bodies from Landsat TM Imagery." *Annals of GI*S 23, no. 3: 141–48. https://doi.org/10.1080/19475683.2017.1340339.

Yang, W., S.L. Carmichael, E.M. Roberts, S.E. Kegley, A.M. Padula, P.B. English, and G.M. Shaw. 2014. "Residential Agricultural Pesticide Exposures and Risk of Neural Tube Defects and Orofacial Clefts Among Offspring in the San Joaquin Valley of California."

American Journal of Epidemiology 179, no. 6: 740–748. https://doi.org/10.1093/aje/kwt324.

Yue, H., Y. Li, J. Qian, and Y. Liu. 2020. "A New Accuracy Evaluation Method for Water Body Extraction." *International Journal of Remote Sensing* 41, no. 19: 7311–7342. https://doi.org/10.1080/01431161.2020.1755740.

Zhu, L., J. Suomalainen, J. Liu, J. Hyyppä, H. Kaartinen and H. Haggren. 2018. "A Review: Remote Sensing Sensors." In *Multi-Purposeful Application of Geospatial Data*, edited by Rustam B. Rustamov, Sabina Hasanova, and Mahfuza H. Zeynalova. InTech. https://doi.org/10.5772/intechopen.71049.

Appendix: A Distributions of NDCI Values

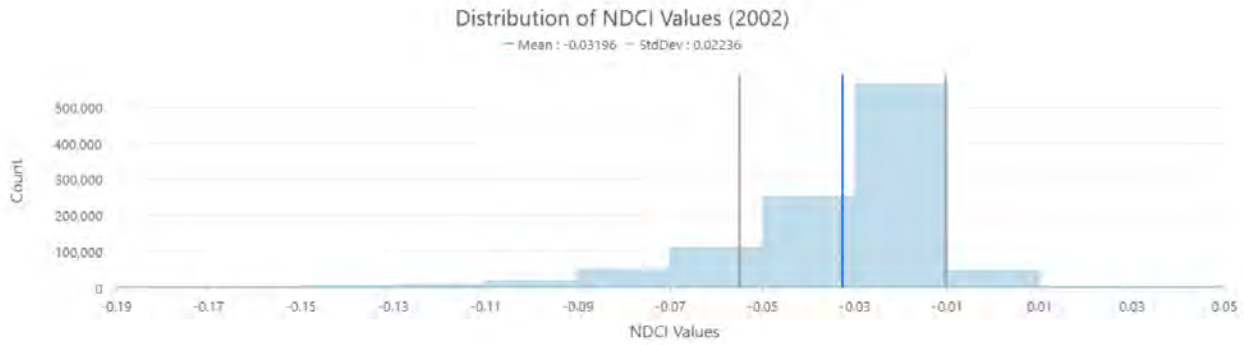
Distribution of NDCI Values (2002)
Mean : -0.03196 StdDev : 0.02236
Count
500,000
400,000
300,000
200,000
100,000
0
-0.19 -0.17 -0.15 -0.13 -0.11 -0.09 -0.07 -0.05 -0.03 -0.01 0.01 0.03 0.05
NDCI Values

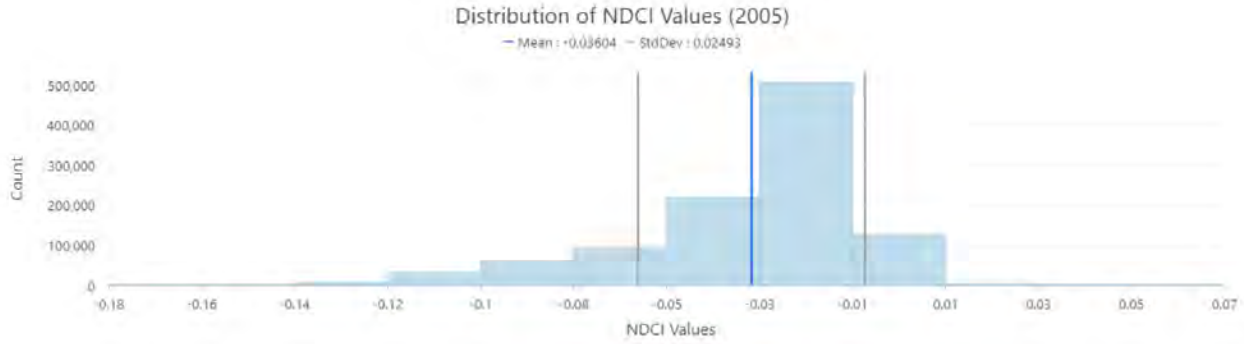
Distribution of NDCI Values (2005)
Mean : -0.03604 StdDev : 0.02493
Count
500,000
400,000
300,000
200,000
100,000
0
-0.18 -0.16 -0.14 -0.12 -0.1 -0.08 -0.05 -0.03 -0.01 0.01 0.03 0.05 0.07
NDCI Values

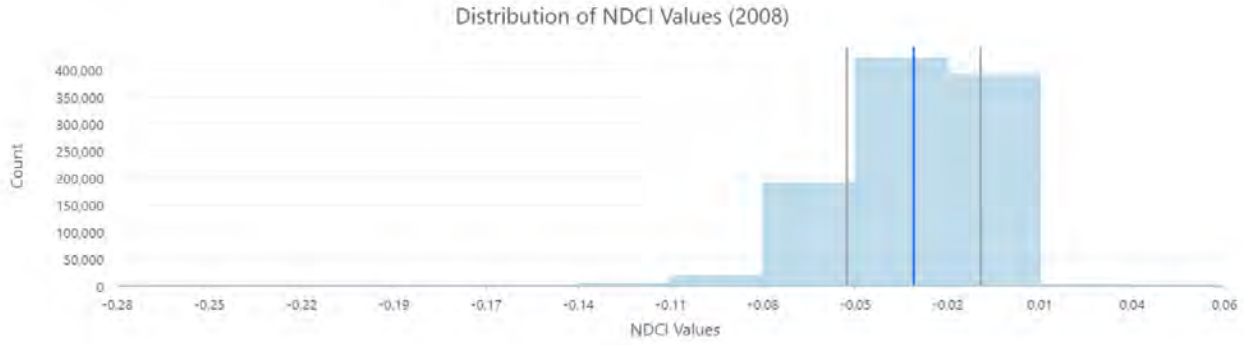
Distribution of NDCI Values (2008)
Count
400,000
350,000
300,000
250,000
200,000
150,000
100,000
50,000
0
-0.28 -0.25 -0.22 -0.19 -0.17 -0.14 -0.11 -0.08 -0.05 -0.02 0.01 0.04 0.06
NDCI Values

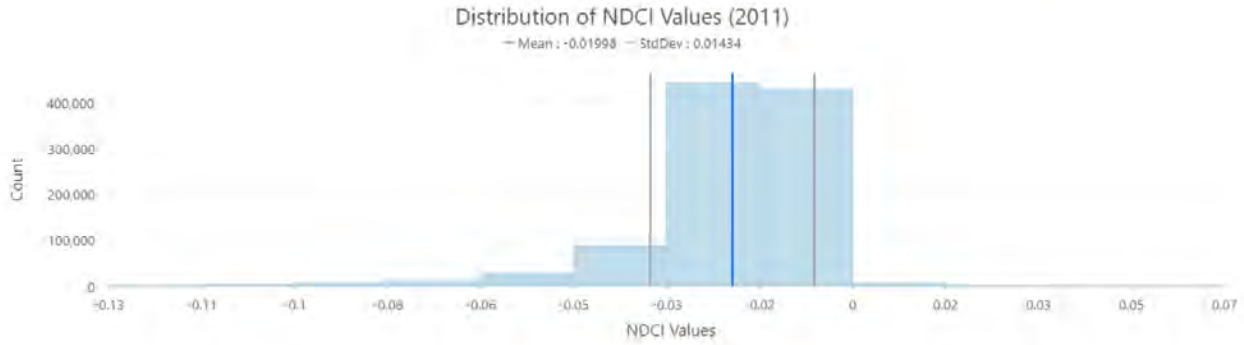
Distribution of NDCI Values (2011)
Mean : -0.01998 StdDev : 0.01434
Count
400,000
300,000
200,000
100,000
0
-0.13 -0.11 -0.1 -0.08 -0.06 -0.05 -0.03 -0.02 0 0.02 0.03 0.05 0.07
NDCI Values

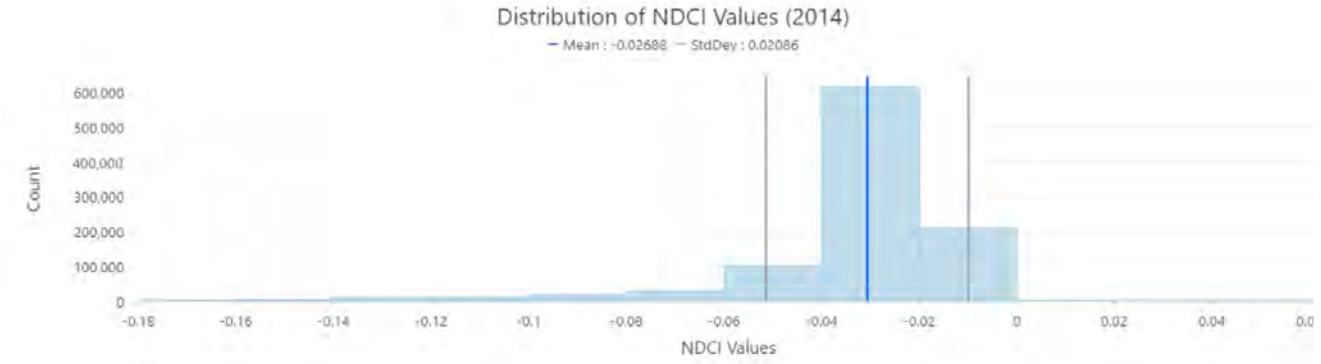
Distribution of NDCI Values (2014)
Mean : -0.02688
StdDev : 0.02086
Count
NDCI Values

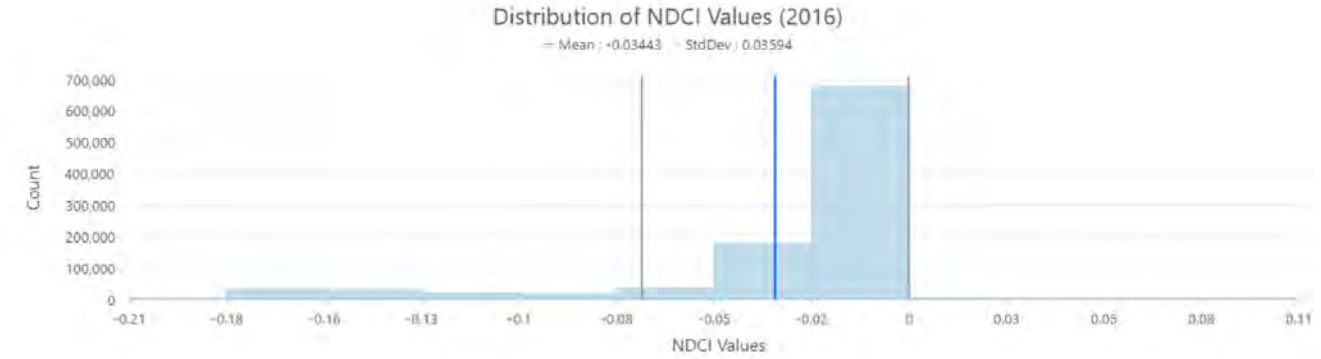
Distribution of NDCI Values (2016)
Mean : -0.03443
StdDev : 0.03594
Count
NDCI Values

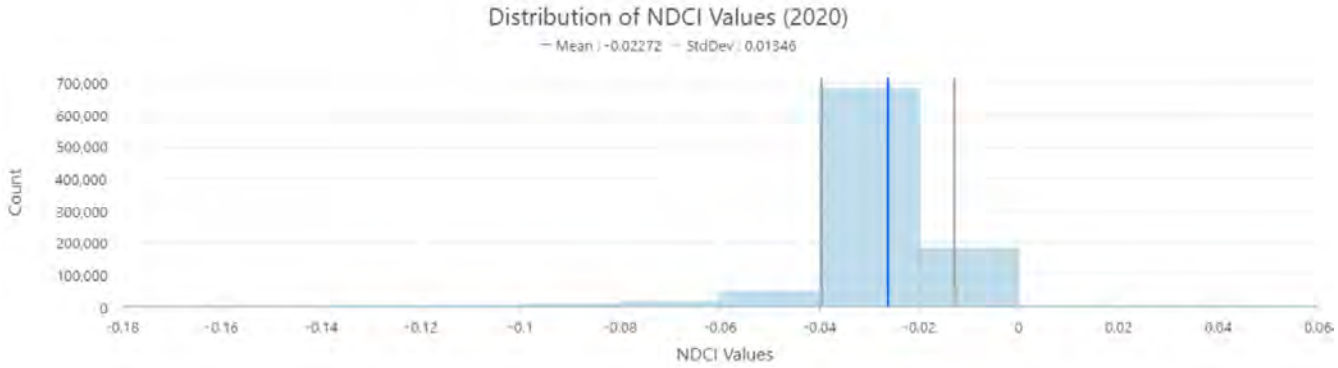
Distribution of NDCI Values (2020)
Mean : -0.02272
StdDev : 0.01346
Count
NDCI Values